Dedication

I dedicate this piece of work to my late father Mr Agho Theophilus A. I still miss you dad. May your soul rest in perfect peace.

Acknowledgements

I wish to express my profound gratitude to the following persons who have contributed or help me in one way or the other during the course of this thesis. I begin by expressing my profound gratitude to my parents who instilled my desire to acquire knowledge even at a tender age. My promoter Prof.dr.ir Filip Meysman was a tremendous help during the study. His critical examinations and practical suggestions helped me especially during difficult moments. I cannot imagine how grateful I am to VLIR for this opportunity to gain international experience and study in Belgium. I say thank you to my colleagues and fellow classmates at ECOMAMA, not leaving out the ECOMAMA staff. I conclude by thanking the following friends: Forsung Clarence, Bolanle Rema, Azong, Eugenia, Queenta, and a whole host of others who have made my stay in Belgium a memorable event.
Finally I thank the Almighty God, Jehovah for all His mercies and favours.

Abstract

Benthic O_2 uptake is the most widely used proxy for estimating organic matter degradation in the ocean floor, which has important implications on global climate, distribution and abundance of benthic communities and provides important information on the biogeochemistry of marine sediments. The quantification of diffusive O_2 uptake (DOU) across the SWI from depth distribution of O_2 is a common technique used in estimating the sediment O_2 uptake. A critical evaluation of DOU estimation procedures was investigated in two different sediment environments, homogeneous and heterogeneous sediments.

In the homogenous environment 1D numerical routines were used to create synthetic "perfect" O_2 depth profiles with different OPD's and subsequently numerically sampled to generate synthetic data O_2 profiles by mimicking different sampling procedures of real sensors. In each case a sensitivity analysis was done to estimate the systematic bias between the "true" DOU extracted from the numerical routines and the sample DOU calculated from the linear gradient fit of the first two and first five sample profile O_2 concentrations. Typically used microelectrodes (50 μ m outer tip diameter and 100 μ m step size) sampling under perfect conditions were found to underestimate the sediments "true" DOU by 5-10 %. However this bias was found to become significantly large (up to 40 %) when the step depths were increased (120-1000 μ m).

Virtual 2-dimensional (2D) O_2 distribution maps with natural spatially dependent hotspots obtained from Sagami Bay (Glud et al., 2009) were created using 2D reactive-transport models and assumed to represent heterogeneous environments. These maps essentially function as a sequence of neighboring O_2 micro profiles measured by a real sensor in typical lateral steps the same as the grid geometry of the 2D model. Sample DOU calculated from the extracted 1D microprofiles approximate well to "true" DOU extracted from the. 2D numerical routines. Compared to the experimental *in situ* DOU data the sample and model DOU's did not displayed any scatter trend from the theoretical homogenous OPD-DOU relationship. The number of 1D micro profiles necessary to underpin the average DOU within the sediment transects with a 10% error limit varied between 5-35 increasing with the heterogeneity of the transects. Random sampling was found to give a better estimate of the average DOU within each transects than selective sampling. Annual organic carbon mineralization rate in Sagami Bay determined from our 2D model was 7.1 g C m^{-2} yr^{-1}.

The study concludes that (1) there is inherent bias in the microelectrode profiling procedure in estimating the DOU using the linear gradient fit below the SWI even under perfect conditions. (2) 1D microprofiling works well in a 3D biogeochemical hotspot environment and, (3) spatial heterogeneity in O_2 uptake rates along the sediment surface due to lateral mosaic hotspot distribution do not create scatter in theoretical OPD-DOU relationship.

Keywords: Benthic O_2 uptake, DOU, microelectrodes, micro-profiles, spatial heterogeneity

Table of contents

List of Figures

List of tables

List of abbreviations

CCD	Couple Charge Device
DBL	Diffusive boundary layer
DOU	Diffusive oxygen uptake
FMOU	Fauna mediated oxygen uptake
TOU	Total oxygen uptake
IPCC	Intergovernmental Panel on Climate Change
SWI	Sediment water interface
OPD	Oxygen penetration depth

CHAPTER 1.

INTRODUCTION AND LITERATURE REVIEW

1.1 The ocean carbon cycle

The oceans contain approximately 60 times more carbon than the atmosphere, and therefore, they exert an important control on atmospheric CO_2. The latter is a major greenhouse gas, and hence, an important factor in the climate system (IPCC, 2007). Effectively, the ocean acts as an important sink for carbon. Of all the CO_2 that is liberated to the atmosphere by anthropogenic emissions, about 30% is taken up by the ocean (a net uptake of 1.7 Gt C per year in Figure 1). Given the pressing concerns about climate change, this provides a valid motivation to better understand the ocean carbon cycle.

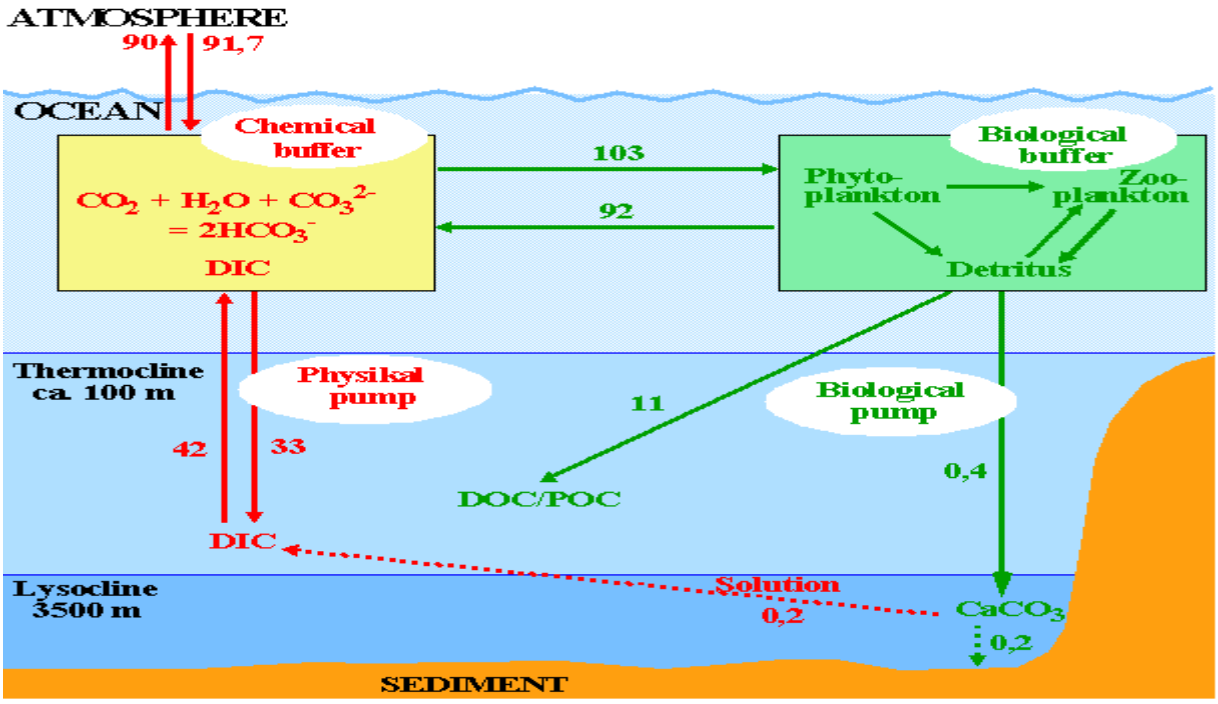

Figure 1. The ocean carbon cycle. Physical and chemical processes are shown in red, while biological processes are in green. All fluxes are in Gt C per year. Source: http://www.hamburger-bildungsserver.de/welcome.phtml?unten=/klima/klimawandel/treibhausgase/carbondioxid/surfaceocean.html

The marine carbon cycle is characterized by two pump mechanisms, which lower the surface concentration of dissolved inorganic carbon relative to the deep ocean. As a result, the carbon storage capacity of the ocean is enhanced. Without these pump mechanisms, the atmospheric CO_2 would rise from the pre-industrial level of 280 ppm to more than 420 ppm, i.e., an

increase of about 50% (Sarmiento and Gruber, 2006). These two pump mechanisms are referred to as:

- Solubility (or physical) pump
- Biological pump

The solubility pump (Figure 2) arises from the circulation of water in the oceans. The main controlling factors are the temperature of water and the partial pressure of CO_2 (pCO_2) in the surface ocean and atmosphere. Surface water flowing towards the poles will cool, thus lowering the pCO_2 and causing an uptake of CO_2 from the atmosphere. The cold, dense CO_2 rich water then sinks to form deep bottom water. The North Atlantic and the Antarctic are the major sites for this deep bottom water formation. The CO_2 rich bottom water flows at great depth in the oceans and eventually wells up to the surface after a period of about 1500 years. The Equatorial Pacific is a major site for such upwelling. The upwelling water is subsequently heated to tropical temperatures, which result in a high pCO_2 and the loss of CO_2 to the atmosphere through outgassing (Sarmiento and Gruber, 2006). The overall effect of the solubility pump is to enhance the storage capacity of dissolved inorganic carbon in the deep ocean.

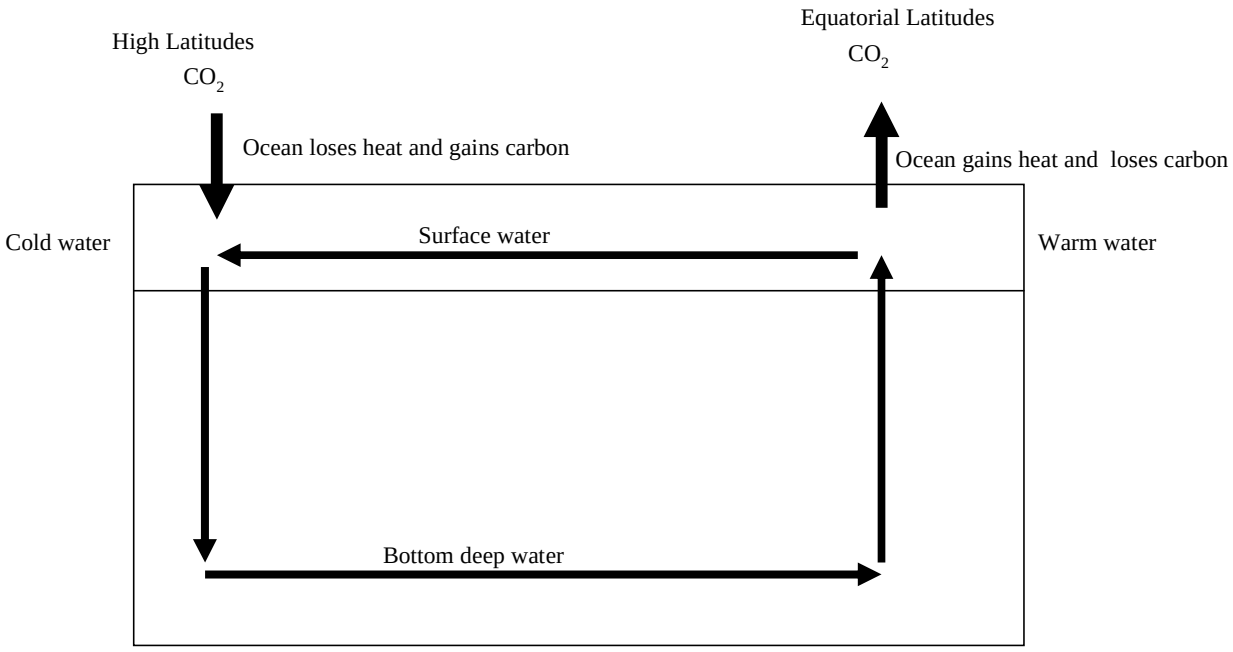

Figure 2. General illustration of the thermo-haline circulation and the solubility pump. Fluxes of heat across the air-sea interface drive the pump.

The biological pump is the sum of all biologically mediated processes that export carbon from the surface water to the deep ocean. The carbon is fixed by primary producers in the euphotic zone where light penetrates and subsequently exported through food-web processes to the dark

ocean below. The main factors that control the biological pump are light and nutrient supply. Two different forms of carbon are exported through the biological pump (Figure 3): organic

carbon (CH_2O), also known as the soft tissue pump, and calcium carbonate ($CaCO_3$), also known as the carbonate pump (Anderson et al., 2004).

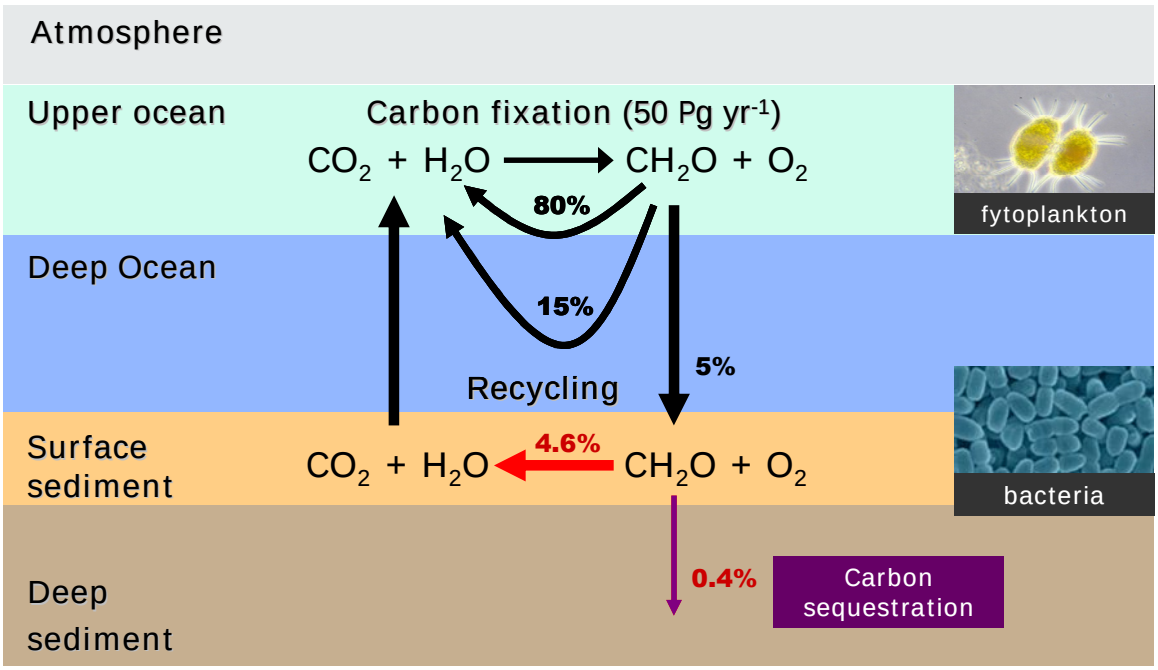

Figure 3. General overview of the soft tissue pump: production, export and mineralization of organic matter in the ocean. Adapted from Sarmiento and Gruber, (2006).

The present thesis studies one particular aspect of the biological pump, namely the fate of the organic matter that arrives at the ocean floor. As shown in Figure 3, a large part of the organic matter fixed by the biological pump is converted back into inorganic constituents by heterotrophic organisms, first within the water column and subsequently in the sediments of the ocean floor. This process is referred to as mineralization. On global average, about 80% of the primary production is mineralized in the upper ocean, 15% in the deep ocean and 4.6% in the surface sediment. The remaining 0.4% (~0.2 Gt C yr^{-1}) is buried into deeper sediment layers, and hence, sequestered over geological time scales. In the present thesis, the goal is to evaluate methods for the quantification of the mineralization rate in ocean floor sediments (the red arrow in Figure 3). Accordingly, the overall goal is to achieve a better quantification of the carbon cycle in the ocean floor.

1.2 The carbon cycle in the ocean floor

1.2.1 Ocean floor as a biogeochemical reactor

The marine ecosystem consists basically of the water column and the ocean floor. The ocean floor covers approximately 71 % of the earth's surface, and thus, encompasses a vast ecosystem. The biogeochemical active compartment of the ocean floor only involves the upper decimeters of sediment, which is 10.000 times smaller than the size of the water column, which has an average depth of 3800 m (Glud, 2008). However, the volume-specific degradation rate of organic matter within the sediments is 100-1000 times higher than the corresponding value for the water column (Glud, 2008). This makes marine sediment a hotspot of biogeochemical activity (Figure 4). About 45% of ocean aerobic respiration takes place in deep sea sediments (Wenzhofer et al., 2001).

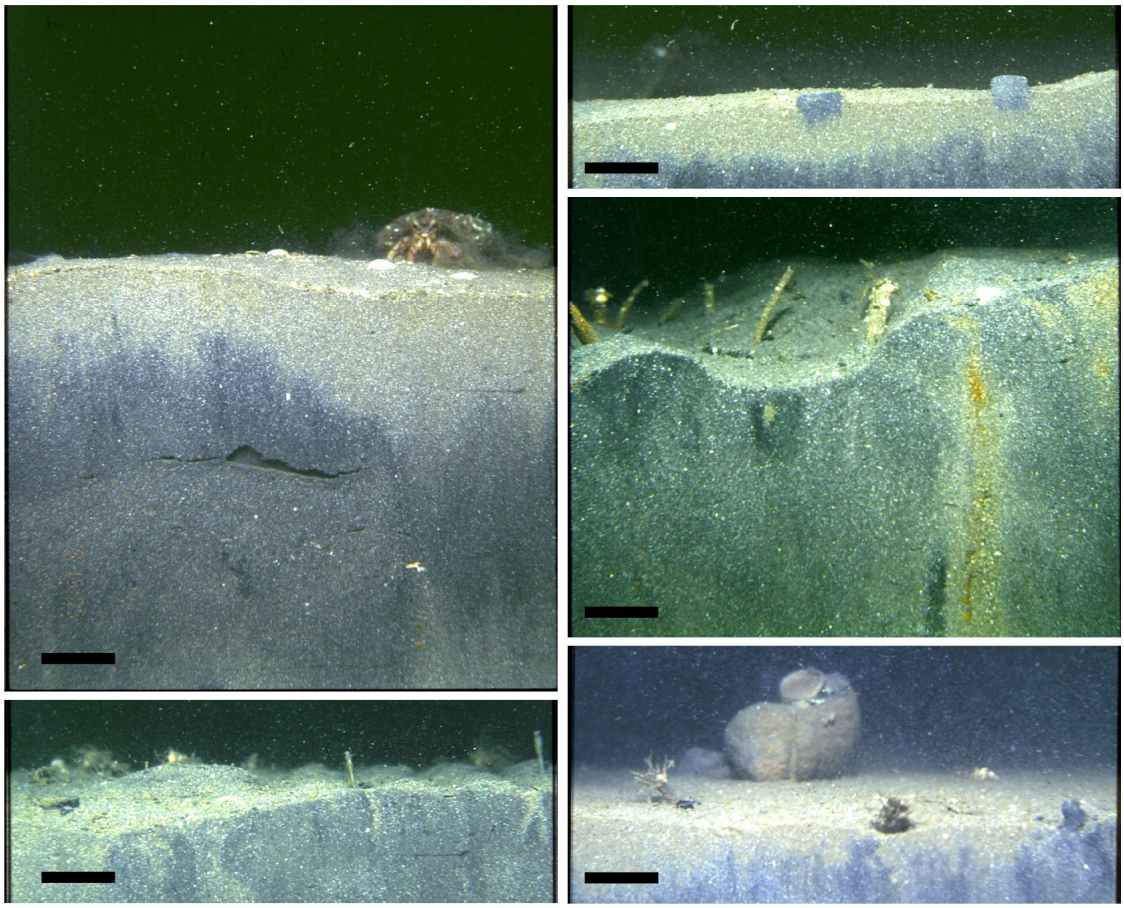

Figure 4. Marine sediments are heterogeneous hotspots of biogeochemical activity, as indicated by the color transitions. Various microbes and macrofauna are involved. Scale bars = 2 cm

The ocean floor acts as a very efficient biogeochemical reactor (Figure 5). Approximately 8 % (0.002-0.12 Gt C yr^{-1} representing 0.01-0.4 % of surface primary production) of the organic

matter reaching the seafloor is sequestered into deeper sediments (Middelburg and Meysman, 2007). This implies that 92 % returns as inorganic carbon to the water column after degradation at the seafloor. This degradation process is mediated by different populations of benthic micro and macro organisms through a complex web of respiratory processes (Seiter et al., 2005; Kim and Kim, 2007; Middelburg and Meysman, 2007).

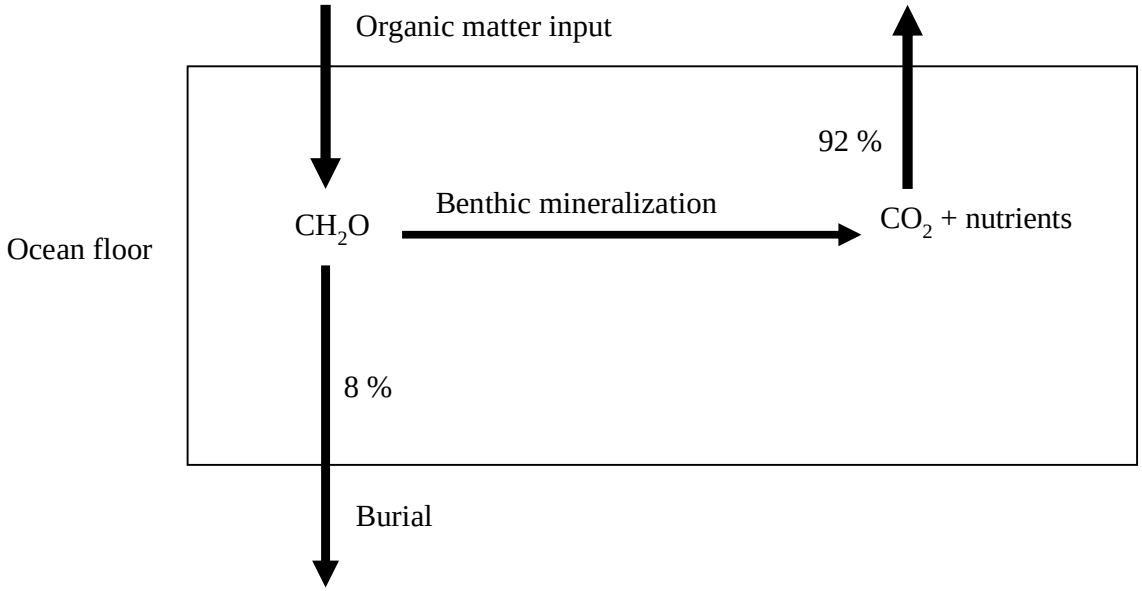

Figure 5. The ocean floor is a very efficient biogeochemical reactor.

Benthic mineralization thus plays an important role in the recycling of nutrients in the oceans and also in determining the ocean's oxygen and carbon balance (Cai and Reimers, 1995). On a short time scale benthic mineralization regenerates inorganic carbon and nutrients sustaining a continued production in the water column (Wenzhofer and Glud, 2002). At the same time, the ocean floor is a sink for carbon where carbon is stored and removed from the marine carbon cycle and thus from the global carbon cycle for long periods of time (Wenzhofer et al., 2001). This burial of organic carbon leads to the accumulation of O_2 in the biosphere and also supports prokaryotes (constituting about 30% of the total biomass on Earth) living deep in the Earth's crust (Middelburg and Meysman, 2007).

Overall, the balance between burial and mineralization of organic matter has a significant impact on the global carbon cycle over both short and long time scales. It is thus highly relevant to accurately quantify turn over rates of organic matter within the sediment, thus allowing a better assessment of natural and anthropogenic perturbations to the carbon cycle in the ocean floor (Wit et al., 1997). The accurate quantification of benthic oxygen consumption is one key aspect to achieve this task.

1.2.2 Pathways of organic matter degradation

There is a high level of biogeochemical activity within the first few centimeters of the sediment. The degradation of organic matter (benthic mineralization) involves different micro and macro fauna using different electron acceptors (Figure 6). Aerobic respiration is the respiratory pathway used by both large organisms, such as clams and worms, and also by aerobic bacteria which can use only oxygen as the electron acceptor. Microbial respiration which uses other electron acceptors such as nitrate, sulphate and metal oxides is termed anaerobic respiration.

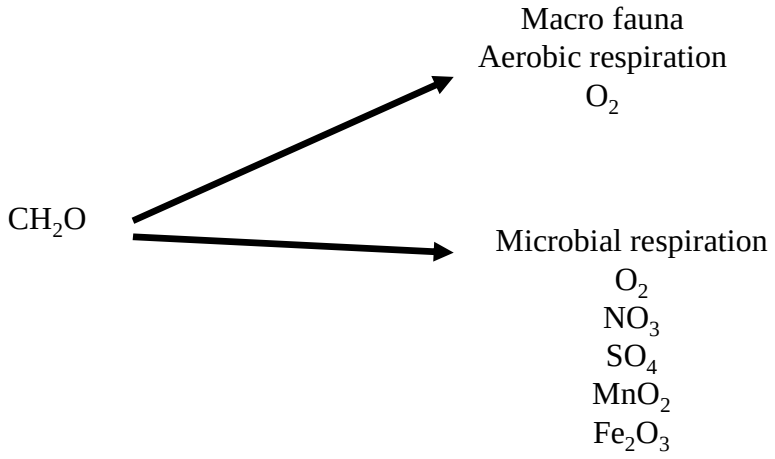

Figure 6. Organic matter degradation pathways in the ocean floor with their associated electron acceptors
.

Oxygen is energetically the most favorable oxidant. However, sea water contains relatively little oxygen and so it is rapidly depleted within few millimeters of the sediment (Cai and Sayles, 1996; Kim and Kim, 2007; Dedieu et al., 2007). As a result, marine sediments can be seen as composing of two distinct layers (Figure 8); an oxic layer representing oxic mineralization (aerobic respiration) and an anoxic layer representing anaerobic carbon mineralization. The reduced substrates formed from anaerobic respiration in deeper sediment layers are eventually transported by diffusion or sediment re-working activities of macro fauna to the oxic-anoxic interface, where they become re-oxidized when they come in contact with oxygen.

1.3 Sedimentary O_2 consumption.

1.3.1 O_2 uptake as a proxy for benthic mineralization

The total sediment O_2 uptake represents the most widely used proxy to estimate benthic carbon mineralization (Thamdrup et al., 2000; Berg et al., 2003; Meysman et al., 2007; Glud et al., 2009). O_2 consumption in marine sediments stems from two main processes (Figure 7): (1)

aerobic respiration activity of bacteria and other sediment fauna and (2) re-oxidation of reduced inorganic products released during anaerobic degradation of organic matter.

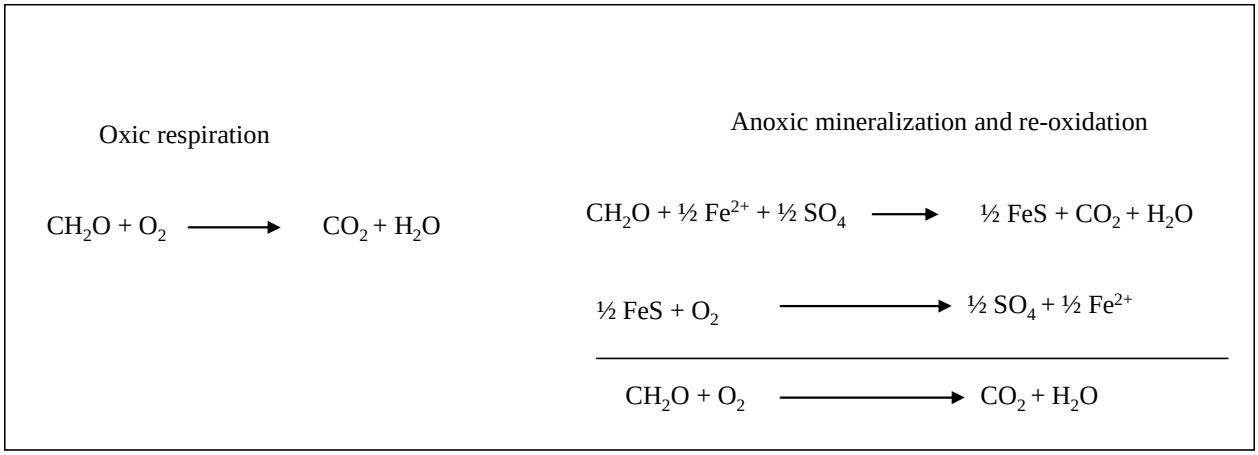

Figure 7. Processes that consume oxygen within sediments

The contribution of both processes to the total sediment O_2 uptake will depend on whether the focus is on deep sea or coastal sediments. In deep sea sediments, aerobic respiration accounts for most of the total sediment O_2 uptake. In coastal sediments, re-oxidation of products from anaerobic mineralization contributes significantly to the total O_2 uptake as a result of shallow water depths, inducing tight benthic-pelagic coupling, and high primary production, which stems from high riverine and terrestrial input of nutrients in these areas (Epping and Helder, 1997)

When steady state is assumed between anaerobic mineralization and re-oxidation processes, and minor electron sinks such as denitrification and FeS and FeS_2 burial are neglected, carbon oxidation and oxygen consumption proceed through stoichiometric ratios, the so-called Redfield ratio (138 mol oxygen/106 mol carbon) (Canfield et al., 1993; Dedieu et al., 2007). As a result, the oxygen consumption rate can be used to quantify carbon mineralization rate.

1.3.2 Components of sediment O_2 consumption

The Total Oxygen Uptake (TOU) represents the total oxygen consumed within the sediment and can be decomposed as (Meysman et al., 2007)

$$TOU = DOU + FMOU \quad [1.1]$$

where DOU is the Diffusive Oxygen Uptake across the sediment water interface (SWI) and FMOU is the Fauna Mediated Oxygen Uptake (Figure 8).

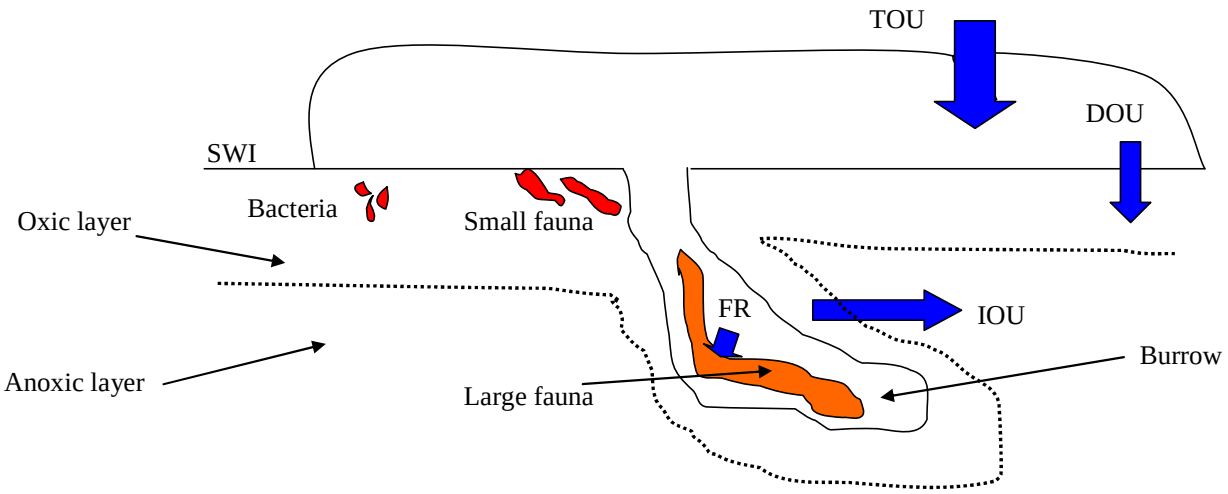

Figure 8. Components of sediment oxygen consumption

The FMOU in its turn can be decomposed as

$$FMOU = IOU + FR \qquad [1.2]$$

where FR is the respiration of the large macrofauna and IOU is the Irrigational Oxygen Uptake representing the oxygen uptake in zone around burrows (deeper micro niches).

The contribution of both terms DOU or FMOU to the TOU will depend on the distance from the shore. In deep sediments the DOU forms the dominant factor and quantitatively accounts for the TOU (Figure 9). However in the near shore marine environments, there is enhanced oxygen uptake by macrofaunal activity and as a result the FMOU contributes significantly to the TOU.

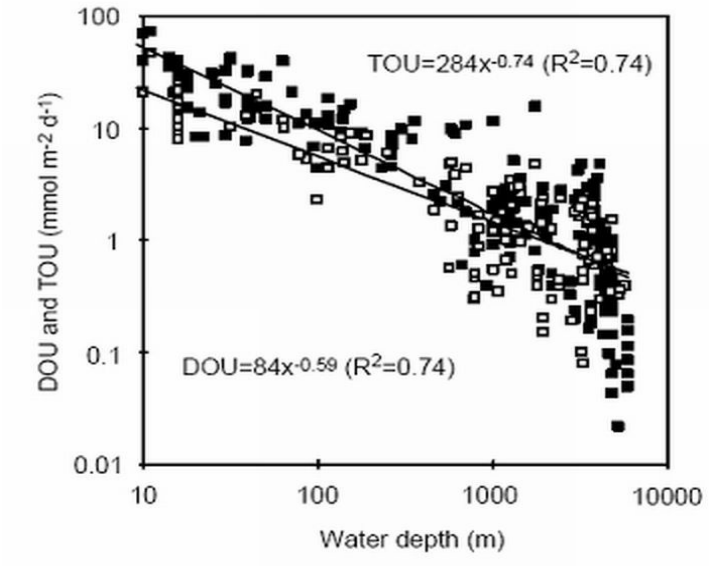

Figure 9. The total O_2 uptake (closed symbols) and the diffusive O_2 uptake (open symbols) plotted as a function of water depth. Source Glud, (2008)

TOU data does not however reveal where oxygen is consumed and how it is distributed within the sediment or interstitial oxygen dynamics. As a result TOU data are always complemented by DOU data, which are obtained by resolving the oxygen distribution within the sediment (Wenzhofer and Glud 2004; Meysman et al., 2007). These O_2 distribution data are often obtained by micro-electrode sensors applied to either recovered sediments or via *in situ* deployment of the micro-electrode sensors (as explained more in detail below). This thesis specifically focuses on how to obtain reliable DOU data.

1.4 Techniques used for estimating sedimentary O_2 consumption

1.4.1 Benthic chambers (TOU)

Benthic chambers (also called boxes, bell jars, flux chamber systems, etc) have been used since the mid-1960s to estimate the total oxygen uptake (TOU) within sediments *in situ* (Reimers et al., 1986; Hall et al., 1989; Archer and Devol, 1992; Viollier et al., 2003). The benthic chamber technique consists of incubating the sediment and following the decrease in the oxygen concentration of overlying water as a function of time. The benthic chambers are placed on the sediment enclosing a known area of sediment and a known volume of ambient overlying water and left to incubate for some weeks (5-7 weeks) with water samples collected periodically to measure changes in oxygen concentration of the overlying water over time. The chambers usually have a box dimension which typically ranges up to 35 cm long with a diameter of about 50 cm (Hall et al., 1989). Before being placed on the sediment the chambers are first cleaned with detergents, soaked with dilute hydrochloric acid, conditioned by suspension in sea water at the sampling sites for about 24 hours, and finally covered with large dark polythene bags to avoid photosynthesis during incubation.

Typically three different chambers are used placed side by side: the regulated chamber, unregulated chamber and the blank chamber (Hall et al., 1989). In the regulated chamber, the dissolved oxygen concentration and pH are maintained close to the original ambient level of the overlying water throughout the incubation period. In the unregulated chamber no such adjustment is made and benthic respiration is allowed to lower the ambient oxygen concentration and pH. Finally, the bottom of the blank chamber is closed with a polythene film instead of sediment and it serves as a control to check if the processes in the water phase contribute to the measured oxygen change (Hall et al., 1989).

A linear fit to the concentration changes of oxygen over the first few days in the enclosed unregulated chamber is used to estimate the TOU within the sediments (Figure 10). The TOU is estimated as (Glud, 2008):

$$TOU = \frac{V}{A}\frac{dC}{dt} \qquad [1.3]$$

where V is the volume of the chamber in liters (L), A is the area of bottom sediment enclosed by the chamber in square meters (m^2), t is time in days and C oxygen concentration μ mol L^{-1}

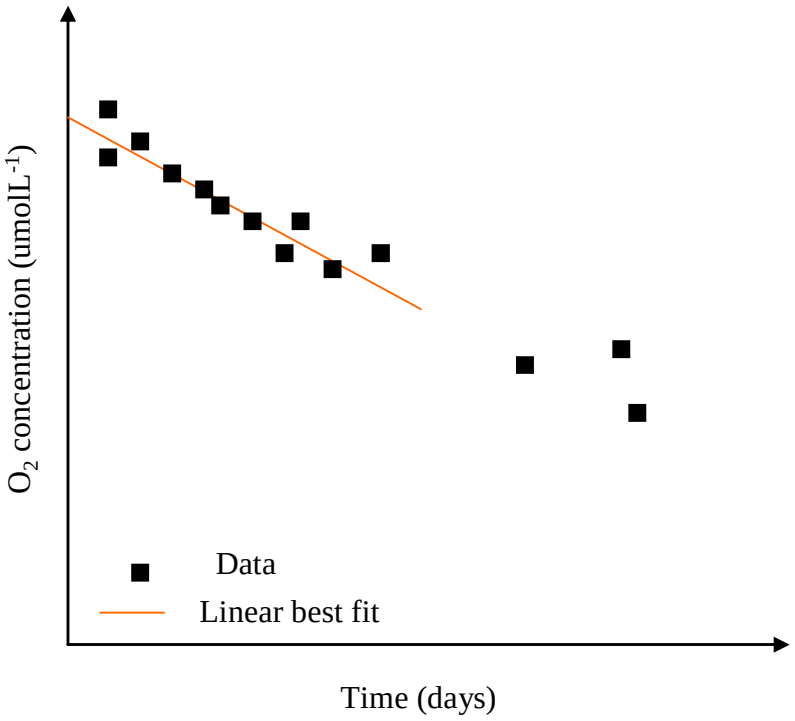

Figure 10. Typical dissolved oxygen curve in the unregulated chamber showing the linear best fit used in estimating the TOU. Adapted from Glud (2008)

Equation [1.3]is based on the following assumptions (Viollier et al., 2003):

- Rates of biogeochemical processes in the overlying water column are negligible compared to those within the sediment.
- The hydrodynamic regime inside the chamber does not alter the oxygen uptake across the sediment water interface compared to natural conditions
- The size of the sampling/measurement area is representative for a larger sea floor area.

The benthic chamber enclosure technique is very useful as it is simple to implement and also because it measures oxygen flux due to bio-irrigation which is often missed by other TOU estimation methods. However the linear curve fitting procedure can only be used under the assumption that the initial decrease in O_2 uptake is mainly due to aerobic heterotrophic processes and that O_2 consumption is depth independent (Hall et al., 1989). This assumption doesn't account for re-oxidation processes and in such instances sophisticated biogeochemical models are required to effectively estimate the TOU (Glud, 2008). The technique also has the disadvantage that it does not provide information about the benthic O_2 distribution or the interstitial O_2 dynamics (Glud, 2005) together with the O_2 penetration depth (OPD). The OPD is formally defined as the depth within the sediment where the oxygen concentration diminishes to zero.

1.4.2 Oxygen micro-electrodes (DOU)

Micro-electrode profiling has been used in a wide variety of studies involving benthic oxygen consumption (e.g. Revsbech et al., 1980; Jorgensen and Revsbech, 1985; Reimers et al., 1986; Jorgensen and Ramussen, 1992; Jorgensen et al., 2005; Kim and Kim, 2007; Glud et al., 2009). The advent of micro-electrodes made it possible to assess the oxygen distribution in marine sediments at sub-millimeter scale resolution and to estimate rates of oxygen production, transport and consumption. In this study a micro-electrode refers both to electrochemical sensors or very small electro-active surfaces embodied within sensors capable of measuring oxygen distribution with a very high spatial resolution (Glud et al., 2000; Reimers, 2007). There are various types of micro-electrode including the Baumgartl and Lubbers, amperometric cathode-type or "Clark-type'' oxygen micro sensors and the voltammetric microelectrode (Figure 11 A-C)

The Clark type oxygen micro-electrode is currently the state of the art both for *in situ* and laboratory studies. The glass plated Clark type oxygen microelectrode senses dissolved oxygen at its gold plated platinum cathode after diffusion across a silicone membrane enclosed at the tip (Figure 11B and D). The electric current between the cathode and an anode (Ag/AgCl reference anode) immersed in an aqueous electrolyte chamber is measured and the magnitude of the current is calibrated to the concentration of oxygen in the surrounding environment (Gundersen et al., 1998). The microelectrode is attached to a micromanipulator which allows measurements to be taken at typical vertical steps of 50 or 100 μm. Table 1.1 shows typical characteristics of a Clark-type sensor. However sensor properties of individual microelectrode may vary and their importance will depend on the specific scientific questions addressed.

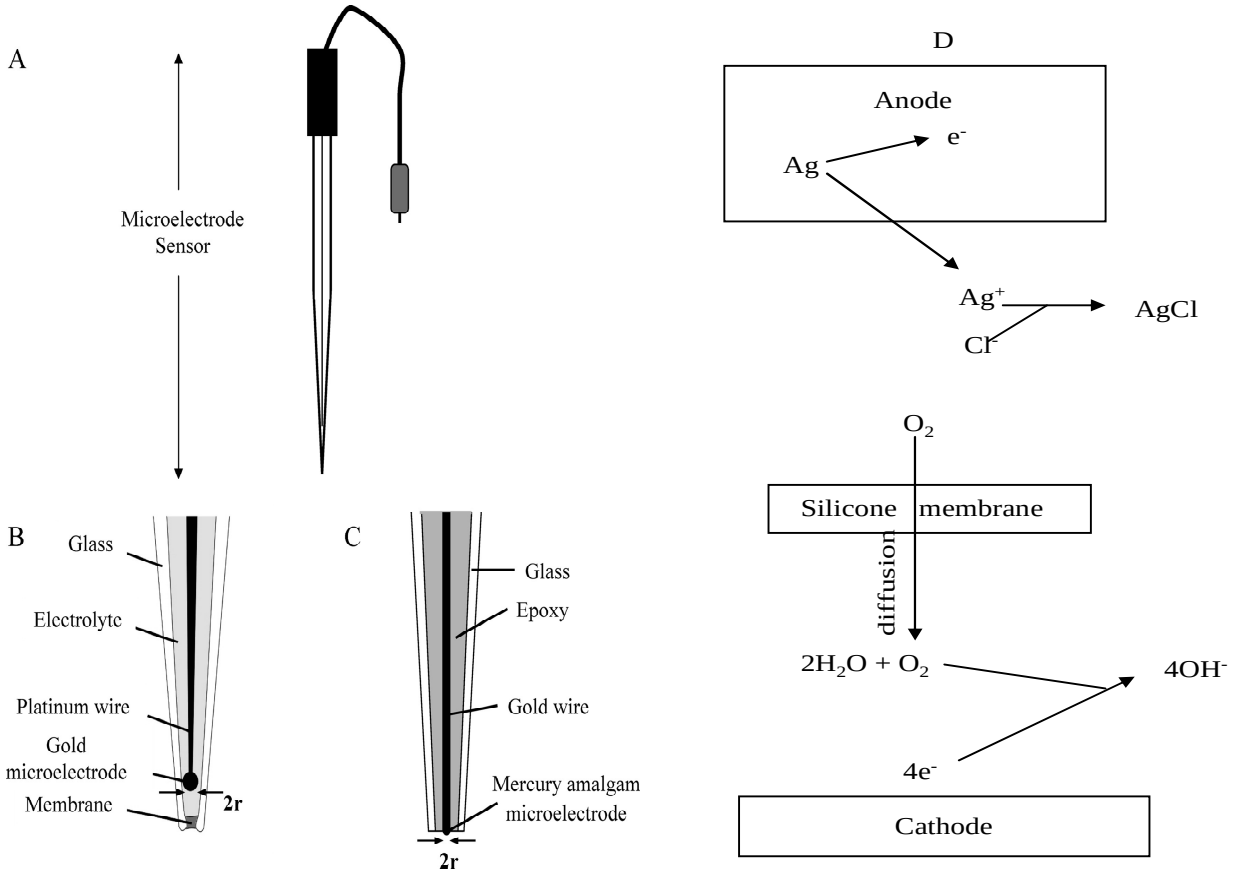

Figure 11. Schematic drawings illustrating the double usage of the term "microelectrode" as both an electrochemical sensor (**A**) and a tiny sensing surface, often located in the tip region of glass capillary constructions (**B** and **C**). **B** resembles the tip of a Clark-type O_2 microelectrode and **C** the tip of a Au-amalgam voltammetric microelectrode. **D** is a schematic illustration of the measurement principle of a Clark-type micro sensor. The upper panel shows the reaction at the anode placed in the bulk electrolyte, while the lower panel illustrates the reactions at the cathode. From Glud et al. (2000) and Reimers (2007).

Sensor characteristics		*Definitions*
Tip outer diameter (μm)	5-1000	The tip size determines the size of the environment that contributes to the sensor signal (spatial resolution)
Stirring sensitivity (%)	0-2	Percentage change in sensor signal when transitioning from a completely anoxic medium to 100 % air saturation.
90 % Response time (t_{90}) (s)	0.5-2	Time required for a sensor signal to reach 90 % of the total signal change after an abrupt change in O_2 concentration
Detection Limit (μmolL-1)	2	Accuracy and precision of sensors to detect O_2. Measurements below this limit are referred to as anoxic signals.
Signal size at air saturation (pA)	50-200	
Main interference	H_2S	The cathode is coated with a membrane that is permeable to ions. This causes interference problems with other dissolve gases in the sediment.

Table 1.1 Typical characteristics of amperometric Clark-type sensors commonly used in benthic research. Adapted from Glud et al., (2000) ; Reimers, (2007)

O_2 microprofiles can be obtained in the lab from recovered sediment cores that are maintained at *in situ* temperature, *in situ* bottom water O_2 concentration and a well-mixed overlying water phase (to obtain trustworthy results). Alternatively, microprofiles can be assessed *in situ* using remotely operated vehicles (so called Benthic Lander systems) that carry benthic chambers and/or a microelectrode profiling unit to the seafloor (Jorgensen and Revsbech 1985; Berg et al., 1998; Glud, 2008). The resulting O_2 microprofiles enable the estimation of (1) the DOU across the sediment water interface driven by molecular diffusion, (2) the oxygen consumption rates within the oxic zone and (3) the oxygen penetration depth using various reactive-transport models (Bouldin, 1968; Rasmussen and Jorgensen, 1992; Dedieu, 2007; Kim and Kim, 2007).

The main advantage of Clark-type sensors is that they allow measurements to be taken at sub-millimeter scales and also make it possible to exploit working principles that normally would not work at macro-scale (Glud et al., 2000). The small tip diameters also minimizes disturbance of surrounding sediment. However because of its small scale, microelectrodes can supply information only at a single point and the profiling depth is limited to about 10-15 cm (Wenzhofer et al., 2001). To be able to capture the spatial heterogeneity of the environment multiple micro profiling is needed which is often very costly.

1.4.3 Optical Microsensors (Microoptodes)

Micro-optodes are a recently developed micro sensor technique to obtain O_2 micro profiles. The basic principle of this method is that it uses the ability of O_2 to dynamically quench a fluorophore (Klimant et al., 1997; Glud et al., 2000; Kazuma et al., 2004; Stockdale et al., 2007). The fluorescence dye is immobilized in a polymer matrix and coated on the tip of a fibre optical cable. The dye which consists of a molecule containing ruthenium, in the absence of O_2 absorbs light at a wavelength of 450 nm and maximally emits light at a wavelength of 610 nm. In the presence of O_2, dynamic quenching takes place and the result is a decrease in the intensity of light emitted. The florescence emitted light is returned through the fibre optic and its intensity is recorded. The intensity measured is inversely proportional to the concentration of O_2 (Glud et al., 2000; Viollier et al., 2003; Stockdale et al., 2007).

Compared to microelectrodes, the oxygen optodes are easier to manufacture, they do not consume oxygen and are therefore insensitive to stirring. For benthic lander use (that is, incorporating the micro-optodes into a Benthic Lander system) they provide long-term stability and are therefore good alternatives to microelectrode systems.

Recently there has been the development of planar optodes that use a modified optical principle from that used in microoptodes. In a planar optode the oxygen quenchable fluorophore is also dissolved in a polymer matrix but applied as a thin layer on to a transparent thick support foil. The planar optode is then mounted onto a small frame of plexiglass which in turn is mounted on to the interior of a glass aquarium. Illumination is provided by a halogen lamp and a CCD camera takes two dimensional (2D) high resolution oxygen image (in principle consisting of numerous neighboring micro profiles) across the sediment water interface (Stockdale et al., 2007).

Planar optode images provide a more detailed insight into the oxygen dynamics of marine sediments than the traditional one-dimensional oxygen micro profiling approach. Planar optodes can also be incorporated in a benthic lander system to study the spatio-temporal heterogeneity of oxygen uptake at a very high spatial resolution of less than 0.1 mm and with a temporal resolution of a few seconds. However at this stage they cannot be used for DBL studies especially in areas where the DBL impedance is significant (Viollier et al., 2003).

1.5 Estimating DOU from micro profiles

The most common procedures often used calculates the DOU from a linear approximation to the O_2 concentration gradient resolved within the diffusive boundary layer (DBL) or a similar a linear fit to the O_2 gradient just below the sediment water interface. The slopes obtained this way are then used in Fick's first law of diffusion (Figure 12). An alternative, but far less frequently used method, is to fit a reactive transport model for O_2 through the data in the sediment, and subsequently extract the flux from the output of this reactive transport model.

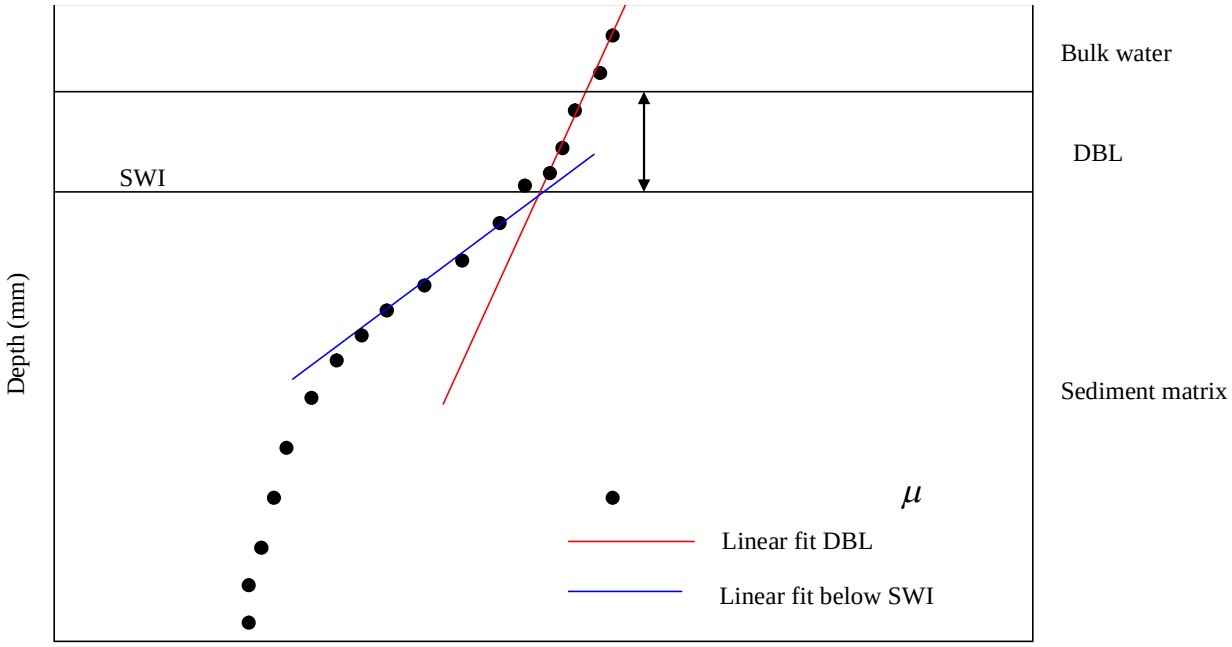

Figure 12. An O_2 micro-scale gradient with linear best fits to estimate DOU.

The DBL is the thin water layer, typically 0.2-1 mm thick, close to the sediment water interface and forms the transition zone which separates the bulk water and the pore water within the sediment matrix. In this layer, viscous forces retard the flow velocity of the overlying water and molecular diffusion progressively becomes dominant in oxygen transport. Because of turbulence in the overlying water, the DBL is generally unstable and the O_2 concentration in the DBL fluctuates. Despite of its modest thickness the DBL can play a significant role in limiting fluxes of nutrients and gasses across the SWI. Below the sediment water interface, molecular diffusion dominates oxygen transport. Diffusion is however reduced because of the convoluted path that molecules need to undertake to circumvent the sediment particles (Glud et al., 1994; Epping and Helder, 1997). There is thus a steeper O_2 gradient just below the SWI than at the DBL (Rasmussen and Jorgensen, 1992).

The DOU from these two common procedures is calculated as (Glud, 2008), the DOU within the DBL

$$DOU\big|_{DBL} = D_{mol}\frac{dC}{dx} \qquad [1.4]$$

and the DOU just below the sediment water interface

$$DOU\big|_{SWI} = \phi D\frac{dC}{dx} \qquad [1.5]$$

where D_{mol} is the molecular diffusion constant, D is the effective diffusion constant in the pore water (accounting for tortusoity) and ϕ the porosity. The porosity is formally defined as the fraction of volume of the sediment that is occupied by open space where the pore water is (Revsbech et al., 1986). A further description of these parameters is given in the modeling methods. The symbol C denotes the pore water O_2 concentration and x is the sediment depth. The DOU as calculated in equation [1.5] will depend on the number of data points included in the linear fit to the gradient, and the delineation of the sediment water-interface.

1.6 Problem statement

This thesis presents a critical evaluation of DOU estimation procedures obtained from 1D oxygen microprofiles. The reliability and accuracy of the method is investigated for two different sediment environments.

1.6.1 Microprofiling in homogeneous environment.

Microprofiling only provides an approximation of the continuous O_2 distribution at a finite resolution. We expect that the DOU as estimated by a microelectrode sensor could be sensitive to (1) the sensing volume of the sensor, (2) the number of points sampled within the oxic zone (e.g. micromanipulator step size) and (3) the number of points included in the fit of the concentration gradient. The question now is: Is there any inherent bias in the microelectrode profiling procedure in estimating the DOU? A literature survey on benthic research involving microelectrodes indicates that this possibility of a systematic bias in the profiling procedure of microelectrodes has not been investigated.

1.6.2 Microprofiling in Heterogeneous environment

Microprofiling is inherently a one-dimensional technique, profiling vertically downwards into the sediment. However, a recent investigation based on high-resolution study of O_2 distribution and consumption in a deep sea environment suggests the seafloor is characterized by extensive micro scale variability on a scale of centimeters (Glud et al., 2009). Furthermore, in coastal sediments, planar optodes have also shown this microscale variability in benthic oxygen distribution (e.g. Wenzhofer and Glud, 2004). Such optodes are more efficient than the micro electrode systems in documenting this heterogeneity, because they in principle consist of numerous neighboring micro profiles. Overall, these studies reveal a far larger heterogeneity in the O_2 consumption than previously anticipated.

The presence of small-scale heterogeneity has two major consequences for DOU estimation procedures:

- Because microprofiling is inherently a one-dimensional technique, the question is whether it works in 3D biogeochemical hotspot context?
- Small-scale heterogeneity implies that there is a great variability in the uptake of oxygen in the ocean floor (on a scale of centimeters) with important implications on benthic mineralization processes. Accordingly, one will need multiple O_2 profiles to arrive at a reliable estimate of the average DOU in a given environment. The question is how many profiles one needs, and whether this number is feasible given current Benthic Lander

technology (currently, technical and logistic constraints limits the number of profiles that can be obtained from a single deployment to 4-8).

The oxygen reactivity of sediments can be expressed by two major indicators: the DOU and the OPD. Currently, plots of DOU versus OPD obtained by *in situ* sampling show substantial scatter, indicating that the two proxies may provide a different assessment of the reactivity of a sediment (which is troublesome). It has been speculated that small-scale heterogeneity could be the source of this scatter. However, this hypothesis has not been investigated up to present.

In this thesis the aim is to investigate DOU estimation procedures within a heterogeneous environment.

1.7 Research objectives

The research presented in this MSc thesis has two following major objectives:

- To test if there is a systematic bias in the different procedures of estimating DOU using microelectrode sensors with different sensing volumes and micro manipulator step size
- To develop virtual sediment transect oxygen distribution maps (similar to optode images) in the ocean floor with natural spatially dependent hotspots using a high resolution two dimensional reactive transport model and to quantify the average DOU within this sediment transects using 1D and 2D approximations.

To achieve the major objectives the following specific objectives were set:

- To develop a spatial 2D reactive-transport model detailing distribution and spatial heterogeneity of benthic oxygen within virtual sediment transects with natural hotpot distributions.
- To quantify the average DOU and average OPD within each transect using 1D and 2D approaches.
- To test if there is systematic bias in 2D and 1D estimation of the average DOU within the sediment transects.
- To estimate the number of micro profiles per sampling needed to better quantify the average DOU within the sediment transects using a real sensor.
- To compare and investigate different sampling procedures used in estimating average DOU within a given sediment area.

CHAPTER 2.

MODELLING METHODS

The quantification of diffusive oxygen uptake (DOU) within the sediment requires the following:

- Oxygen data depth profiles: These oxygen depth profiles are usually collected using oxygen micro-sensors.
- Reactive transport models: Mathematical equations that describe the distribution of oxygen within the sediment. These equations are used for creating and/or numerically fitting oxygen depth profiles.
- Model simulation platform: Appropriate computer programs and packages to numerically solve the reactive transport models and visualize the model output.

In this thesis we use reactive transport models to create high-resolution oxygen depth distributions. These oxygen distributions essentially function as virtual sediments. Associated with this profiles comes a "true" DOU. These "perfect" O_2 distributions are subsequently numerically "sampled" to create synthetic oxygen data profiles. The numerical sampling procedure mimics the sampling procedure of an actual oxygen microsensor. From the synthetic data profiles, we then extract an estimate for the diffusive oxygen uptake (DOU). This "sampled" DOU is then compared to the "true" DOU associated with the original high-resolution oxygen depth distribution.

2.1 Software platform

The platform used for simulation was the open source programming software R (v.2.8.1). R is a freely available modeling and statistical program available through the internet under the General Public License (GPL). It provides a platform environment in which you can perform statistics and produce graphics (Dalgaard, 2009). Numerical routines in the R package `ReacTran` developed by Soetaert and Meysman (2009) were used to specify and formulate the reactive-transport model. The numerical routines in the R package `rootSolve` (Soetaert, 2008) were used to integrate the resulting partial differential equations of oxygen reactive-transport models. The R-package `ReacTran` contains routines (`tran.1D` and `tran.2D`) that enable the development of reactive transport models in one-dimensional (1D) and two-dimensional (2D) model geometry respectively in aquatic systems (rivers, lakes), porous media (floc aggregates, sediments,...) and even idealized organisms (spherical cells, cylindrical worms,...). The package rootSolve is used to solve the steady-state conditions for 1D and 2D reactive transport models using numerical routines `steady.1D` and `steady.2D` respectively. The output from these steady state simulations are sediment depth oxygen distributions – a vector in the case of 1D simulations or a matrix in the case of 2D simulations.

2.2 1D reactive transport model

2.2.1 Model domain geometry

In a one dimensional (1D) model description, the sediment surface is represented by a model domain with a fixed thickness L. The x-coordinates represent the depths in to the sediment. The origin is attached to the sediment-water interface (SWI) with the depth layer L subdivided in to a finite number of grid cells (N) with Δx_i being the thickness of each grid cell. In this model geometry the oxygen concentration is defined in the middle of the grid cells while the oxygen fluxes are defined at the interfaces of the grid cells (Figure 13).

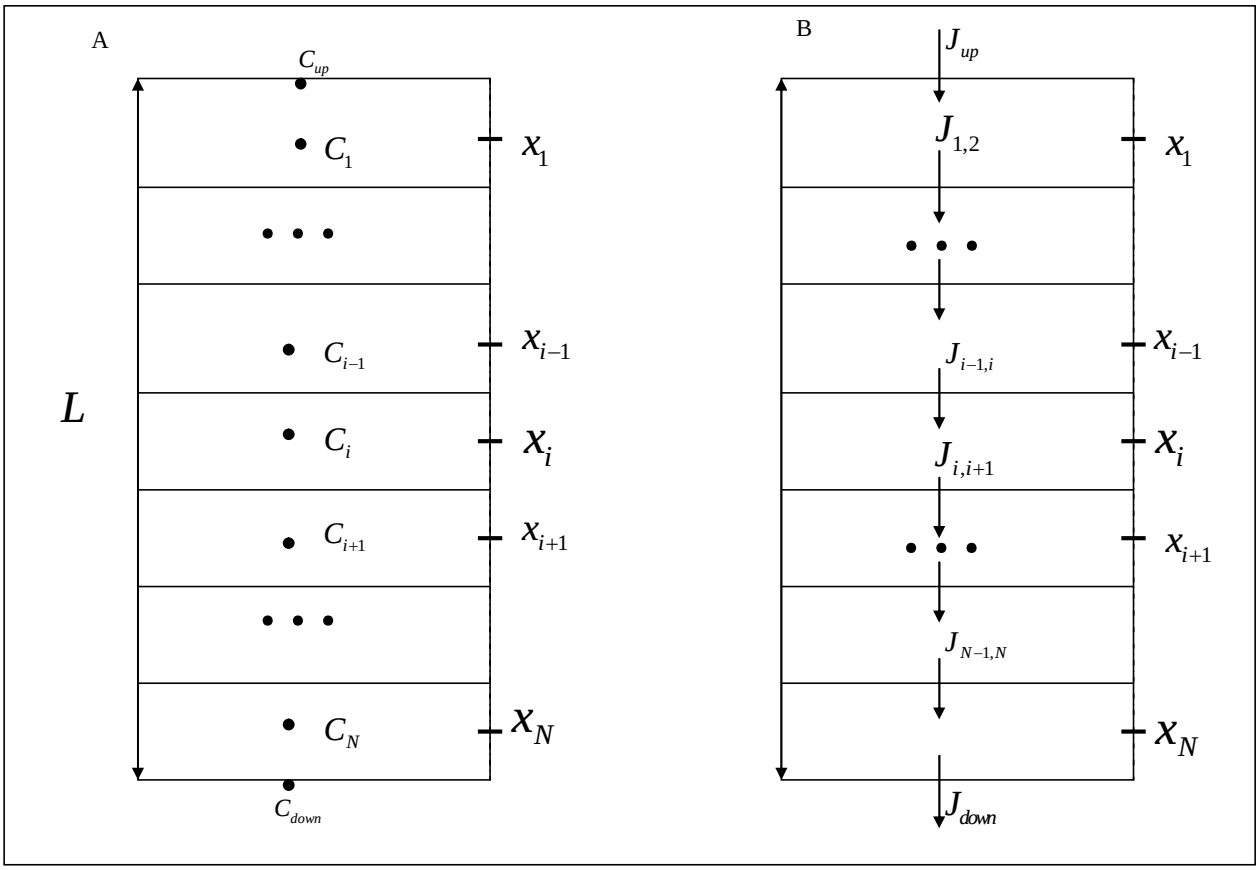

Figure 13. A. Concentrations are defined in the centre of the grid cells. **B.** Fluxes are defined at the box interfaces. Adapted from Soetaert and Herman (2009).

2.2.2 Mass balance statement

In a one-dimensional model description, the oxygen distribution within the sediment is governed by the general mass balance equation (Boudreau, 1997)

$$\frac{\partial(\phi C)}{\partial t} = -\frac{\partial J}{\partial x} - \phi R(x,t) + \phi I(x,t) \qquad [2.1]$$

The quantity C denotes the pore water oxygen concentration, ϕ the porosity, J is the oxygen flux, R the oxygen consumption rate (expressed per unit volume of pore water) and I the non-local input of oxygen through physical or biological irrigation.
The following simplifying assumptions were adopted:

- Solute transport by advection is assumed to be negligible compared to the diffusive transport, and is not considered
- Non-local irrigation as a result of wave and current movements or macro fauna bio irrigation is ignored
- The porosity of the sediment is considered constant with depth and time.
- The oxygen concentration is assumed to be in steady state.

The flux J defines the amount of oxygen that passes through a unit surface per unit of time. Because we assumed that transport is principally governed by molecular diffusion, J can be expressed as (Boudreau, 1997; Soetaert and Herman, 2009);

$$J\big|_{diffusion} = -\phi D \frac{\partial C}{\partial x} \qquad [2.2]$$

The effective diffusion constant is calculated as $D = D_{mol}/\theta^2$ from the molecular diffusion constant D_{mol} corrected with the tortuosity factor θ^2. This tortuosity correction is needed because the water molecules and ions follow a convoluted (tortuous) pathway in the porous sediments unlike the free random linear pathways in water. The molecular diffusion constant of oxygen is calculated in units of $m^2\ s^{-1}$ using the R package `marelac` as (Soetaert et al. in prep)

$$D_{mol} = \left(0.2604 + 0.006383\frac{T}{\mu}\right)10^{-5} \qquad [2.3]$$

with T and μ the temperature and dynamic viscosity of sea water respectively, expressed in deg C and centipoises ($g\ m^{-1}\ s^{-1}$) respectively. The tortuosity factor is calculated from the porosity as (Boudreau, 1997)

$$\theta^2 = 1 - 2ln(\phi) \qquad [2.4]$$

Implementing the above simplifications, one arrives at the simplified mass balance statement

$$D\left(\frac{\partial^2 C}{\partial x^2}\right) = R(x) \qquad [2.5]$$

This equation says that oxygen concentration observed in the pore water basically results from a balance between molecular diffusion and consumption.

2.2.3 The oxygen consumption rate

We applied two different kinetic rate laws to model the oxygen consumption rate $R(x)$, which is expressed per unit volume of pore water. The Bouldin model assumes that the oxygen consumption rate is constant over the oxygenated zone (Bouldin, 1968)

$$R(x) = \begin{cases} R_{\max} & for\, C > 0 \\ 0 & for\, C = 0 \end{cases} \qquad [2.6]$$

An alternative (and more realistic description) of sedimentary oxygen consumption is the Monod model, which explicitly accounts for rate limitation at low oxygen levels

$$R(x) = R_{\max}\frac{C}{C + K_s} \qquad [2.7]$$

The parameter $R_{\max}$ now denotes the maximum consumption rate of oxygen. In terms of model complexity this adds a second parameter, K_s, the half saturation constant for oxygen uptake. Both $R_{\max}$ and K_s are assumed to be constant with depth. The difference between the Monod model and the Bouldin model depends on the value of K_s. When $K_s \to 0$ the Monod rate law reduces to the Bouldin model.

2.2.4 Boundary conditions

Because oxygen distribution is modeled in 1D, there are 2 boundary conditions. The oxygen concentration at the SWI is kept at a constant value and is the same as the bottom water oxygen concentration (we ignore a diffusive boundary layer).

$$C(x)\big|_{x=0} = C_o \qquad [2.8]$$

The flux at the lower boundary of the model domain (x=L) should vanish

$$J\big|_{x=L} = -\phi D\left.\frac{\partial C}{\partial x}\right|_{x=L} = 0 \qquad [2.9]$$

Typically, oxygen concentration will also vanish at this depth L.

2.2.5 The diffusive oxygen uptake

The diffusive oxygen uptake (DOU) is formally defined as the flux of oxygen into the sediment across the sediment-water interface (SWI)

$$DOU = -\phi D \left.\frac{\partial C}{\partial x}\right|_{x=0} \qquad [2.10]$$

The total oxygen consumption within the sediment is defined as

$$R_{TOT} = \int_0^L \phi R(x)\,dx \qquad [2.11]$$

The mass balance for oxygen over the whole sediment domain is obtained by integration of [2.1] over the layer L (Figure 14).

$$\frac{d}{dt}\left[\int_0^L \phi C(x)\,dx\right] = J_{in} - J_{out} - R_{TOT} \qquad [2.12]$$

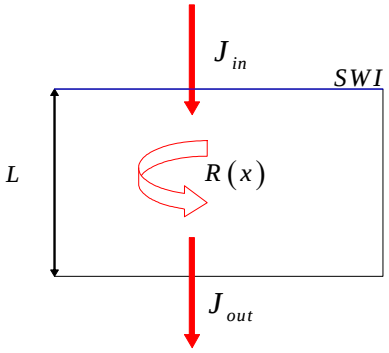

Figure 14. Input and output fluxes across the main sediment boundaries in 1-D model domain geometry.

Because we assume a steady state, and there is no flux of oxygen to deeper sediment layers ($J_{out} = 0$ - see boundary conditions above), the DOU ($= J_{in}$) must equal the total oxygen consumption within the sediment

$$DOU = R_{TOT} \qquad [2.13]$$

In our numerical simulations, this condition was verified to ensure the consistency of the numerical calculations.

2.2.6 Oxygen penetration depth

The oxygen penetration depth (OPD), represented by the symbol δ, is formally defined as the depth where the oxygen concentration (C) diminishes to zero. In reality however, one has to account for the accuracy and precision of the sensors that generate the oxygen profiles. Current operational practice is to use a threshold oxygen concentration of 2 μmol L^{-1} for micro-electrodes under field conditions (R. Glud pers. comm.). Oxygen concentrations below this level are considered to be zero (anoxic signal). Here, we used this same detection limit to calculate the OPD.

$$C(x)\big|_{x=\delta} = 2\ \mu\text{mol L}^{-1} \qquad [2.14]$$

Once the oxygen profile $C(x)$ is calculated, the penetration depth δ can be solved from equation [2.14] via a non-linear root finding procedure.

2.2.7 Bouldin model: analytical solution

The analytical solution to the Bouldin model is well known. The expressions for the oxygen concentration profile, oxygen penetration depth and the DOU are respectively (Revsbech et al., (1980);

$$C(x) = \frac{R_{\max}}{2D}\left(x^2 - 2x\sqrt{\frac{2DC_o}{R_{\max}}} + \frac{2DC_o}{R_{\max}} \right) = C_0\left(1 - \frac{x}{\delta}\right)^2 \qquad [2.15]$$

$$\delta = \sqrt{\frac{2DC_o}{R_{\max}}} \qquad [2.16]$$

$$DOU = \phi\sqrt{2C_o D R_{\max}} \qquad \text{`[2.17]}$$

The expression for the oxygen penetration depth [2.16] can be used to estimate the oxygen consumption rate $R_{\max}$ that is associated with a given oxygen penetration depth.

2.2.8 Monod model: numerical solution

The routine `tran.1D` from the R-package `ReacTran` was used to formulate and implement our Monod model over a 1D sediment finite difference grid created using the routine `setup.grid.1D`. The routine `setup.grid.1D` also in the R package `ReacTran` first subdivides the virtual sediment domain in to equal sediment layers, while `tran.1D` estimates the transport and flux terms over each of these sediment layers. The Monod model was then solved numerically under steady state conditions using the routine `steady.1D` from the R-package `rootSolve` to produce synthetic "perfect'' oxygen micro profiles (see chapter 3 for details). The oxygen concentrations are defined in the middle of the sediment layers. The use of the various R routines is shown in the R script below.

```
#=================================================================
# Setting grid for the model
grid <- setup.grid.1D(x.up=0,L=L.x,N=N.x)

# Defining the reactive transport model
monod.ddt <- function (time=0, y, parms=NULL, Rmax)
{
tran <- tran.1D(C=y,C.up =O2.BW,C.down=O2.low,dx=grid,VF = por.grid,
D = D.grid,full.check = FALSE, full.output = FALSE)$dC
reac <- -Rmax*y/(y+Ks)
ddt <- tran+reac
return(list(ddt=ddt))
}

# Steady state solution
monod <- function(Rmax)
{
O2.profile <- steady.1D(runif(N.x), func=monod.ddt, parms=NULL,
Rmax=Rmax, nspec=1, pos=TRUE)$y
dummy <- tran.1D(C=O2.profile.A, C.up =O2.BW, C.down=O2.low,
dx=grid, VF = por.grid, D = D.grid,full.check = FALSE, full.output =
FALSE)
depth <- grid$x.mid
flux.x.up <- t_fac*dummy$flux.up
return (list(x=depth, C=O2.profile.A,flux.x.up=flux.x.up))}
#=================================================================
```

2.2.9 Example application: Creating 1D oxygen profiles

The numerical routine described above could be used to numerically fit generated model synthetic O_2 profiles to sampled O_2 data profiles collected from the field. The parameter values used in the numerical routines, in this case must reflect values obtained from the sampling sites. Table 2.1 shows parameter values used in generating the numerical synthetic profile shown in Figure 15. The data O_2 profile was obtained from shallow sediments just outside the Nioo-knaw research centre in the Netherlands during winter. This example is presented to illustrate how generated synthetic O_2 profile numerically fits well with the real data profile and could be assumed to represent actual measurements obtained by micro electrodes.

Parameter	Value	Units
Temperature (T)	10	^{o}C
Salinity (S)	33	dimensionless
Pressure (P)	1.0	bar
Porosity (ϕ)	0.8	dimensionless
Oxygen consumption (R_{max})	5.12×10^{-5}	μmol L^{-1} s^{-1}
Effective diffusion coefficient (D)	$1.56\ 10^{-9}$	m^2 s^{-1}
Half saturation constant (K_s)	5	μmol L^{-1}
SWI concentration (C_o)	235	μmol L^{-1}
Threshold oxygen concentration	2	μmol L^{-1}

Table 2.1 Application of 1D numerical solution procedure. Parameter values used in generating synthetic O_2 profile

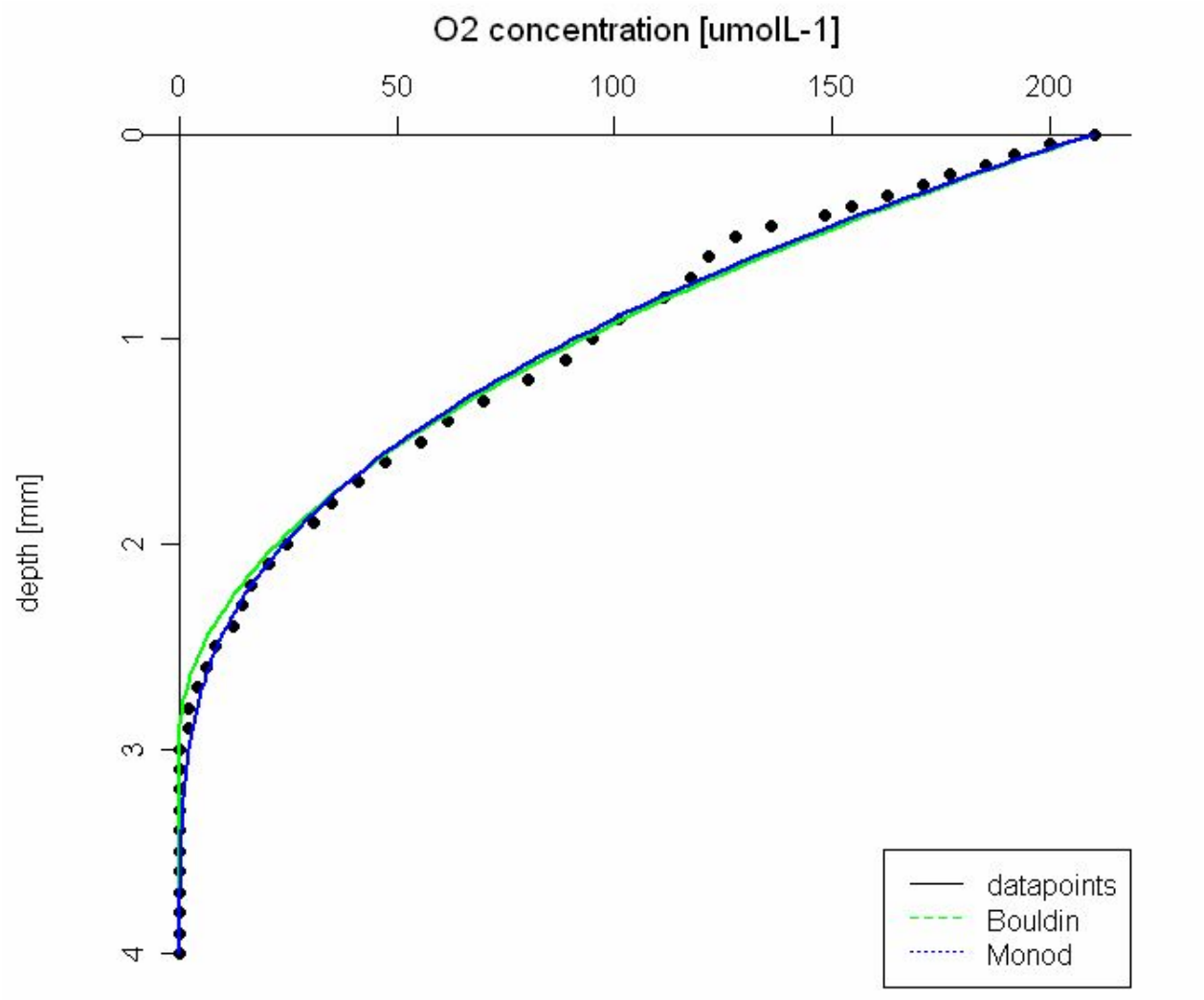

Figure 15. Generated numerical profile fits well with experimental data profile

The initial curvature at the SWI is similar for both the numerical profiles and the experimental data profile and as such the linear O_2 gradient will be the same for all three profiles. However at deeper depths Bouldin numerical profile deviates from the Monod profile because of different underlying assumptions of O_2 consumption within the oxic zone (already described above).

2.3 2D reactive transport model

2.3.1 Model domain geometry

In a two-dimensional (2D) reactive transport model description, the oxygen transport is modeled both in the x (vertical depth coordinates) and y (horizontal coordinates) directions. The sediment is approximated as a rectangular box of length L_x and width L_y (Figure 16). This box is subdivided into a $N_x \mathrm{x} N_y$ matrix of rectangular grid cells. The quantities $\left(\Delta x_i, \Delta y_j\right)$ denote the size (length and width) of the $i-th$ cell in the x-direction and the $j-th$ cell in the y direction respectively. Note that in either direction the grid cells do not have to be equidistant. Typically, we used an equidistant grid in the y-direction and a grid in the x-direction with higher resolution near the sediment water interface.

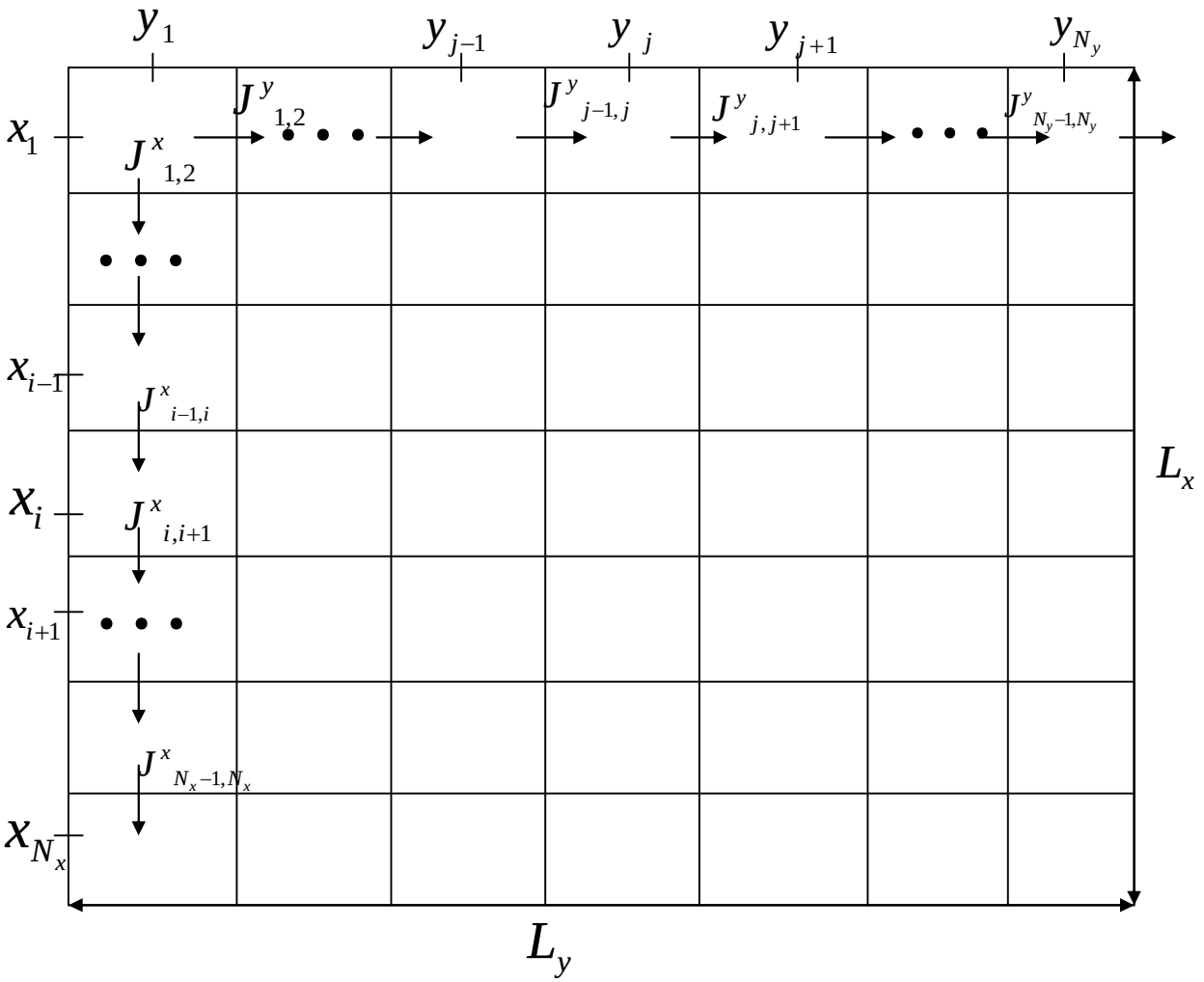

Figure 16. Finite difference grid indicating the sediment depth and horizontal distance coordinates. Fluxes are defined on the box interfaces.

2.3.2 Mass balance statement

In two dimensions, the general mass balance statement is given by (Boudreau, 1997)

$$\frac{\partial(\phi C)}{\partial t} = -\frac{\partial J_x}{\partial x} - \frac{\partial J_y}{\partial y} - \phi R(x,y) - \phi I(x,y) \qquad [2.18]$$

where the fluxes J_x and J_y are the fluxes at the horizontal and vertical interfaces of the model domain respectively. Adopting the same assumptions as in the 1D model, the 2D steady state mass balance statement governing the oxygen distribution within the sediment is given by:

$$D\left(\frac{\partial^2 C}{\partial x^2} + \frac{\partial^2 C}{\partial y^2}\right) = R(x,y) \qquad [2.19]$$

where D is the effective diffusion coefficient of oxygen, and $R(x,y)$ is the oxygen consumption rate per unit volume of pore water.

2.3.3 Oxygen consumption rate

The oxygen consumption rate $R(x,y)$ needs to be defined over the two-dimensional sediment domain. Two different cases were investigated: a homogeneous and a heterogeneous sediment. The baseline case assumed perfectly homogeneous sediment. Here, oxygen consumption rate is implemented via the classical Monod dependence,

$$R(x,y) = R_{base}\frac{C(x,y)}{C(x,y)+K_s} \qquad [2.20]$$

In a second case, we evaluated models that have a spatially dependent oxygen consumption rate. In particular, we investigated the presence of so-called hotspots, that is, localized zones with increased oxygen consumption. To this end, the following expression was used

$$R(x,y) = \left(R_{base} + \sum_{h=1}^{n} R_h(x,y)\right)\frac{C(x,y)}{C(x,y)+K_s} \qquad [2.21]$$

The total oxygen consumption is hence composed of a baseline rate R_{base}, and added to it, the increased consumption R_h at the h-th hotspot. This hotspot consumption is modeled on the basis of a normal distribution by

$$R_h(x,y) = R_{\max}^h \exp\left[-\frac{1}{2}\left(\frac{x-x_h}{\sigma_{x,h}}\right)^2 - \frac{1}{2}\left(\frac{y-y_h}{\sigma_{y,h}}\right)^2\right] \qquad [2.22]$$

where $R_{\max}^h$ is the maximal oxygen consumption rate at the center of a hotspot, the coordinates (x_h, y_h) denote the location of centre of the h-th hotspot, and $(\sigma_{x,h}, \sigma_{y,h})$ denote the width of the hotspot in the x and y direction respectively.

2.3.4 Boundary conditions

We need to specify 4 boundary conditions i.e., one on each side of the rectangular model domain (Figure 17).

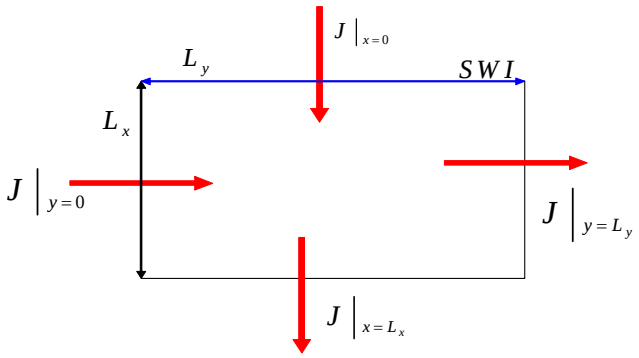

Figure 17. Boundary fluxes located each side of the rectangular box geometry

The oxygen concentration at the SWI is kept at a constant value and is the same as the bottom water oxygen concentration

$$C(x,y)\big|_{x=0} = C_o \qquad [2.23]$$

The left and right interfaces are considered closed, and so the flux is considered equal to zero

$$J\big|_{y=0} = -D\phi \left.\frac{\partial C}{\partial y}\right|_{y=0} = 0 \qquad [2.24]$$

$$J\big|_{y=L_y} = -D\phi \left.\frac{\partial C}{\partial y}\right|_{y=L_y} = 0 \qquad [2.25]$$

The flux at the lower boundary of the model domain is also considered to be equal to zero

$$J\big|_{x=L_x} = -D\phi \left.\frac{\partial C}{\partial x}\right|_{x=L_x} = 0 \qquad [2.26]$$

2.3.5 The Diffusive Oxygen Uptake

The total oxygen consumption R_{TOT} is the integral of the oxygen consumption rate over the whole sediment domain

$$R_{TOT} = \int_0^{L_y}\int_0^{L_x} \phi R(x,y)\,dxdy \qquad [2.27]$$

The average oxygen consumption within the sediment is then given by

$$R_{AVG} = \frac{1}{L_x L_y} R_{TOT} \qquad [2.28]$$

The average fluxes through a particular plane in the x and y direction are given by;

$$\langle J_x \rangle(x) = \frac{1}{L_y}\int_0^{L_y} J_x(x,y)\,dy = \frac{1}{L_y}\sum_{j=1}^{N_y} J^x_{j-1,j}\Delta y_j \qquad [2.29]$$

$$\langle J_y \rangle(y) = \frac{1}{L_x}\int_0^{L_x} J_y(x,y)\,dx = \frac{1}{L_x}\sum_{i=1}^{N_x} J^y_{i-1,i}\Delta x_i \qquad [2.30]$$

The average fluxes at the left, right and lower boundaries of the model domain are equal to zero (see boundary conditions). The average sum of all the fluxes at the SWI along the distance coordinate L_y is the average DOU.

$$\langle DOU \rangle = \langle J_x \rangle(x=0) \qquad [2.31]$$

The mass balance for oxygen over the whole sediment domain is obtained by integration of [2.18] over the model domain (L_x, L_y).

$$\frac{\partial}{\partial t}\left(\int_0^{L_y}\int_0^{L_x} \phi C(x,y)\right)dxdy = L_y\langle J|_{x=0}\rangle - L_y\langle J|_{x=L_x}\rangle + L_x\langle J|_{y=0}\rangle - L_x\langle J|_{y=L_y}\rangle - R_{TOT} - I_{TOT} \qquad [2.32]$$

Because of the steady state, no irrigation, and closed boundaries (left, right and down), this immediately reduces to

$$\langle DOU \rangle = \frac{1}{L_y} R_{TOT} = L_x R_{AVG} \qquad [2.33]$$

The average DOU therefore should scale with the total oxygen consumption.

2.3.6 Oxygen penetration depth

The same assumptions as in the 1D model were adopted in the 2D model.

$C(x,y)\big|_{x=\delta} = 2\ \mu\text{mol L}^{-1}$

2.3.7 Numerical solution procedure

`Setup.grid.2D` in the R package `ReacTran` was used to create a rectangular finite difference grid over the model domain. The 2D Monod reactive-transport model was implemented over this grid using the numerical routine `tran.2D` from `ReacTran`. This routine estimates the transport terms J_x and J_y over the sediment grid created by `setup.grid.2D`. The Monod model was then solved numerically for steady state using `steady.2D` from the package `rootSolve`. This produced 2D oxygen distribution maps, which essentially consist of a sequence of neighboring 1D vertical O_2 profiles. The use of the various R routines is shown in the R script below.

```
#=================================================================

# Model geometry: setting up the grid
x.grid <- setup.grid.1D(x.up=0,L=L.x,N=N.x)
y.grid <- setup.grid.1D(x.up=0,L=L.y,N=N.y)
grid2D <- setup.grid.2D(x.grid,y.grid)

# Defining the reactive transport model
model_A <- function (time,y,parms=NULL)
{
  C <- matrix(data=y,nrow=grid2D$x.N,ncol=grid2D$y.N)
  tran <- tran.2D(full.check=TRUE,full.output=TRUE,
  C=C,D.x=D.O2,D.y=D.O2,v.x=0,
  v.y=0,VF.x=Por,VF.y=Por,grid=grid2D,C.x.up=O2_BW)$dC
  reac <- -C/(C+Ks)*(Rmax + O2.cons(grid2D,R))
  dydt <- as.vector(tran+reac)
  return(list(dydt = dydt))
}

# Definition of the oxygen consumption at hotspots
# modified BND function
mod.BND <- function(x,y,mu.x,mu.y,sd.x,sd.y)
{
z <- (x-mu.x)^2/(sd.x^2) + (y-mu.y)^2/(sd.y^2)
return(exp(-z/2))
}
```

2.3.8 Example application: Creating 2D oxygen distribution maps

Figure 18 is an example of a 2D oxygen distribution map with two hotspots created using the 2D numerical procedure described above. The parameter values used in creating the hotspots are shown in Table 2.2.

Parameter	Value	Units
Temperature (T)	10	^{o}C
Salinity (S)	30	dimensionless
Pressure (P)	150	bar
Porosity (ϕ)	0.8	dimensionless
Baseline O_2 consumption (R_{base})	5.0×10^{-4}	μmol L^{-1} s^{-1}
Hotspots O_2 consumption (R_h)	25×10^{-4}	μmol L^{-1} s^{-1}
Effective diffusion coefficient (D)	$1.32\ 10^{-9}$	m^2 s^{-1}
Half saturation constant (K_s)	5	μmol L^{-1}
SWI concentration (C_o)	200	μmol L^{-1}
Threshold oxygen concentration	2	μmol L^{-1}

Table 2.2 Parameter values used in generating 2D O_2 distribution maps. O_2 consumption in the two hotspots was the same.

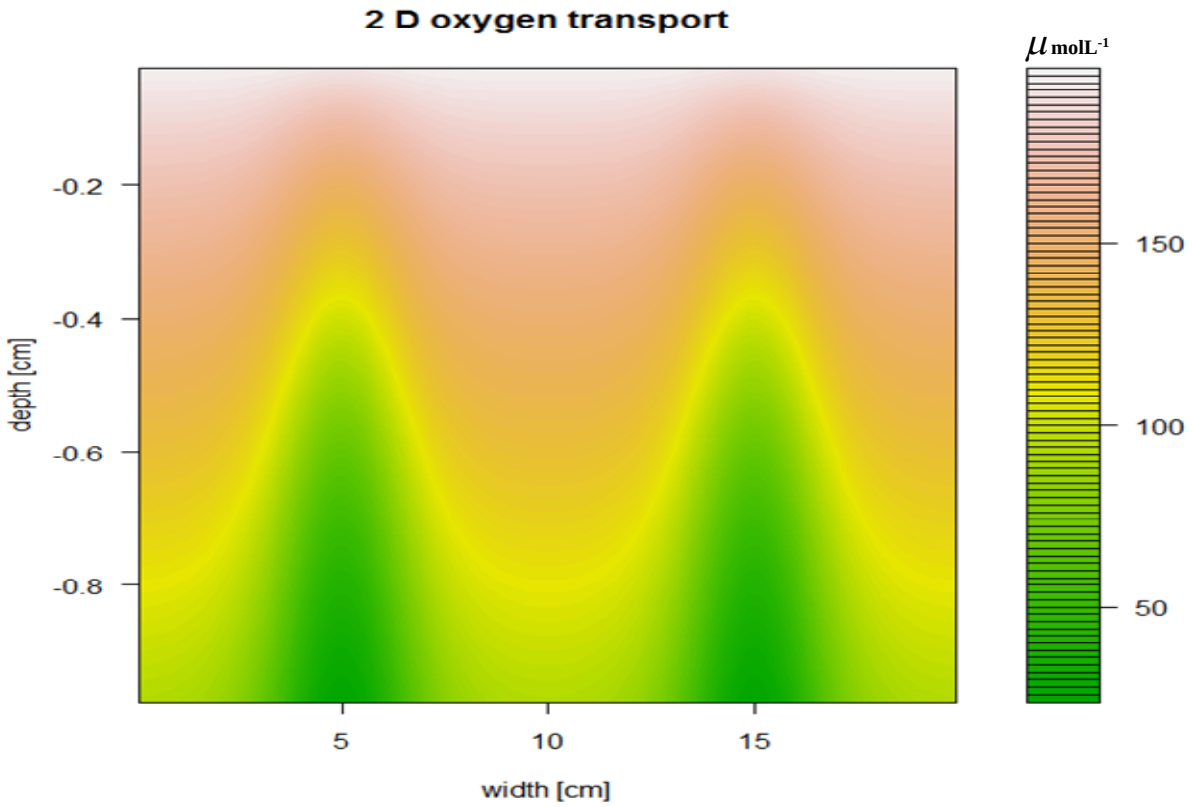

Figure 18. 2D oxygen distribution map with two hotspots created using the numerical procedure described above. The Gaussian shaped gold glowing structures represent the individual hotspots. Note the change in O_2 distribution at the hotspots.

CHAPTER 3.

O_2 MICROPROFILING AND DOU ESTIMATION IN HOMOGENEOUS SEDIMENTS

3.1 Introduction

In this chapter, we present a theoretical investigation of potential biases in the DOU estimation from oxygen microprofiles. To this end, we first created synthetic O_2 profiles using the numerical routines described under 1D modeling methods in Chapter 2. The DOU calculated by the numerical routines was assumed to represent the "true'' DOU of the virtual sediment. Subsequently, sampling procedures of real sensors were mimicked and used to virtually "sample" these synthetic O_2 profiles in order to generate synthetic O_2 "data" profiles. From these data a "sampled" DOU value was estimated. A sensitivity analysis was done to investigate the systematic bias between the "true" DOU and the "sampled" DOU under different sensor sampling procedures.

3.2 Investigating Sensor's bias

3.2.1 Creation of synthetic "perfect" O_2 profiles

The routine `setup.grid.1D` in the R package ReacTran was used to create a virtual 1D sediment at a very high resolution (very many thin sediment layers). The geometry specifications of this virtual sediment are shown in Table 3.1.

Sediment geometry	*Values*	*units*
L	50	mm
N	50000	
Δx	1	μm

Table 3.1 Grid specifications of created virtual 1D sediment.

Using this very fine grid, synthetic "perfect'' O_2 profiles were created for a range of sediments with OPD's ranging from 1-50 mm (Figure 19 shows a number of examples). The parameter values used in generating these synthetic O_2 profiles are shown in the Table 3.2. All parameters were kept constant except the oxygen consumption rates. The oxygen consumption rates were varied by selecting a particular value for the OPD and calculating the associated

oxygen consumption rate using the Bouldin formula ($R_{\max} = (2C_o D)/\delta^2$). The resulting microprofiles on this high resolution grid can be regarded to represent measurements obtained by a Perfect Sensor sampling sediments with different oxygen consumption rates at a step size and sensing volume the same as very small grid cell thickness of 1 μm. Obviously, in any real sediment setting such a high sampling resolution is not achievable.

Parameters	*Values*	*Units*
SWI concentration (C_o)	50	μmol L^{-1}
Temperature (T)	10	deg C
Pressure (P)	150	bar
Salinity (S)	30	dimensionless
Porosity (ϕ)	0.91	dimensionless
Effective diffusion coefficient (D)	1.33e-09	m^2 s^{-1}
Half saturation constant (K_s)	5	μmol L^{-1}

Table 3.2 Parameter values used in generating a "perfect synthetic oxygen profile" from a homogeneous virtual sediment

.

The “true” DOU value of these “perfect’’ O_2 profiles were obtained by extracting the flux across the upstream boundary of the model domain as calculated by the numerical routine `tran.1D`. These DOU values were hence assumed to represent the best DOU value one can possibly get from analyzing the synthetic “perfect’’ O_2 profiles. The true DOU’s of the virtual sediments analyzed are shown in the table below.

δ *(mm)*	R_{max} *(mmol m^{-3} s^{-1})*	*‘‘True DOU’’ (mmol m^{-2} d^{-1})*
1	0.132	9.12
2	0.0332	4.56
4	0.0083	2.28
5	0.0053	1.82
8	0.0021	1.14
16	0.0005	0.57
32	0.0001	0.22
50	5.3×10^{-5}	0.094

Table 3.3 True DOU's for selected virtual sediments with different oxygen consumption rates.

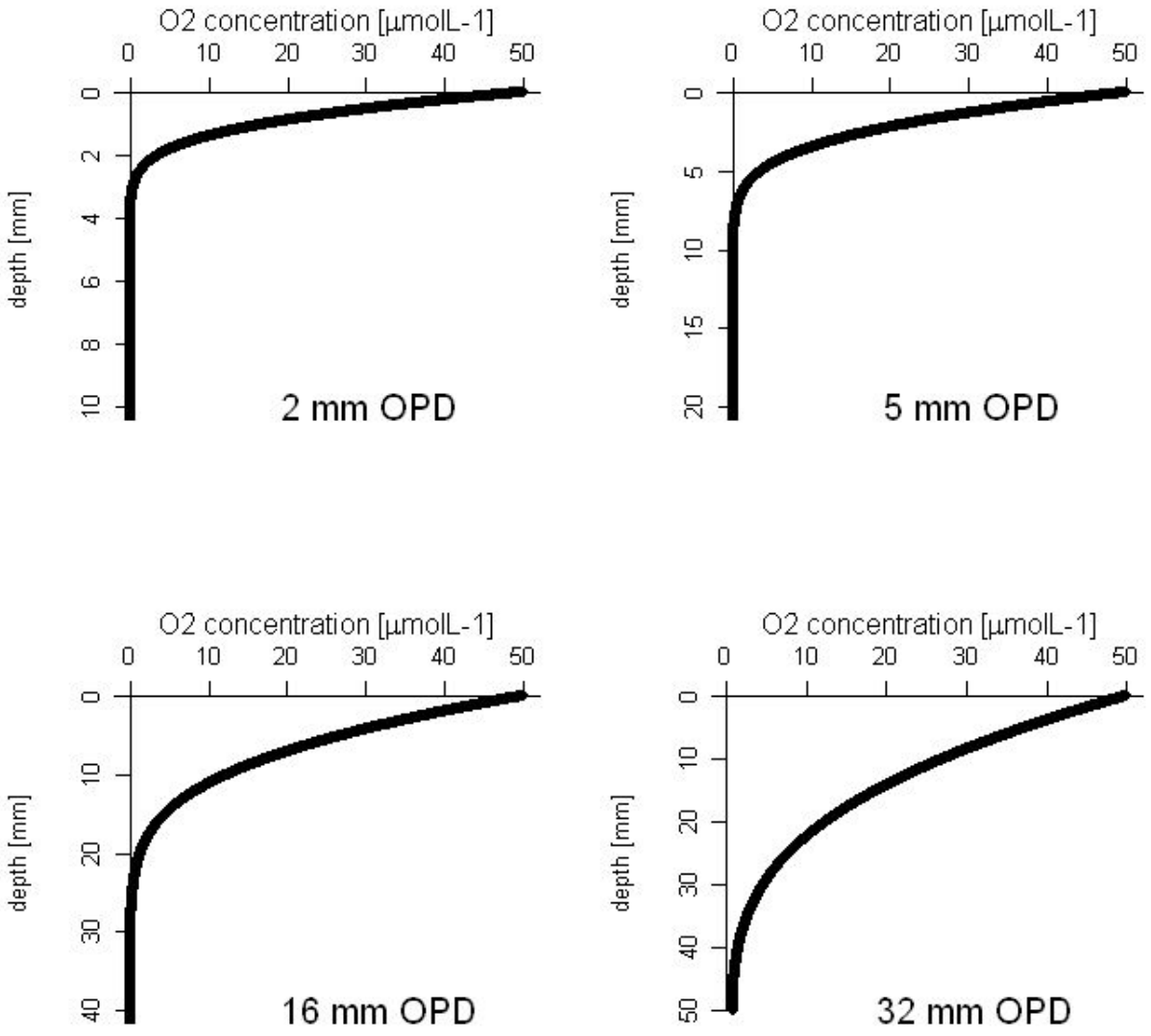

Figure 19. Perfect O_2 profiles as would be measured by a Perfect Sensor.

3.2.2 Virtual sampling of the "perfect" O_2 profiles

The perfect O_2 micro profiles were sampled to generate synthetic "data'' O_2 profiles by mimicking the measurement procedure of a real O_2 microelectrode sensor. The sample profile as measured by a real sensor depends on (1) the sensing volume of the microelectrode and (2) the step size of the micromanipulator.

The “sensing volume” of a micro-electrode sensor is defined as the sediment volume that contributes to the sensor signal. In a micro-electrode, the O_2 flux towards the sensor tip is controlled by radial diffusion (Reimers, 2007). Therefore, the sensing volume can be approximated by a diffusion sphere with a diameter b (Figure 20). In general, the diameter of the sensing volume is estimated to be twice the diameter a of the sensor’s outer tip. This is also the spatial resolution of the sensor (Unisense, 2008).

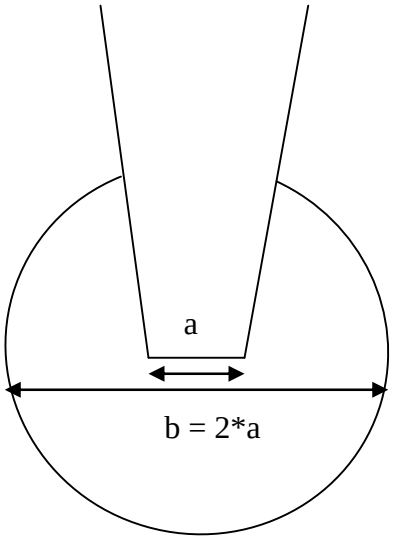

Figure 20. The sensor provides an output signal that integrates over the diffusion sphere. Sensor diameter (a), diameter of the diffusion sphere (b).

The step size of the micromanipulator determines the depth resolution of the sampled O_2 profile. This step size d (Figure 21) is hence the distance between two sampling points. The step size d should be larger than the diameter of the sensing volume in order to avoid overlapping diffusion spheres. In practice, this is nearly always the case.

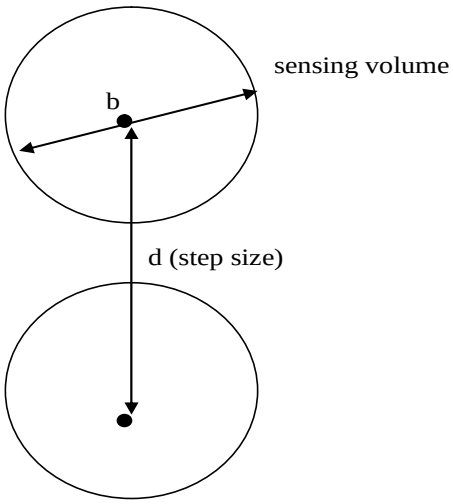

Figure 21. Sensor’s micro manipulator step size (d) not the same as sensing volume.

The sampled “data” profiles were generated by suitably averaging the oxygen concentrations of the perfect O_2 micro profiles over the sensing volumes (diffusion sphere). This procedure mimics the sampling procedure of a real sensor. Examples of sampled O_2 data micro profiles obtained by this procedure are shown in Figure 22.

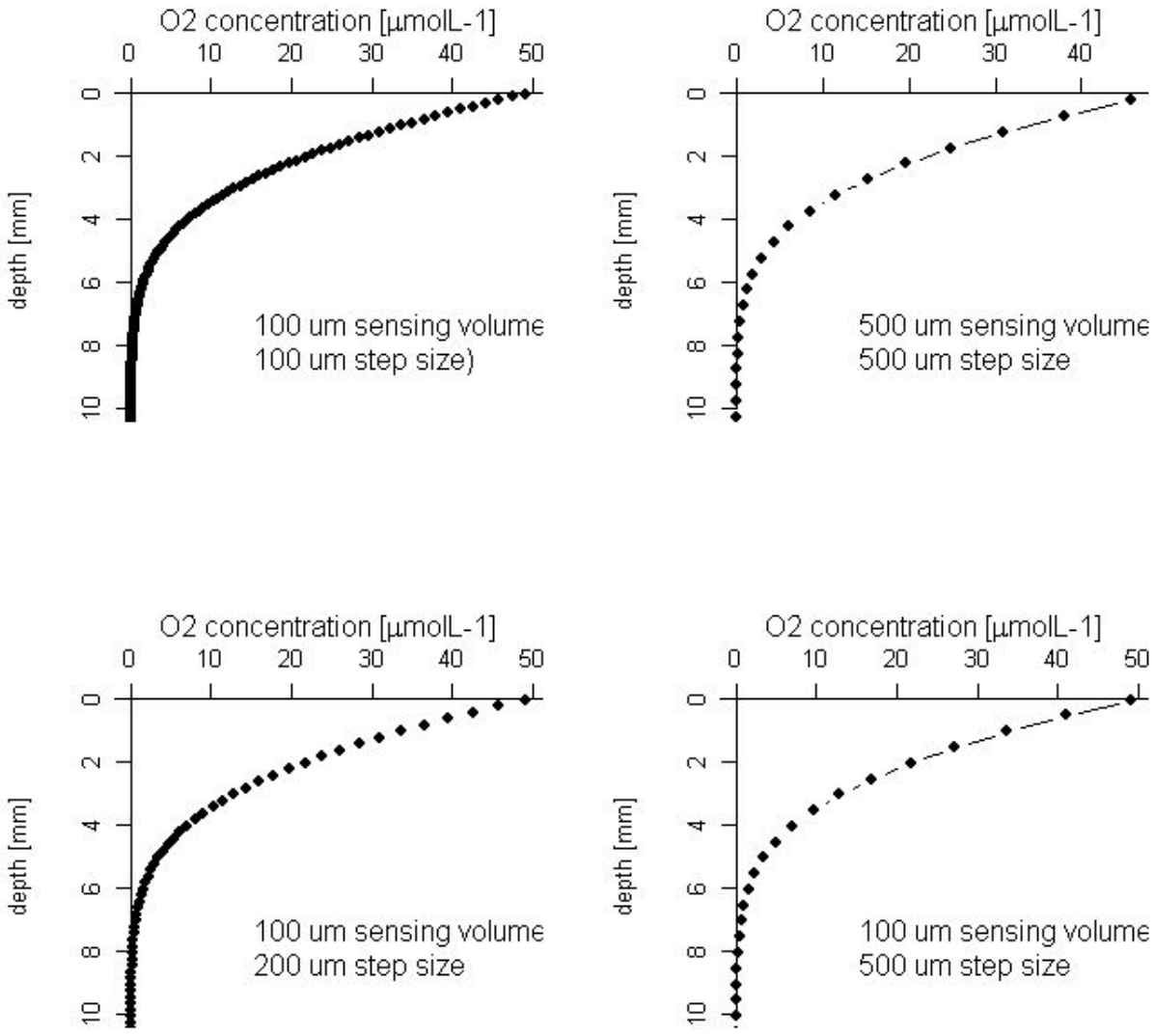

Figure 22. Different “sample” O_2 profiles generated from the same “perfect” profile mimicking the sampling procedure of different sensors (with different step size and sensing volume).

3.2.3 Estimating the DOU from the sampled O_2 profile

The DOU method investigated here is based on fitting the oxygen concentration gradient in the pore water near the sediment-water interface. The least squares method was used to linearly fit a line (Figure 23) across the sampled micro profiles (depth coordinates are at the mid points of the grid cells). The resulting fit becomes

$$C(x) = xm + c \qquad [3.1]$$

where m is slope and c is the intercept of the fitted trend line. The fit depends on the number of data points $\left(n_{dp}\right)$ included in the model. Two different values for n_{dp} were tested in the least square fitting two and five data points.

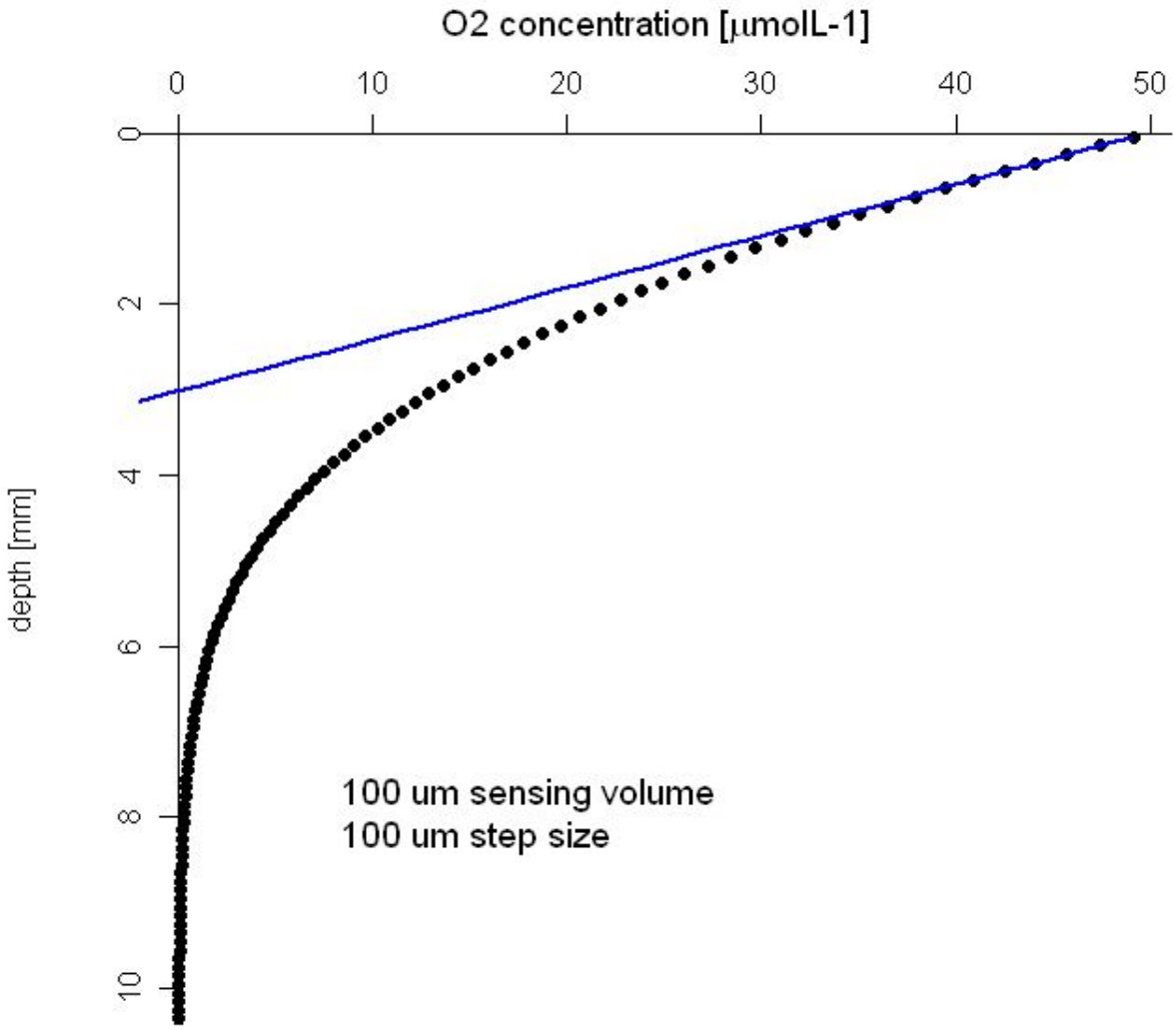

Figure 23. Sampled O_2 data profile with the linear best fit line used in estimating the DOU. In this case we used the first five data points.

Based on the value of m, the "sampled" DOU, can be calculated as

$$DOU = -\phi Dm = -\phi D \left. \frac{\partial C}{\partial x} \right|_{x=1,\ldots,n_{dp}} \quad [3.2]$$

3.2.4 Sensitivity analysis

Given the above, the sample DOU estimate will depend on three main parameters:

- The sensing volume of the micro sensor
- The number of points sampled within the oxic zone of the sediment by the sensor (which is dependent on both the micro-manipulator step size and the OPD)
- The number of sample points (n_{dp}) included in the DOU fit

A sensitivity analysis was performed for each of these parameters. Each time we determined the bias between the "true'' DOU obtained from the perfect O_2 profiles and the sample DOU obtained from the virtual DOU estimation.

Sensitivity on the sensing volume (coarse vs. fine sensors)

The sensitivity on the sensing volume was assessed under two different conditions. In the first case, sensors with sensing volumes of 10 μ m, 50 μ m, 100 μ m , 200 μ m , 300 μ m , 500 μ m , 800 μ m and 1000 μ m were mimicked and used to sample the 5 mm OPD Perfect O_2 profile. The micro manipulator step size was kept the same as the sensor's sensing volumes. In the second case, we mimicked sensors with the same micro-manipulator step size (100 μ m) but different sensing volumes (1 μ m, 5 μ m, 10 μ m, 20 μ m, 30 μ m, 40 μ m, 50 μ m, 60 μ m, 70 μ m, 80 μ m, 90 μ m, 100 μ m). The range of sensing volumes was chosen because microelectrodes used in benthic research typically have tip diameters in the range of 1-50 μ m and often sample at typical step size of 100 μ m.

Sensitivity on the number of sampling points within the oxic zone.

The number of points (n) sampled within the oxic zone can be calculated as

$$n = \frac{\delta}{d} \quad [3.3]$$

The sensitivity on the number of sampling points will depend on the both the OPD and the step size. Both were investigated. In a first case, the number of sampling points within the oxic zone was changed for a fixed OPD but changing the step size. A fixed sensing volume of 100 μm was used as commonly used in actual field sensor measurements. The sediment reactivity was set as to have a 5 mm OPD. The micro manipulator step size was varied as $(120\mu m, 150\mu m, 200\mu m, 300\mu m, 500\mu m, 800\mu m, 1000\mu m)$.

In a second case, the number of sampling points within the oxic zone was changed for a fixed step size but different OPD's. Again a fixed sensing volume of 100 μm was used (mimicking a typical oxygen sensor with a 50 μm outer tip diameter). The step size was fixed at 100 μm.

Sensitivity on the number of sample points included in the DOU fit

To investigate this sensitivity two conventional methods that is, gradient of first two sample points and first five sample points were used to estimate the sample DOU's of the O_2 profile generated from the sensitivity analysis described above.

3.2.5 Sensors uncertainties

An O_2 sensor doesn't measure the O_2 flux at a particular point in space but integrates the O_2 flux over a diffusion sphere. This therefore means that there is a certain amount of uncertainty in the measurement procedure of sensors at each profiling depth. This was investigated as follows:

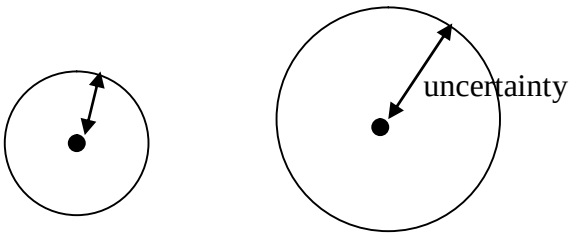

Figure 24. Measured O_2 flux uncertainty at each profiling depth. The uncertainty depends on the sensor sensing volume.

We calculated the O_2 signal uncertainty for all the mimicked sensors at each profiling depth. From the profiling depth uncertainty we estimated the overall uncertainty for a given mimicked sensor.

3.3 Results

3.3.1. Sensing volume the same as micro manipulator step size

The two fitting approaches (two points gradient vs. five points gradient) used in calculating the sample DOU showed considerable bias (Figure 25) in estimating the true DOU when the sensing volume is the same as the step size. The results are summarized in Table 3.4.

Tip diameter μ *m*	*Sensing volume* μ *m*	*Step size* μ *m*	*n*	*Two Point*		*Five Point*	
				DOU	*% bias*	*DOU*	*% bias*
0.5	1	1	5000	1.823	0.00	1.823	0.00
2.5	5	5	1000	1.821	0.10	1.818	0.26
5	10	10	500	1.819	0.21	1.814	0.52
25	50	50	100	1.804	1.04	1.776	2.60
50	**100**	**100**	**50**	**1.785**	**2.08**	**1.728**	**5.19**
100	**200**	**200**	**25**	**1.747**	**4.15**	**1.635**	**10.3**
150	300	300	17	1.710	6.22	1.543	15.4
250	500	500	10	1.635	10.3	1.362	25.3
400	800	800	6	1.524	16.4	1.108	39.2
500	1000	1000	5	1.451	20.4	0.952	47.8

Table 3.4 DOU (mmol m^{-2} d^{-1}) calculated from micro profiles (OPD=5 mm) obtained using mimicked oxygen sensors with different sensing volumes (spatial resolution). Micro manipulator step depths the same as sensor's spatial resolution. The first row represents the Perfect Sensor. Typical Clark microelectrodes are given in bold.

The sampled DOU deviates more strongly from the True DOU with increasing sensing volume. At very small tip diameters (1-5 μ m) the True DOU is approached. There is a strong correlation ($r^2 = 0.998$) between the sample DOU and its sensing volumes/step size. Typical micro electrodes with a tip diameter of 50-100 μ m showed a 5-10 % bias in estimating the True DOU using the five-point gradient method. Over the whole range, the bias in the five point DOU fit is approximately twice that of the two point DOU fit (Figure 25).

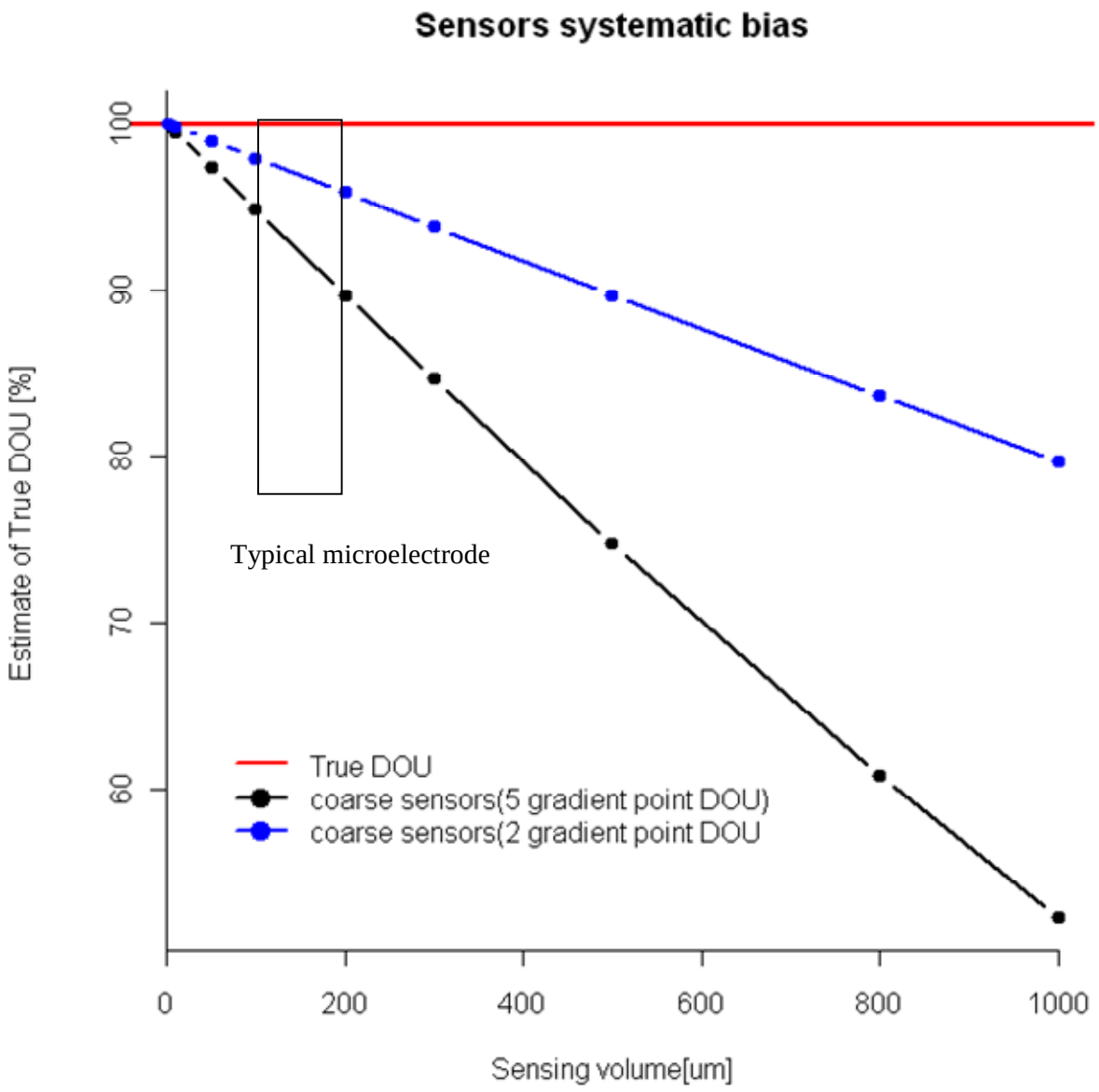

Figure 25. Estimating true DOU using sensors with different sensing volumes. Micro manipulator step size was the same as the individual sensor's sensing volume.

3.3.2 Sensitivity on the sensing volume

The sensing volume has little influence on the systematic bias between sampled DOU and True DOU, which is small compared to the case above in which the step size was the same as the sensing volume (Table 3.5 - Figure 26). When changing the sensing volume over the range from 1 µm up to 100 µm the bias only changes by 2 %.

Tip diameter µ m	*Sensing volume µ m*	*Step size µ m*	*n*	*Two Point*		*Five Point*	
				DOU	*% bias*	*DOU*	*% bias*
0.5	1	100	5000	1.823	0.00	1.823	0.00
0.5	1	100	50	1.804	1.05	1.747	4.16
2.5	5	100	50	1.803	1.09	1.746	4.20
5	10	100	50	1.802	1.14	1.745	4.26
10	20	100	50	1.800	1.25	1.743	4.36
15	30	100	50	1.798	1.35	1.742	4.46
20	40	100	50	1.796	1.46	1.740	4.57
25	50	100	50	1.795	1.56	1.738	4.67
30	60	100	50	1.793	1.66	1.736	4.77
35	70	100	50	1.791	1.77	1.734	4.88
40	80	100	50	1.789	1.87	1.732	4.98
45	90	100	50	1.787	1.98	1.730	5.08
50	100	100	50	1.785	2.08	1.728	5.19

Table 3.5 DOU (mmol m^{-2} d^{-1}) calculated from micro profiles (OPD = 5 mm) obtained using mimicked oxygen sensors with different sensing volumes (spatial resolution). Micro manipulator step depths was the same in all cases.

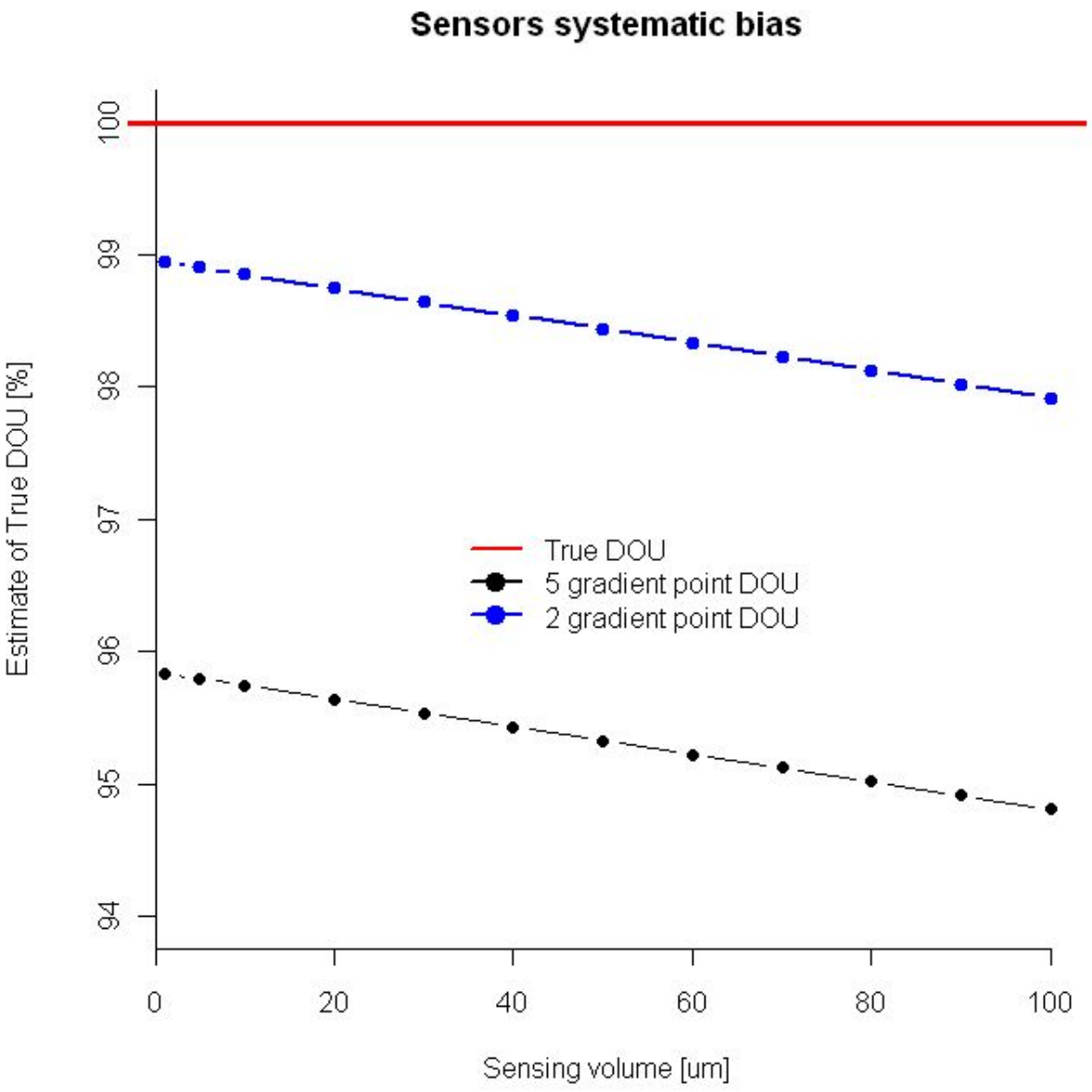

Figure 26. Systematic bias of different sensors in estimating the true DOU. Micro-manipulator step size in all cases was the same (100 μ m).

3.3.3 Sensitivity to the micro manipulator step size

The bias of the five point DOU fitting method was approximately three times that of the two gradient point method. This is shown in Table 3.6 and Figure 27. The bias of typically used O_2 microelectrodes (50 μm tip diameter) becomes very large as the step depths are increased.

Tip diameter μm	*Sensing volume* μm	*Step size* μm	*n*	*Two Point*		*Five Point*	
				DOU	*% bias*	*DOU*	*% bias*
0.5	1	1	5000	1.823	0.00	1.823	0.00
50	100	100	50	1.785	2.08	1.728	5.19
50	100	120	42	1.781	2.29	1.713	6.01
50	100	150	33	1.776	2.60	1.691	7.25
50	100	200	25	1.766	3.12	1.653	9.29
50	100	250	20	1.757	3.64	1.616	11.3
50	100	300	17	1.747	4.15	1.580	13.4
50	100	500	10	1.710	6.22	1.434	21.3
50	100	800	6	1.654	9.29	1.226	32.7
50	100	1000	5	1.617	11.3	1.097	39.8

Table 3.6 DOU (mmol m^{-2} d^{-1}) calculated from micro profiles obtained using a 50 μmm tip diameter oxygen sensor with different micro manipulator step depths

In Figure 27 the deviation from the True DOU with changing micro manipulator size depths is plotted.

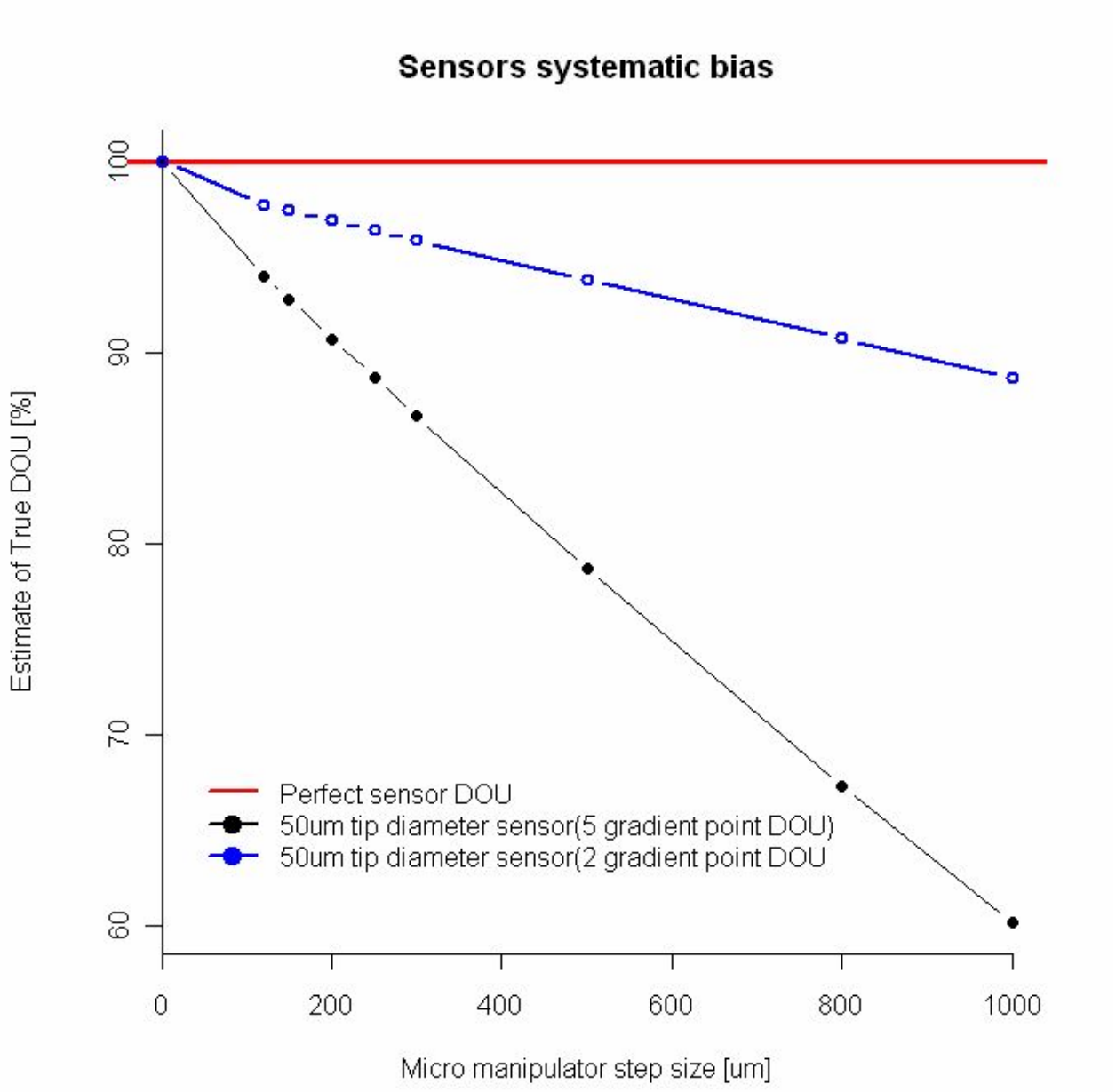

Figure 27. Estimating "true'' DOU using typical 1-50 μ m outer tip diameter microelectrode with different micro-manipulator step size.

3.3.4 Sensitivity to the OPD

The bias of typical microelectrode reduces significantly at large OPD's and as such the estimated DOU approaches the True DOU. This is illustrated in figure 28 below.

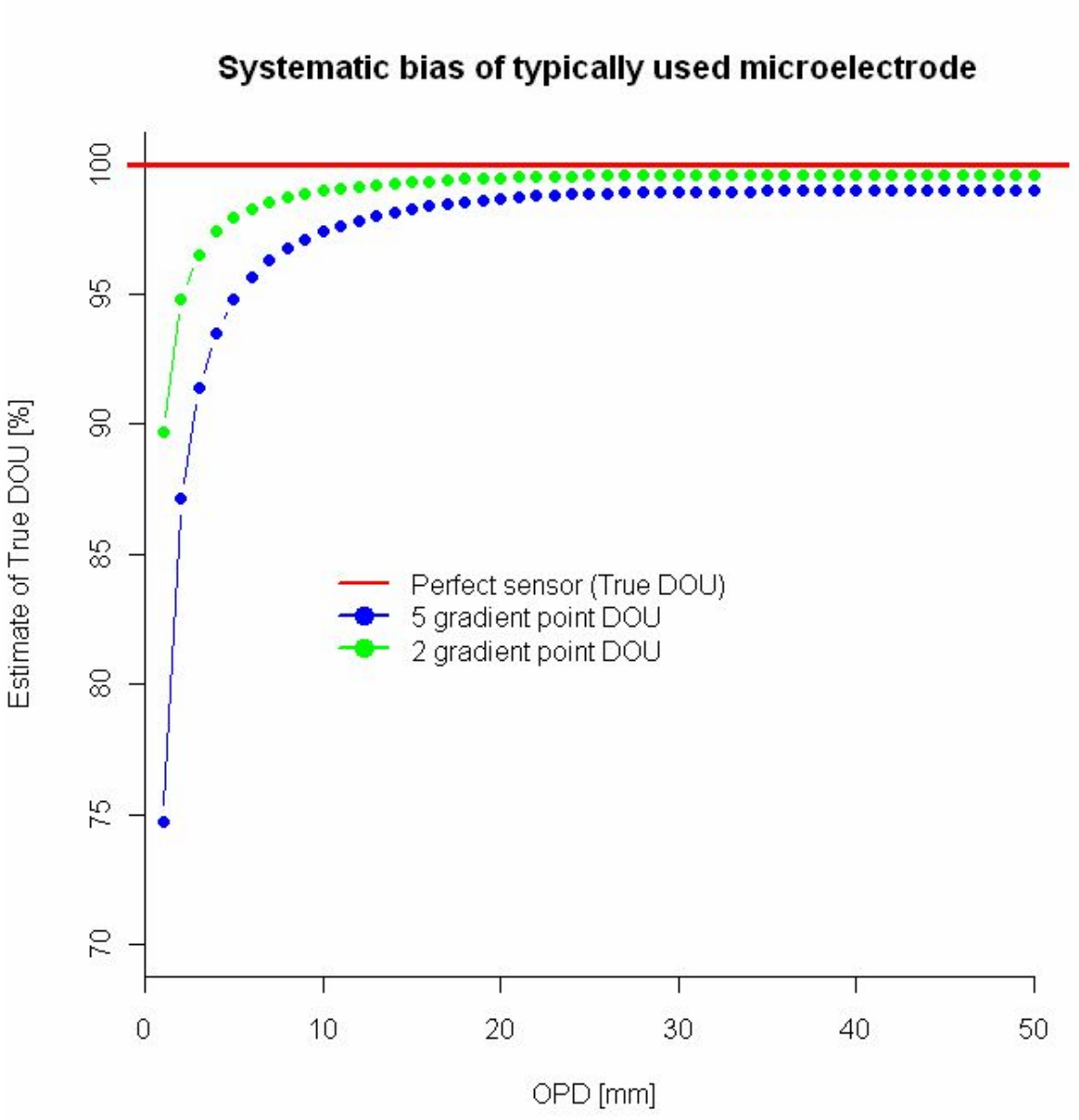

Figure 28. Estimated bias of typical 1-50 μ m outer tip diameter microelectrode sampling virtual sediments with different OPD's with a step size of 100 μ m

3.4 Sensors uncertainties

The O_2 signal uncertainty for each mimicked sensor at each profiling depth decreased linearly within the sediment oxic zones and became zero after the OPD (Figure 29). The initial decreased is probably as a result of linear O_2 gradient generated from a constant O_2 consumption rate within the sediment oxic zone. Below the OPD there is no O_2 consumption and as such no O_2 gradient making the uncertainty to be zero within this domain.

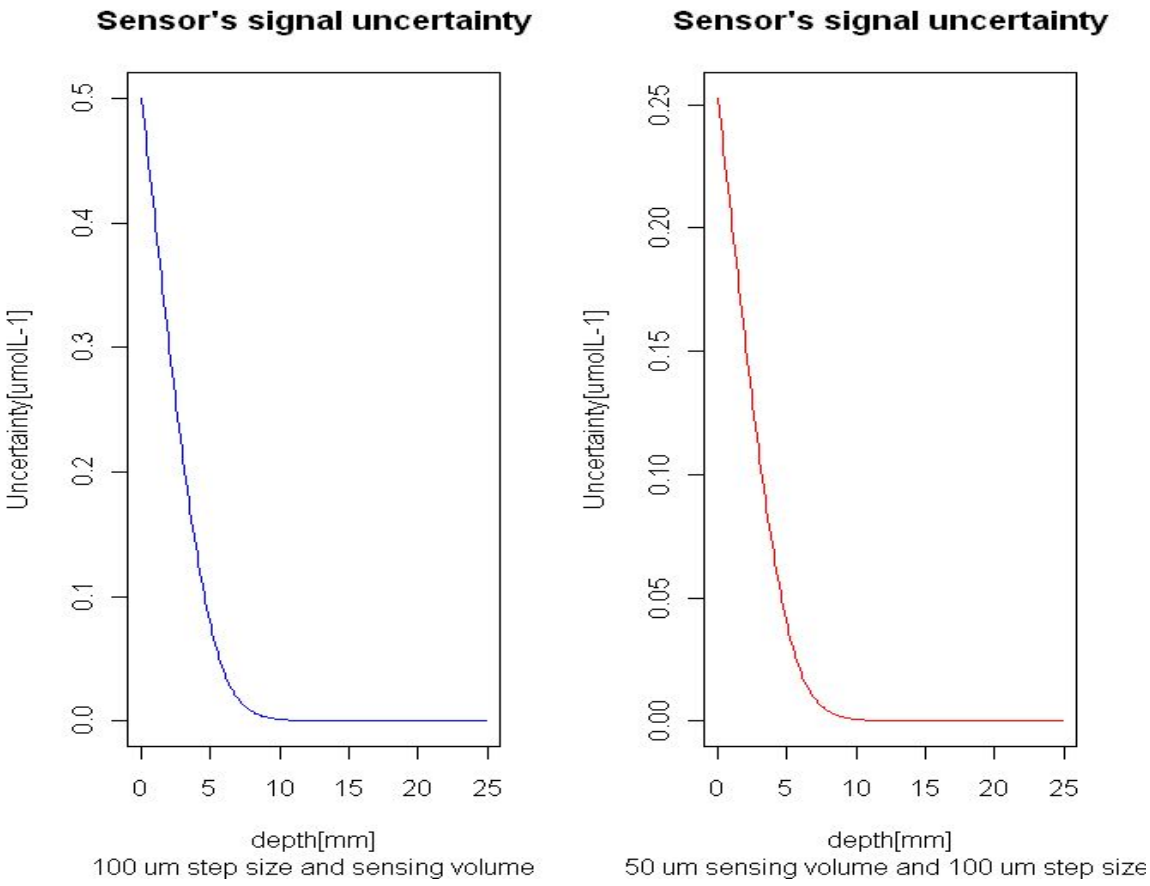

Figure 29. Sensors uncertainty at each profiling depth

The standard error of the profiling depths uncertainties is representative of the overall uncertainty of a sensor. This overall individual sensor's uncertainty showed a perfect linear relationship ($r^2 = 1$; Figure 30) to their respective sensing volumes. The uncertainty of all the mimicked sensors was in all cases independent of the micromanipulator step size.

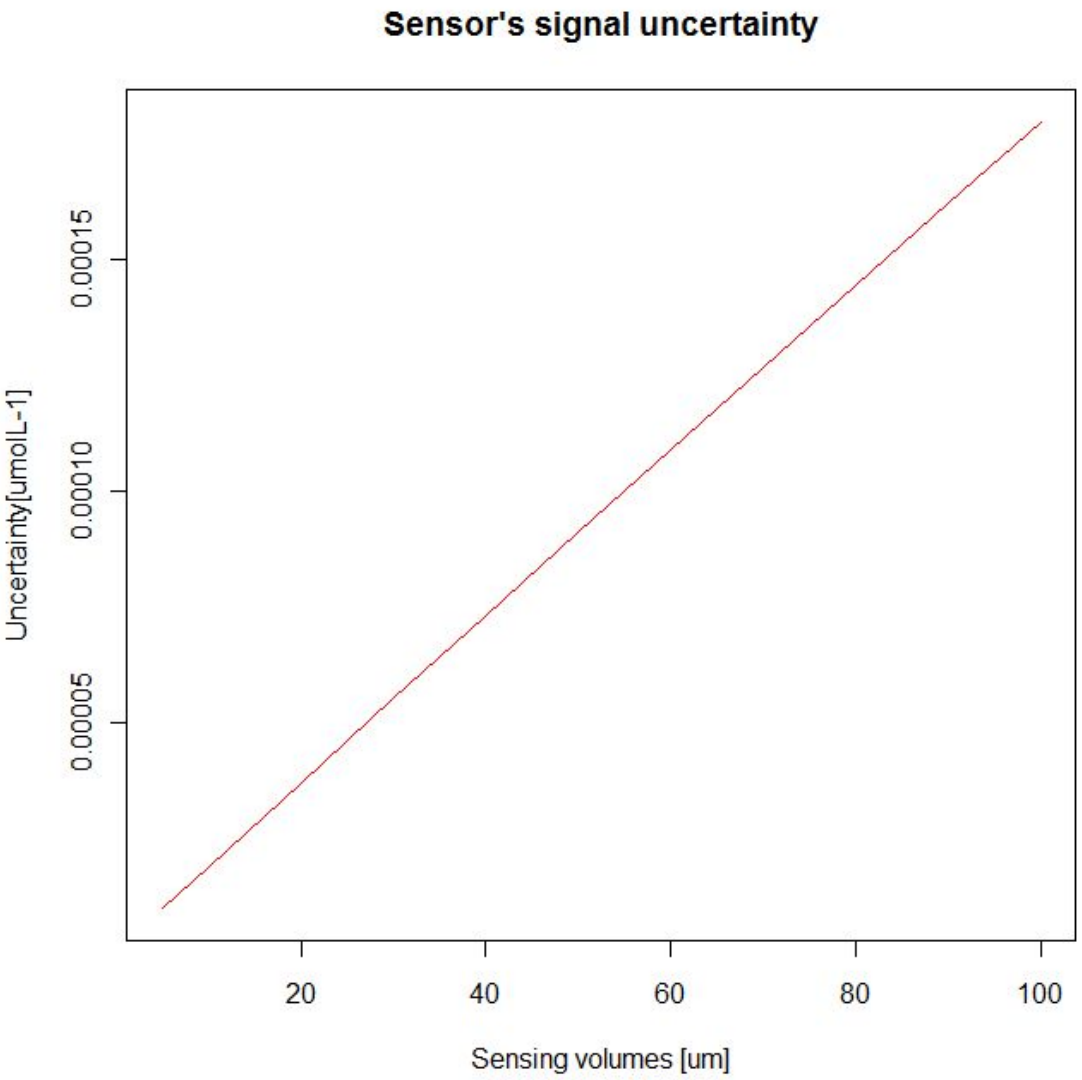

Figure 30. Individual sensor's overall uncertainty

3.5 Discussion

Sensitivity analysis

In most benthic mineralization studies involving micro profiling with Clark type O_2 sensors little attempt has been made to quantify the systematic bias posed by these sensors with respect to their tip diameter and micro manipulator step size in estimating the DOU. Focus at the moment is placed on the sensitivity of the sensors from its physical dimensions, temperature, salinity and bottom water oxygen concentration and the DBL (Revsbech, 1989; Ramussen and Jorgensen, 1992; Gundersen et al., 1998; Glud et al., 1994; Reimers, 2007). It was thus difficult to compare our findings with other similar research studies. However we were able to show that the sensor's signal is also sensitive to varying sensing volumes and micro manipulator step size. This sensitivity will eventually lead to systematic bias in the estimated DOU using either the two points or five points' gradient methods. The two point gradient method in all cases gave a better estimate of the DOU than the five point gradient method. The reason for this is because the estimated O_2 gradient at the sediment interface generally decreases as the distance of extrapolation increases (Reimers and Smith, 1986).

In this thesis we mimicked sensors with commonly used outer tip diameters and micromanipulator step depths (Glud et al., 1998; Wenzhofer et al., 2001; Whenzhofer and Glud 2002; Grenz et al., 2003; Whenzhofer and Glud 2004; Jorgensen et al., 2005; Dedieu et al., 2007). In both cases we tested how the systematic bias to the estimated DOU varies when the sensors sensing volumes and step size are the same or different. 5 mm OPD O_2 micro profile was used for the theoretical analysis because the OPD reported in most coastal benthic research varies between 1-10 mm with an average of 5 mm (Glud, 2008). Our findings showed that the microelectrode step depth was the most sensitive parameter in estimating the DOU. This is because the bias becomes significantly larger when the step size is increase for a given sensing volume. The step depth determines the positions in the sediment where the O_2 flux is registered and the number of sampling points within the oxic zone. As the step depth increases there is a gradual shift of the depth coordinates at which the output signal is registered. This shift far from the SWI increases the extrapolation distance for the linear gradient line (gradient fit becomes increasing vertical than horizontal) (Figure 31). As a result this vertical gradient cannot capture the initial abrupt decrease in O_2 concentration at the SWI. A small step depth captures the abrupt linear O_2 gradient at the DBL and just below the sediment surface than a larger step depth (Wenzhofer et al., 2001). This corresponds well with the results of our sensitivity analysis. A step size of 100 μm or less has been proposed as ideal to better capture the O_2 gradient at the DBL and just below the SWI (Rasmussen and Jorgensen, 1992; Wenzhofer et al., 2001). In this thesis we were able to show that even typically used Clark type O_2 microelectrode with an outer tip diameter of 1-100 μm and step depths of 100 μm underestimate the DOU (using the five gradient approach) by 5-10 % under perfect conditions (no stirring effect, hydrodynamic disturbance etc). This bias may increase significantly (up to 40 %) when the step depths becomes large (100-1000 μm).

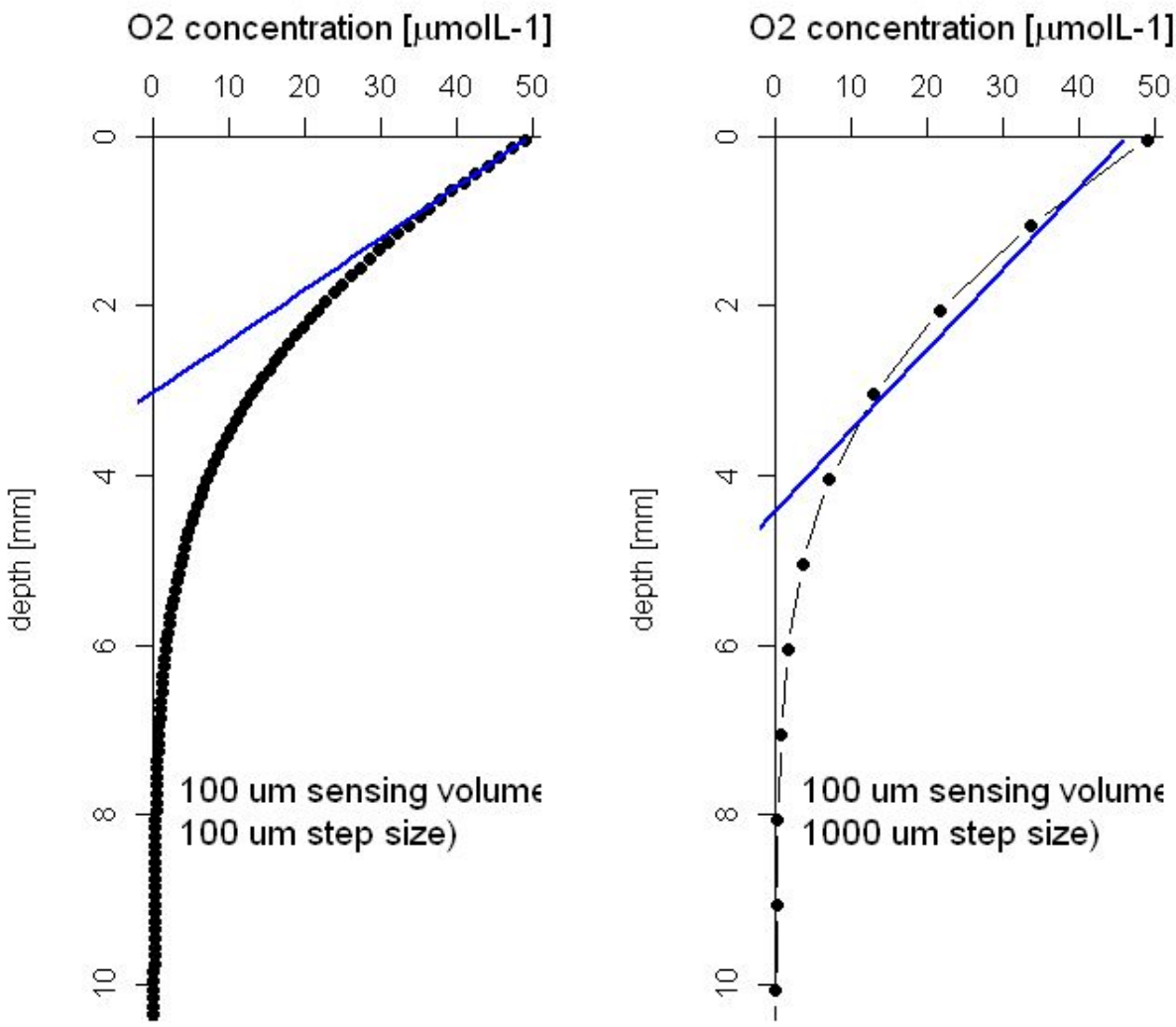

Figure 31. Extrapolation distance (gradient line) increases as the step depths becomes larger.

The estimated DOU was also sensitive to the microelectrodes sensing volumes. Large sensing volume underestimates the DOU in both the two point and five gradient approach. A possible explanation for this is that because the sensor records the O_2 signal at a profiling depth after integrating over a diffusion sphere, the uncertainty in this integration procedure will be larger for a large sensing volume than for a smaller sensing volume (Figure 30). This uncertainty was however extremely small and as such the bias in the estimated DOU for typically used microelectrode is also small (2 %).

This method of sensitivity analysis is purely theoretical because we integrated the grids and O_2 concentrations generated by a reactive transport model to mimic possible output signals from sensors with different tip diameter and step size. However care should be taken when extrapolating the results to deep ocean sediments with large OPD's .This is because our analysis demonstrated that the bias decreases significantly as the OPD increases in the case of

typically used microelectrode (Figure 28). In these large OPD sediments we expect the O_2 uptake rates to be very low (Glud et al., 2005). The O_2 profiles curvature in these deep sea sediments will be small and as such a linear fit at the SWI will give a good approximation of the DOU.

CHAPTER 4.

O_2 MICROPROFILING AND DOU ESTIMATION IN HETERGOGENEOUS SEDIMENTS

4.1 Data collection

For the 2D analysis in this chapter we used O_2 consumption rates that are based on data collected at 1450 m water depth in central Sagami Bay by Glud et al. (2009). Below is a summary of the study area and the data collection methods from Glud et al. (2009).

4.1.1 Study site

Sagami Bay is a 3000 km^2 large embayment at Honshu (Japan), which faces the Pacific Ocean (Figure 32).

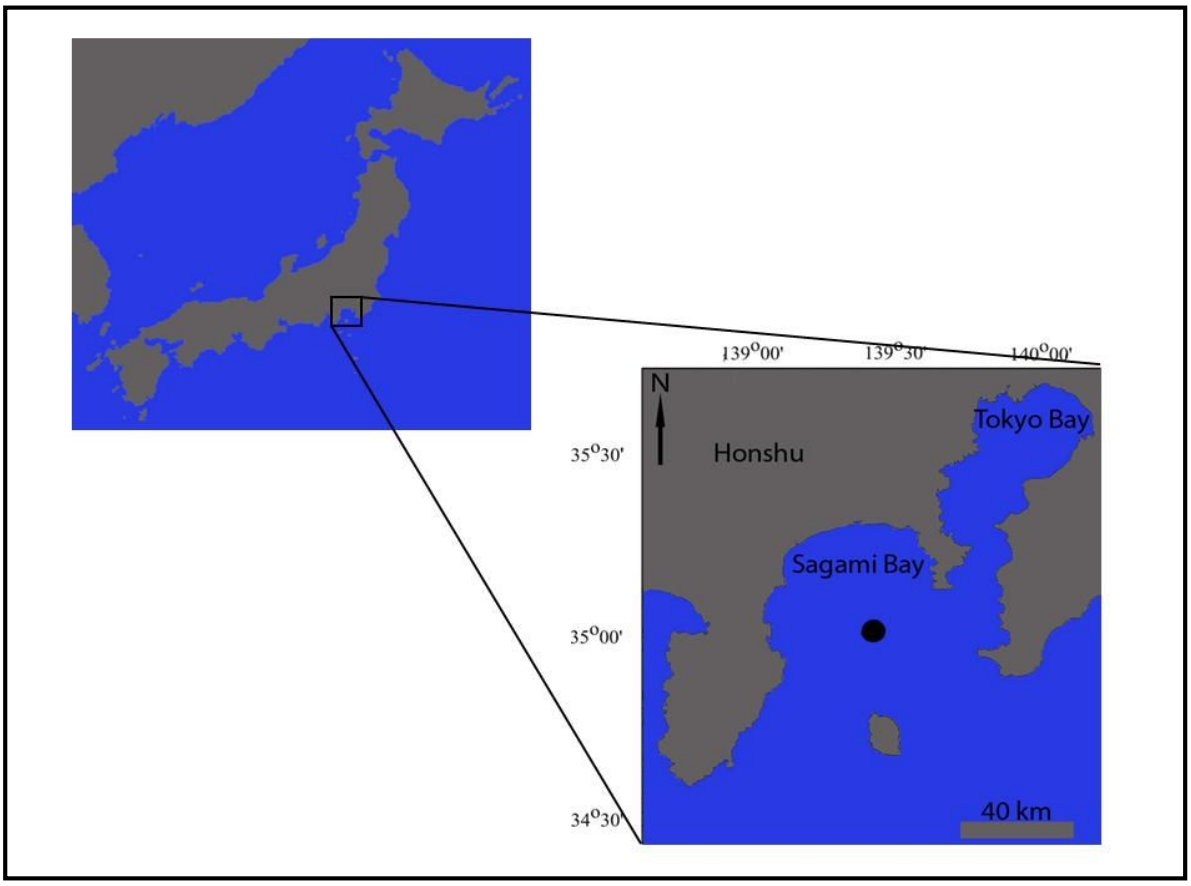

Figure 32. Sagami Bay with the investigated site indicated by a black dot: modified from Glud et al. (2009)

Towards the north east, Sagami Bay is connected to the relatively shallow and eutrophic Tokyo Bay. The bathymetry is dominated by a central canyon, which extends from the sill at the Tokyo Bay to the central part of Sagami Bay, which has an average depth around 1500 m. Depth integrated concentration of Chlorophyll over the upper 50 m water column was found to vary between 20 and 80 mg m^{-2} with peaks during spring and minima during mid winter (Kanda et al., 2003). Intense mineralization in the water column results in oxygen depleted water, leading to values around 50 µmol L^{-1} at 1200-1400 m water depth. Approximately 10% of organic carbon deposited in central Sagami Bay is mineralized within the upper 10 cm of the sediment depth, while ~90% is retained in the deeper sediments layers. Figure 33 shows the estimated carbon budget for the Sagami Bay area

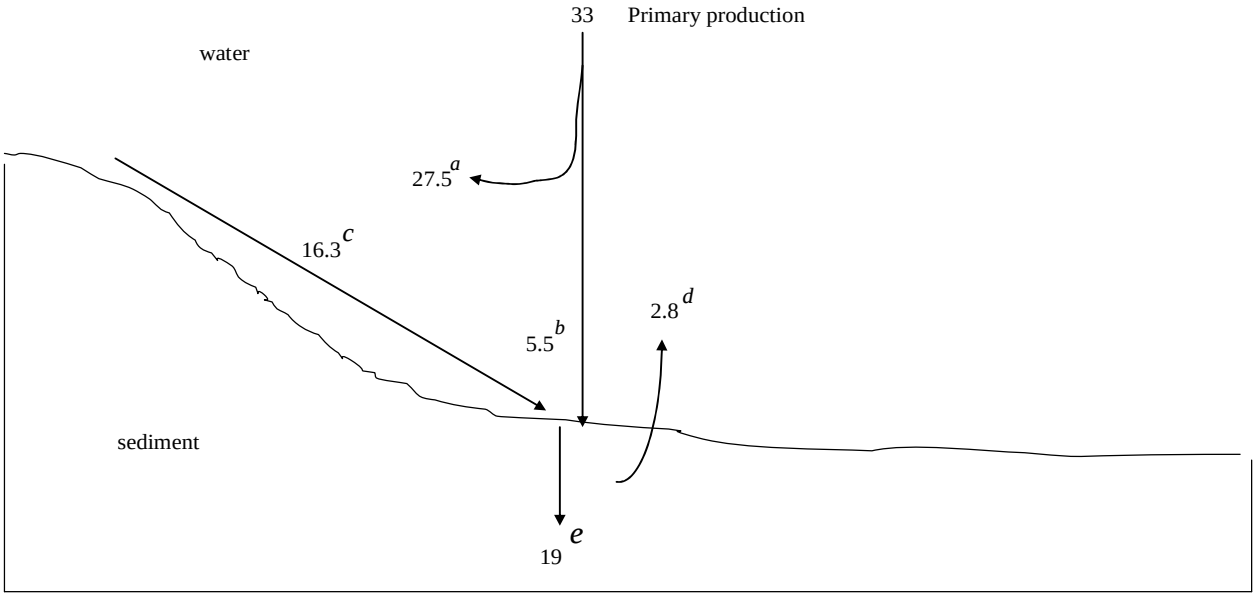

a Annual average water column mineralization

b Average vertical organic carbon sedimentation measured by sediment traps positioned 350m above the sea bed

c Average annual down slope of organic carbon

d Average DOU rate

e Average annual burial rates of organic carbon measured at 10 cm sediment depth

Figure 33. An estimated carbon budget (mmol C m^{-2} d^{-1}) for central Sagami Bay. Modified from Glud et al. (2009).

4.1.2 In situ O_2 profiling

A transecting profiler equipped with an electronic cylinder carrying 4 microelectrodes and one resistivity sensor was used to obtain micro profiles from the bay floor. The microelectrodes were of the Clark type with an internal reference and a guard cathode, tip diameters of ~10 μm, t_{90} < 2 s and stirring sensitivities < 2 % (Revsbech 1989a). The profiling unit was mounted in a benthic lander tripod (Figure 34) and placed on a sledge which could move a total horizontal distance of 90 cm in increments of 0.7 cm. A set of micro profiles was collected at each increment position. A remotely operated vehicle (ROV) controlled from the research mother ship was used to carefully and slowly move the benthic lander tripod from the ship to a site that remained undisturbed from any potential bow wave. The tripod was equipped with a wooden triangle to avoid sinking in to the sediment once it landed and during the course of the profiling routine.

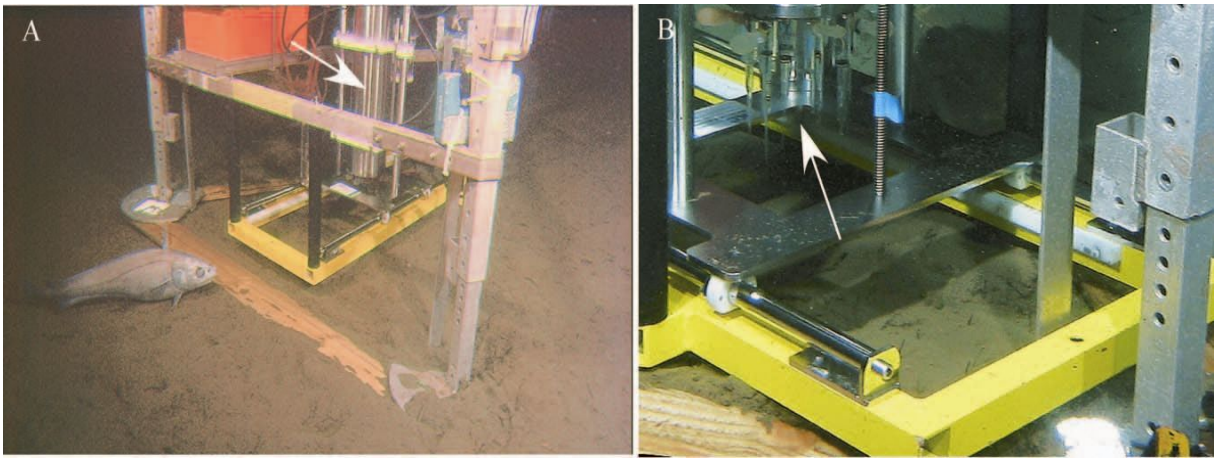

Figure 34 A. Benthic lander tripod with transecting profiler placed on a sledge. **B.** A closer look at the micro electrode array. Source Glud et al., 2009.

Once the lander was positioned on the bay floor the ROV activated the electronic cylinder and the micro electrodes are moved continuously vertically towards the sediment surface. With a 10 % drop in the resisitivity sensor signal indicating the relative position of the SWI the vertical movement stops and the electronic cylinder receded 3.0 cm. The sledge now moved horizontally at increments of 7 mm. At each increment position the electronic cylinder holding the micro sensor array was lowered at 0.1 mm increment for a total distance of 70 mm before moving back to its initial vertical position. This measurement routine was repeated 33 times and required a total deployment time of 28 hours. Due to breakage of one sensor towards the end of the measurement procedure a total of 129 O_2 depth profiles (instead of 132) were measured along four mini transects ~20 cm long. The parallel transects were separated by a few cm and all profiles were measured within a sediment area of ~190 cm^2. After completion of the measurement routine the ROV grabbed and lifted the lander tripod back to the sea surface where both instruments were recovered to the mother ship. Microprofile transect data were collected during the period 08-16 December 2006, while additional support data from the same location were measured on three other cruises which took place 24 September-10 October 2003, 22-27 march 2006 and 17-23 January 2008.

4.1.3 Two dimensional O_2 consumption maps

The oxygen distribution or neighboring micro profiles for each transect were plotted as isopleths (Figure 35).

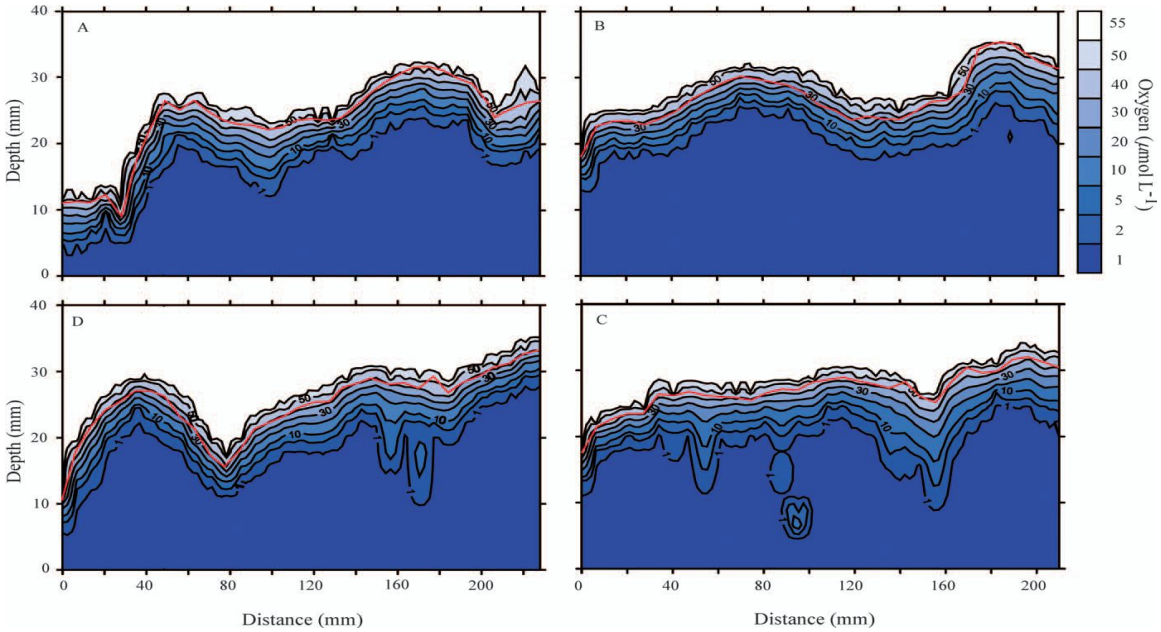

Figure 35. (A-D) The benthic oxygen distribution isopleths along four parallel transects measured by the transecting micro profiler. The red lines indicate the relative position of the sediment surface.

The 3D isopleths showed extensive small scale variability in the oxygen distribution within each transect and also a varied topographic relief at the sediment surface. To create the O_2 consumption rate maps for each transect (Figure 36), the volume-specific oxygen consumption activity was calculated from the isopleths using the simplified 1D approach after correcting for micro topographic consequences of the variable sediment surface topography (see details in Glud et al. 2009). This variable topographic relief enlarges the sediment area across which diffusive exchange takes place and causes horizontal concentration gradients within the sediments and diffusive boundary layer (DBL). Such factors not accounted for in 1D DOU calculations. The geometric correction was done by estimating the average angle of the sediment relief and the overlying DBL in relation to the horizontal plane.

The result of this analysis was a 2D distribution map of the oxygen consumption rate in the sediments for each of the 4 transects (Figure 36). These maps show a very heterogeneous oxygen consumption rate within the surface sediment, characterized by hotspots: zones of intensified oxygen consumption separated by patches of insignificant activity.

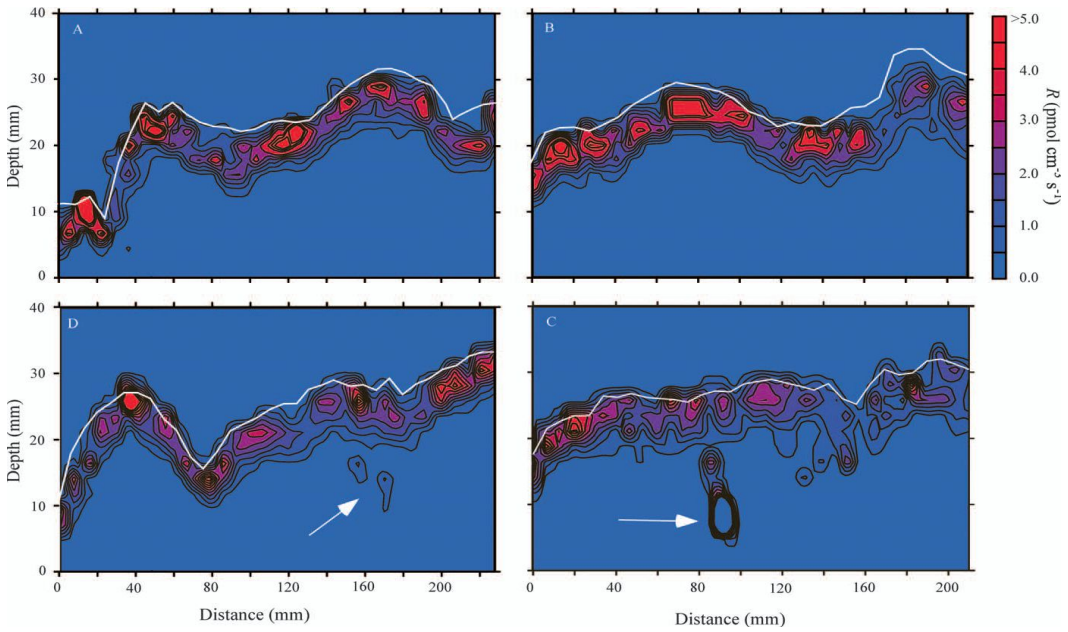

.

Figure 36. (A-D) The calculated volume-specific oxygen consumption rate R as calculated from the the oxygen distribution of the four parallel transect presented in Fig 5.The white lines indicate the estimated position of the sediment surface and the white arrows penetrated infauna burrow

4.2 Creation of virtual heterogeneous 2D sediment transects

Four virtual 2D sediments were created using the oxygen consumption maps associated with each of the 4 transects in Glud et al. (2009) as given in Figure 36. Each sediment transect has the same rectangular geometry and covers an area of 25 cm^2. The geometry specifications that were used to create the 2D finite difference grid using the routine `setup.grid.2D` in the R package `ReacTran` are given in Table 4.1.

Sediment transect Geometry	*Values*	*Units*
L_x	1.8	cm
L_y	21	cm
N_x	180	
N_y	2100	
Δx	100	μ m
Δy	100	μ m

Table 4.1 Sediment transects geometry.

For each 2D oxygen consumption map in Glud et al. (2009) the position of the hotspots $(x_{h,}y_h)$ and their widths $(\sigma_{x,h},\sigma_{y,h})$ were measured using a ruler. Equation [2.22] was then used to parameterize the oxygen consumption at each hotspot. The sum of all hotspots provides an oxygen consumption field for each 2D transect. This hotspot oxygen consumption field was implemented in a 2D reactive transport model for oxygen. Using the `tran.2D` routine we formulated this 2D reactive transport model for the fours sediment transects. Parameter values used in these 2D simulations of the oxygen field are shown in Table 4.2 below. The routine `Steady.2D` was used to calculate the 2D steady state oxygen distribution map for each of the four sediment transects.

The flux at the upstream boundary in each grid cell along the SWI was extracted from the routine `tran.2D`. These fluxes represent the "true DOU" in each grid cell (and account for vertical and horizontal concentration gradients within the sediment).

Parameters	*Values*	*Units*
C_o	50	μmol L^{-1}
Temperature (T)	10	deg C
Pressure (P)	150	bar
Salinity (S)	30	
Porosity (ϕ)	0.91	dimensionless
Effective diffusion coefficient (D)	1.33e-09	m^2s^{-1}
Half saturation constant (k_s)	5	μmol L^{-1}
R_{max}	0.004	μmol $L^{-1}s^{-1}$
R_{base}	0.001	μmol $L^{-1}s^{-1}$

Table 4.2 Parameter values incorporated in 2D simulations.

4.3 Real sensor sampling

4.3.1 Infinite sampling effort

These oxygen distribution maps are analogous to oxygen images obtained using planar optodes at spatial resolution of 100 μ m. Each 2D oxygen distribution map in principle can be regarded as consisting of 2100 juxtaposed 1D O_2 micro profiles as measured by a 50 μ m tip diameter oxygen sensor. This involves extracting all the individual columns of the O_2 concentration matrix generated by our 2D numerical procedure. Each column in principle represents an O_2 micro profile measured by a 50 μ m tip oxygen sensor, taking lateral steps of 100 μ m along the SWI over the whole transect with a width L_y = 21 cm. We call this "infinite sampling effort" because all possible micro profiles are extracted. The "sampled" DOU of each 1D micro profile was then calculated using the SWI gradient method based on two fitting points as already described above.

4.3.2 Finite sampling effort

In reality, it is plainly impossible to be able to investigate the sediment with a 100 μ m lateral resolution! Glud et al., (2009) effectively use a 7 mm lateral resolution. Real sampling procedures will extract therefore much less than 2100 profiles in one transect. Under field conditions it is not possible to sample all the neighboring micro profile along the SWI. Such real sampling procedures mimicking actual field measurements were simulated (random vs. selective sampling). We then used this sampling procedure to sample different 1D oxygen micro profiles along the SWI of each virtual sediment transect. As a result, a finite number of micro profiles are selected from the whole set of 2100 either randomly or selectively along the SWI. This is referred to as "finite sampling effort".

.

4.4 Statistical analysis

The "true'' DOU values in each grid cell from all the 4 transects were pooled and assumed to represent the normal population distribution of all true DOU's within Sagami Bay area (this provides 2100 true DOU values per transect (25 cm^2 sediment area) and 8400 in total) . For each grid cell, the "sample" DOU column was also extracted using the gradient of the first two micro profile concentrations (this provides 2100 sample DOU values per transect and 8400 in total). The sample DOU's were also pooled together and assumed to represent the normal population distribution of all sample DOU's within Sagami Bay.

A dependent t-test at 5% significance level was used to test for a significant difference between the mean of the pooled true DOU's and the mean of the pooled sample DOU's. This was done to ascertain if there is any systematic bias in the microprofiling method based on infinite sampling effort. Because a normal distribution was assumed in both cases a Monte Carlo simulation was also used to calculate the true significance level of the dependent t-test. A non-parametric Wilcoxon signed rank test was also used to ascertain the level of bias given the assumptions of normal distribution were flawed.

Assuming an error tolerance level of 10 % standard error of the mean, and adopting a 5 % significance level, the number of measurements (n) needed to quantify the average DOU within a given pool and transect using either 1D microprofiling or 2D measurements (incubation boxes) was calculated as,

$$n = \left(\frac{1.96\sigma}{0.1\bar{X}} \right)^2 \qquad [4.1]$$

where σ is the standard deviation from the average DOU represented by $\bar{X}$.

This estimation was done for each of the individual transects (25 cm^2 sediment area – 2100 DOU values) and as well for the whole Sagami Bay area as a whole (pooled 8400 DOU values).

The average DOU obtained using our mimicked 1D microprofiling was then compared with that obtained by Glud et al., (2009) for each transect and for the whole Sagami Bay. Note that the experimental DOU values were obtained by applying Fick's law of diffusion over the diffusive boundary layer.

4.5 Results

4.5.1 Sediment oxygen maps

Figure 37 A-D shows the 2D oxygen maps created from each transect in Glud et al., (2009).

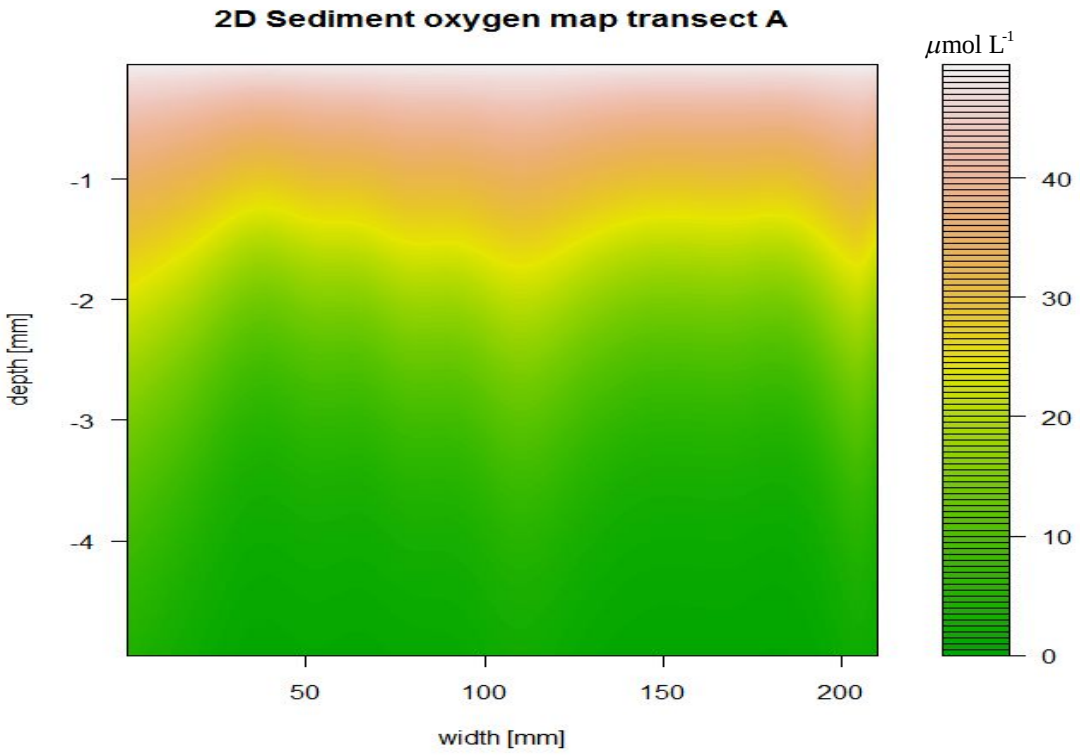

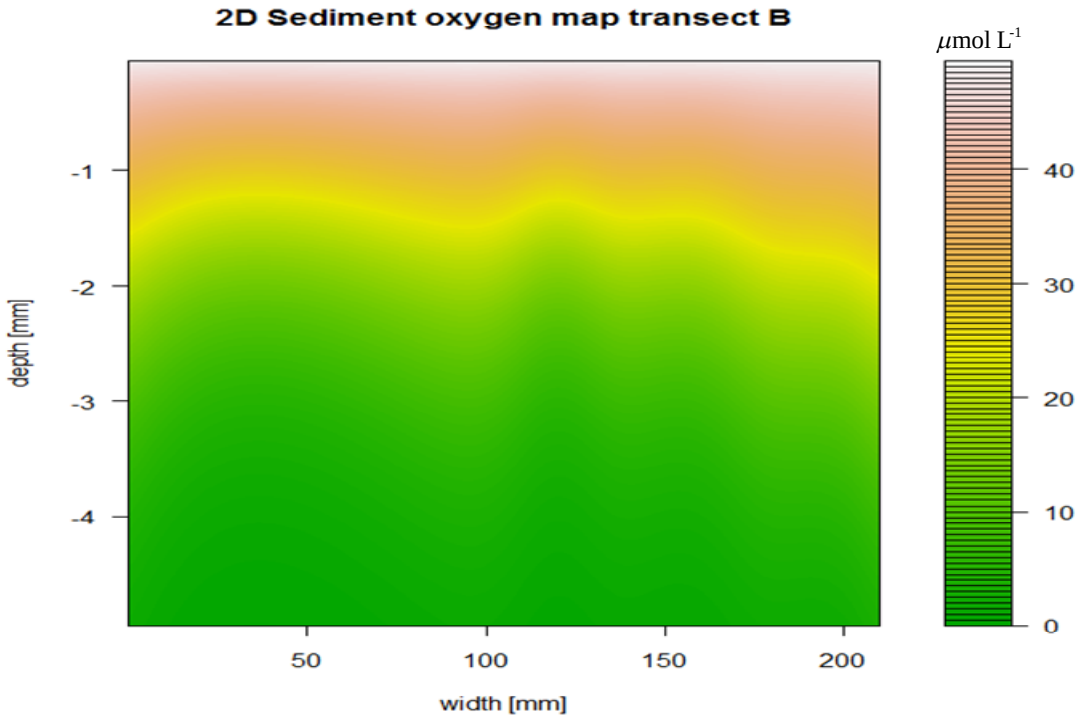
2D Sediment oxygen map transect B
µmol L-1
depth [mm]
-1
-2
-3
-4
50
100
150
200
width [mm]
40
30
20
10
0

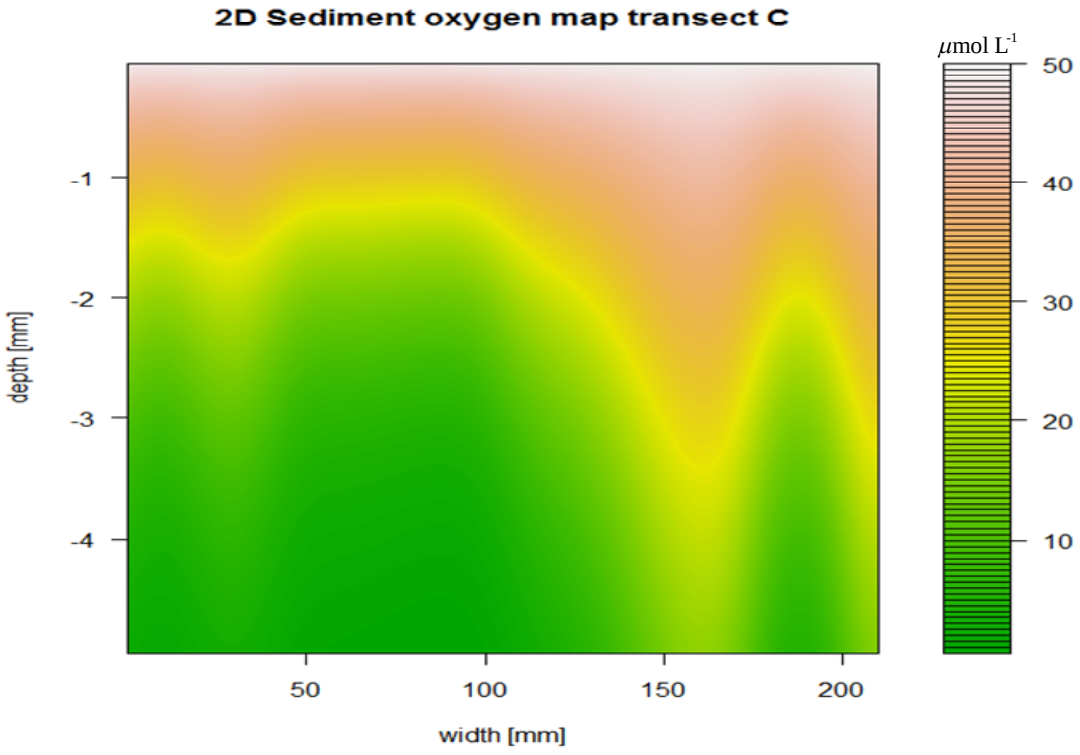
2D Sediment oxygen map transect C
µmol L-1
depth [mm]
-1
-2
-3
-4
50
100
150
200
width [mm]
50
40
30
20
10

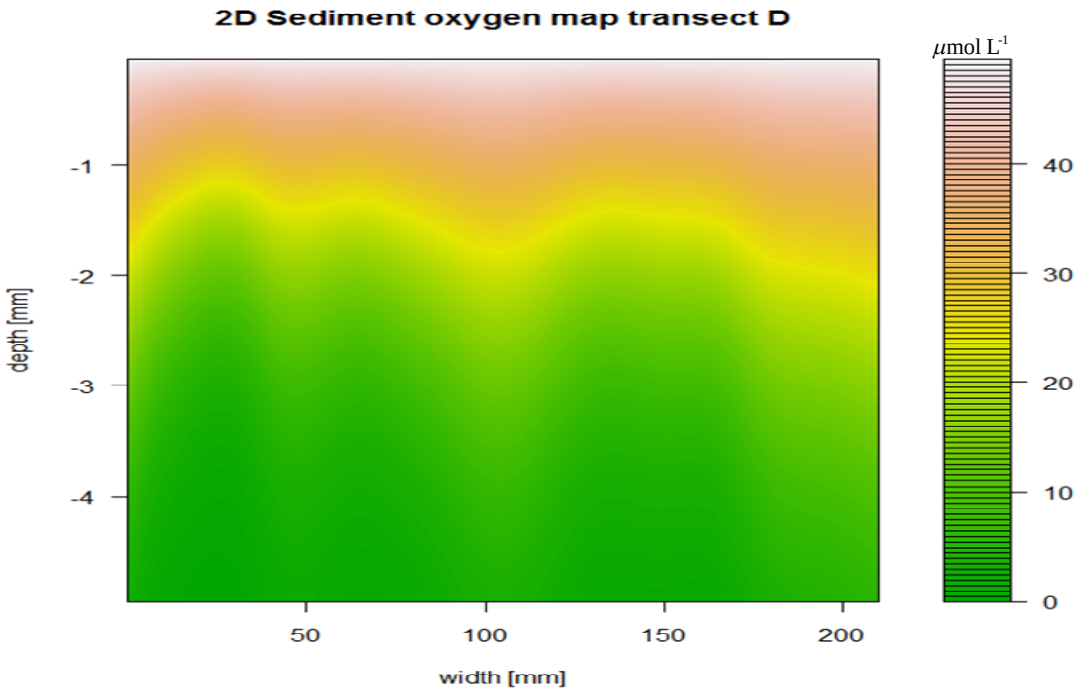

Figure 37. (A-D) Virtual sediment distribution maps generated from respective natural transect hotspot data in Glud et al., (2009)

The generated 2D distribution maps were quite similar to the ones obtained by Glud et al., (2009) indicating that our simulated 1D micro profiling procedure is representative of actual sampling in Sagami Bay. The gold structures within the maps represent the relative position of the hotspots. Note how the O_2 distribution changes along these structures. The O_2 isopleths displayed a bell-shape around the hotspots indicating intense O_2 consumption at the center of these structures.

4.5.2 DOU statistics: infinite sampling effort

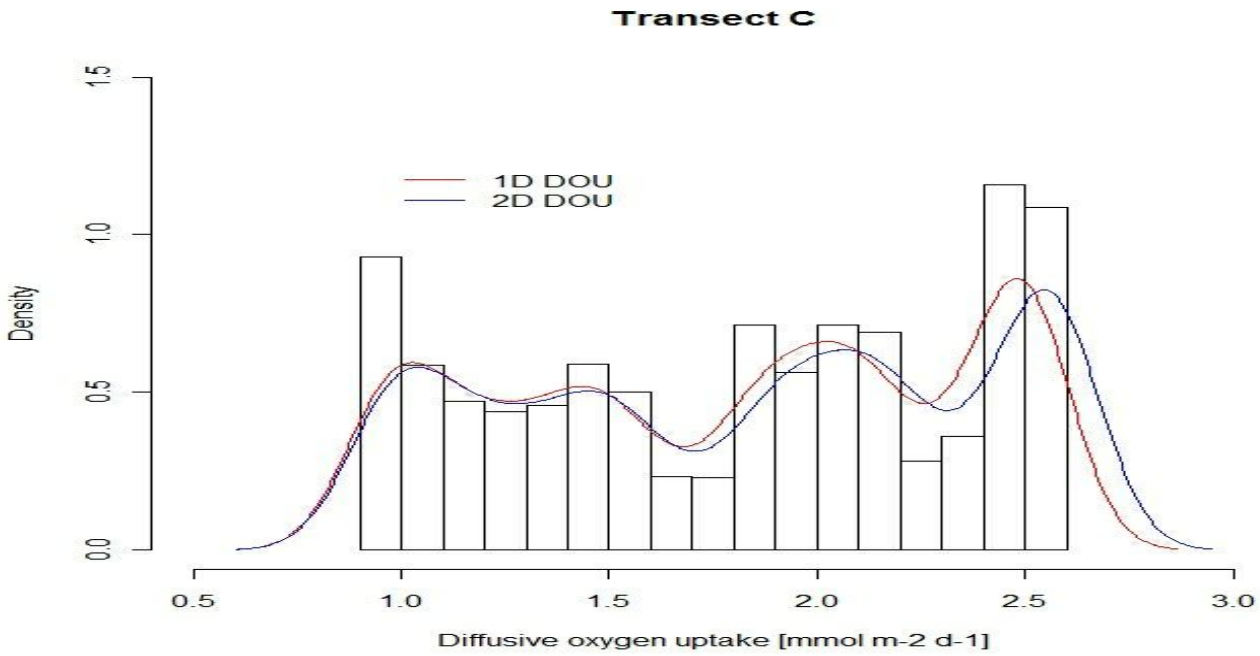

Figure 38. Histogram and density plots of true and sample DOU's of transect C.

Histograms and density plots (Figure 38) of true and sample DOU's of transect C shows a heterogeneous distribution of oxygen along the SWI. This spatial heterogeneity is due to lateral hotspots heterogeneity which creates heterogeneous O_2 consumption rates along the SWI. The difference in the density plots is due to inherent systematic bias in the 1D micro profiling procedure in estimating the DOU using linear gradient fit below the SWI.

The DOU and OPD calculated from the 2D oxygen maps and the extracted O_2 micro profiles (real sensor) are compared with *in situ* experimental data obtained by Glud et al., (2009) in Table 4.3. Sediment transect C had the most heterogeneous oxygen distribution along the SWI. The number of sampling measurements (real sensor vs. 2D incubation boxes) to best quantify the DOU varied for each transect. This number was the same for each transect irrespective of the measurement procedure.

Transects	*DOU (mmol m^{-2} d^{-1})*			*OPD (mm)*		*n*		*Coefficient of variation (%)*	
	2D	*1D*	*in situ*	*Model data*	*in situ*	*2D*	*1D*		
A	2.18 ± 0.25	2.14 ± 0.24	1.62 ± 0.73	5.22 ± 0.65	8.02 ± 3.28	5	5	11.49	11.11
B	2.28 ± 0.27	2.23 ± 0.26	1.68 ± 0.52	5.13 ± 0.46	5.89 ± 1.52	6	5	12.26	11.85
C	1.84 ± 0.56	1.81 ± 0.54	1.60 ± 0.71	7.79 ± 3.08	6.83 ± 2.59	36	35	30.53	30.02
D	2.08 ± 0.30	2.04 ± 0.29	2.15 ± 0.76	5.74 ± 0.97	5.54 ± 1.63	8	8	14.32	14.06
Pool transects	2.10 ± 0.40	2.05 ± 0.38	1.76 ± 0.71	5.97 ± 1.98	6.61 ± 2.56	14	14	19.26	18.89

Table 4.3 DOU and OPD calculated from the sediment transects using 2D and 1D approximations and *in situ* values obtained from Glud et al., (2009). n = Number of sampling measurements needed to quantify the DOU at 95 % confidence interval with a 10 % error tolerance level. The coefficient variation to compare spatial heterogeneity in the different sediment transects. Pooled data from the four transects to be representative of the DOU distribution within the Bay area.

However in all transects with the exception of transect D the in situ DOU values were about 32% lower than the DOU estimated (using the two gradient linear fit method) from the extracted infinite 1D microprofiles .

The average OPD obtained from the 2D transect maps using 1D and 2D approximations was the same for each transect because we used the same O_2 detection limit. This was not the same for the average DOU. True significance level calculated from Monte Carlo simulations (p-value = 0.049), dependent two sample t-test (p-value = 4e-11) and the Wilcoxon signed rank test (p-value < 2.2e-16) showed significant difference between average DOU calculated from the extracted O_2 micro profiles using the two gradient point method and the 2D integration method. We attribute this difference to be as a result of inherent systematic bias in 1D profiling procedures.

4.5.3. DOU statistics: finite sampling effort

Sediment transect C showed the largest heterogeneity and was used as a test case. We compared random and equidistant sampling procedures. From the total pool of 1D O_2 microprofiles, a number of profiles (5,7,9,10,20,50,70,100,130,170,210,500,1000,2100) were selected randomly and at regular intervals. The true DOU and sampled DOU of these microprofiles were calculated using the two point gradient method. Empirical distribution of the DOU's of the different sampling procedures is shown in Figure 39 below. The random sampling procedure was done a hundred times. This means to sample say 5 random sample from the pool of 2100 we selected 5 profiles each at random from the pool without replacement a hundred times. This was done to generate an empirical distribution of random DOU's for a given number of random samples.

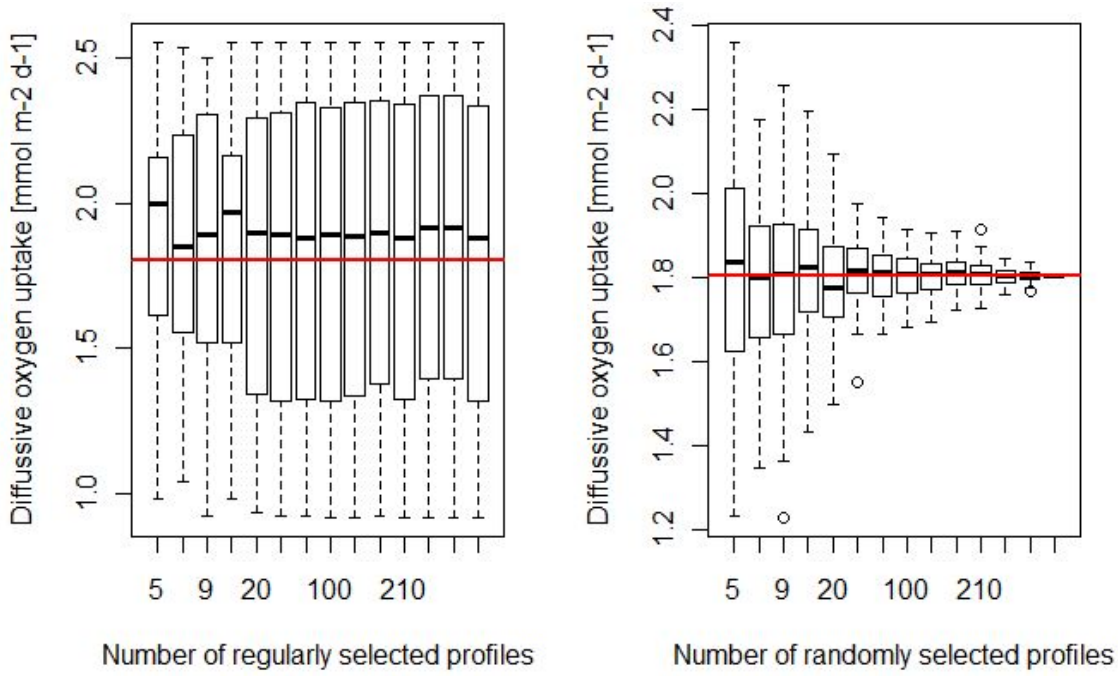

Figure 39. Empirical DOU distribution generated using different sampling procedures to approximate the true DOU.A. Regular sampling. B. Random sampling. The horizontal redline indicates the true average DOU calculated from the sediment transects

As the number of sampling profiles approaches our calculated number of profiles required to quantify the DOU within Sagami Bay at 10% error limit random sampling gave a better estimate of the true DOU than regular sampling.

4.6 Discussion

The theoretical 2D model confirms the presence of small scale heterogeneity along the SWI in Sagami Bay. Spatial 2D model captures the variability in O_2 uptake within sediment transects. This variability is usually not captured by a single micro profile because it supply information only at a single point (Glud et al, 2005). The spatial 2D model showed that the Sagami bay floor is not a laminated surface with a homogenous O_2 uptake at each point in space but rather a mosaic structure embedded with hotspots of different oxygen consumption rates at different point in space separated by zones of insignificant O_2 consumption activity. These hotspots are probably formed by settling debris of fresh organic matter and subsequently invite a consortium of highly populated microbial communities resulting in intensified O_2 consumption (Middelboe et al., 2006; Glud et al., 2009). This spatial heterogeneity in the DOU has also been reported for a number of coastal environments (Jorgensen et al., 2005; Dedieu et al., 2007).

Cai and Sayles, 1996 proposed that for a homogeneous sediment the OPD and DOU are related inversely by the equation

$$\delta = 2\phi D\left(\frac{C_o}{DOU}\right) \qquad [4.2]$$

This inverse relationship has been used as an indication for steady-state O_2 distribution, uniform distribution of organic matter and negligible irrigation in shelf and continental margin sediments (Cai and Sayles, 1996). Although there was a major discrepancy between the experimental winter data obtained by Glud et al., (2009) and our model data, both sets of data displayed the general trend of the inverse relationship reported by Cai and Sayles, (1995). The experimental data displayed a more scatter trend from the inverse relationship than the model data (Figure 40). Glud et al., (2009) reported that scatter trends from the homogenous OPD-DOU relationship are as a result of inherent heterogeneity of O_2 uptake due to lateral hotspots distributions. However our 2D simulations did not display this scatter trend. There are two probable reasons for the scatter trend in the experimental data (1) The DOU's calculated from the experimental microprofiles is bias. This is because it underestimates the DOU extracted from the model 1D microprofiles by 16%. The experimental DOU was calculated by applying Fick's law of diffusion over the DBL. This calculation is however bias because it is very difficult to determine the SWI with much accuracy. (2) The experimental O_2 profiles were not at a steady state. Flow velocity along the SWI changes a lot, this strongly affects the thickness of the DBL bringing the O_2 concentration at different depths out of steady state. Doing measurement at different places and times will give you measurements at different time series in the evolution of steady. Some of the profiles will be closer to steady state while others will be far from it. The theoretical OPD-DOU relationship assumes a steady state.

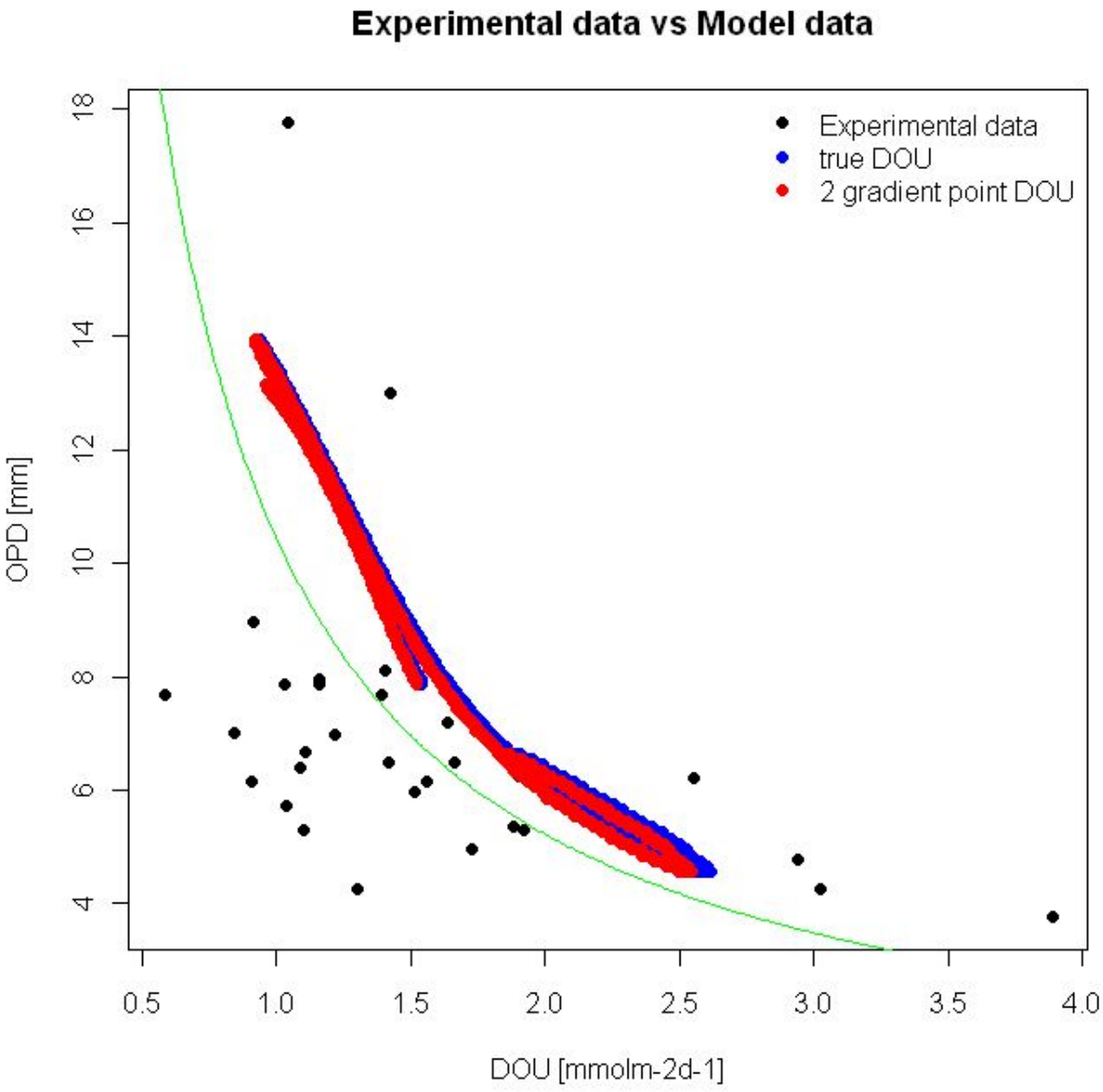

Figure 40. OPD-DOU relationship. The solid green line is the proposed relationship by Cai and Sayles, (1996)

The question now is does the average DOU obtained from infinite micro electrodes sampling within a sediment transect area approximates to the model 2D DOU calculated using our reactive transport model. This question is very important because 1D profiling is essentially a one dimensional technique and does not account for later O_2 gradients present in heterogeneous hotspots environments. Our simulations showed that DOU estimated from 1D microprofiles can significantly quantify the average DOU within 3D biogeochemical hotspot environments. The statistical difference ($p < 0.05$) is because of the inherent bias in the 1D profiling procedure in estimating the DOU described in the sensitivity analysis above. This was further confirmed as the possible reason for this difference because sampling all transects with a mimicked Perfect sensor produced average 1D DOU value that showed no statistical difference with the model average 2D DOU. The average DOU calculated from the central Sagami using our simulation approached was 2.10 ± 0.40 mmol m^{-2} d^{-1}.The model 2D DOU underestimates the experimental DOU obtained by Glud et al., (2009) by 9 %. A possible

explanation for this difference is because our model simulation assumed the sediment surface is a flat plane. The seafloor in reality has a varied topographic landscape and accounting for this topography generally increases the DOU in coastal sediments by approximately 10 % (Roy et al., 2002; Glud et al., 2003). Assuming a molar organic $C:O_2$ remineralization ratio of 106/138 (redfield ratio), the benthic carbon mineralization rate in Sagami Bay is 7.1 g C m^{-2} yr^{-1} as calculated by our 2D model.

Under normal field conditions it is not possible to carry out infinite micro profiling so we tried to quantify the number of profiles to better estimate the average DOU within a given sediment heterogeneous transect area (25 cm^2) in the Bay. Current operational practice in *in situ* benthic research limits this number to between 4 and 8 because of logistic and technical constraints. However in our model simulations this number ranges from 5 to 35 depending on the transect's spatial heterogeneity scale. For the Sagami Bay area 14 micro profiles at random positions are enough to quantify its average DOU with a 5% error limit.

Current operational practices in in situ benthic research used selective sampling as a model to sample the seafloor. Our results demonstrated that random sampling is a better option because the degree of spread of its DOU data is much smaller than that obtained through selective sampling. This degree of spread remains the same irrespective of the number of selective samples unlike in the case of random sampling in which the degree of spread reduces as the number of random samples increases. Increasing the number of random samples thus gives a better approximation of the true average DOU within a heterogeneous transect. A possible explanation for this is that hotspots in the ocean floor do not occur at regular intervals but are determined by factors such as settling of organic debris which do not follow regular patterns.

CHAPTER 6.

CONCLUSIONS

In this thesis DOU estimation procedures were investigated under two different environments-homogenous and heterogeneous sediments.

In the homogenous sediment synthetic perfect O_2 profiles were generated and later sampled using mimicked sensors with different outer tip diameters and step size to produced synthetic data O_2 profiles. The goal was to test if there is any inherent bias in the profiling procedures of microelectrodes in estimating the DOU. Our results indicate that;

- DOU estimated from micro profiles are very sensitive to their microelectrodes step depths and sensing volumes with the step depth being the most important factor.
- Typically used Clark type O_2 with an outer tip diameter of 1-50 μm and step depths of 100 μm sampling under perfect conditions underestimate the DOU by 5-10 %. This bias becomes significantly large (up to 40 %) when the step depths are increased (120-1000 μm).Even though this bias may be small it is very important to account for the bias in order to establish accurate quantification of benthic mineralization rate.

The thesis study concludes that there is inherent bias in the microelectrode profiling procedure in estimating the DOU using either the two point or five point linear fit gradient.

In the heterogeneous environment virtual sediment transects with natural hotspot distribution were generated using a spatial 2D reactive-transport model. The goal was to demonstrate and quantify the spatial heterogeneity of O_2 uptake at very small scale (cm) and to test if the 1D O_2 profiling procedure works in 3D biogeochemical hotspot heterogeneous environments. Our results indicate that;

- Sagami Bay is characterized by a lateral mosaic ocean floor with a very heterogeneous oxygen distribution at very small scales.
- Heterogeneity in O_2 uptake rates along the SWI due to lateral hotspots heterogeneity do not create scatter in the homogenous OPD-DOU relationship.
- 1D micro profiling within sediment transects approximates significantly the true average DOU in a 3D biogeochemical heterogeneous environment.
- Four-teen micro profiles are necessary to obtain a reliable estimate of the DOU within a sediment environment.

CHAPTER 7. RECOMMENDATIONS

The following recommendations could be made from this Msc thesis study:

- The step size of microelectrodes should be kept very small, possibly < 50 μm to increase the number of sampling points within the oxic zone so as to reduce the systematic bias of profiling procedures in estimating the DOU using linear gradient fit at the SWI.
- Gradient of first two points below the SWI is ideal for estimating the DOU of 1D O_2 profiles.
- In the cases where determination of the SWI is difficult reactive transport models will give a better estimate of the sediment reactivity.
- Single deployment of Benthic Lander systems should retrieve at least twenty microprofiles to get a good estimate of the average DOU within the sediment environment.

References

Anderson, J. H., W. M. J. Wijsman, M. J. P. Herman, J. J. Middelburg, K. Soetaert, AND C. Heip. (2004). Respiration patterns in the deep ocean. Geophysical Research Letters **31,L03304**: doi:10.1029/2003GL018756.

Archer, D. A., A. Devol. (1992). Benthic oxygen fluxes on the Washington shelf and slope: a comparison of in situ microelectrode and chamber flux measurements. Limnology and Oceanography **37**: 614-629.

Berg, P., H. Roy, F. Janssen, V. Meyer, B. B. Jorgensen, M. Huettel AND D. Beer. (2003). Oxygen uptake by aquatic sediments measured with a novel non-invasive eddy-correlation technique. Marine Ecology Progress Series **261**: 75-83.

Berg, P., N. Risgaard-Petersen, S. Rysgaard. (1998). Interpretation of measured concentration profiles in sediment pore water. Limnology and Oceanography **43**(7): 1500-1510.

Boudreau, B. P. (1997). Diagenetic models and their implementation. Springer.

Bouldin, B. P. (1968). Models for describing the diffusion of oxygen and other mobile constituents across mud-water interface Journal of Ecology **56**: 77-87.

Brotas, V., A. Amorim-Ferreira, C. Vale, F. Catarino (1990). Oxygen profiles in intertidal sediments of Ria Formosa (S. Portugal). Hydrobiologia **207**: 123-129.

Cai, W. J., AND C. E. Reimers. (1995). Benthic oxygen flux, bottom water oxygen concentration and core top organic carbon content in the deep northeast Pacific Ocean. Deep-Sea Research I **42**(10): 1681-1699.

Cai, W. J., AND F. L. Sayles (1996). Oxygen penetration depths and fluxes in marine sediments Marine Chemistry **52**: 123-131.

Canfield, D. E., B. B. Jorgensen, H. Fossing, R. N. Glud, J. K. Gundersen, N. B. Ramsing AND OTHERS. (1993). Pathways of of organic carbon oxidation in three continental margin sediments. Marine Geology **113**: 27-40.

Dalgaard, P. (2008). Introductory Statistics with R, Springer.

Dedieu, K., C.Rabouille, G. Thouzeau, F. Jean, L. Chauvaud, J. Clavier, V. Mesnage AND S. Ogier. (2007). Benthic O_2 distribution and dynamics in a Mediterranean lagoon (Thau France): An in situ microelectrode study Estuarine, Coastal and Shelf Science **72**: 393-405.

Epping, E. H. G., AND W. Helder (1997). Oxygen budgets calculated from in situ microprofiles for Northern Adriatic sediments. Continental Shelf Research **17**(14): 1737-1764.

Glud, R. N., H. Stahl, P. Berg, F. Wenzhofer, O. Kazumas, AND H. Kitazato. (2009). In situ microscale variation in distribution and consumption of O_2: A case study from a deep ocean margin sediment (Sagami Bay, Japan) . Limnology and Oceanography **54**(1): 000-000.

Glud, R. N. (2008). Oxygen dynamics of marine sediments. Marine Biology Research **4**: 243-289.

Glud, R. N., F. Wenzhofer, A. Tengberg, M. Middelboe, K. Oguri, H. Kitazato (2005). Distribution of oxygen in surface sediments from central Sagami Bay, Japan: In situ measurements by microelectrodes and planar optodes. Deep-Sea Research I **52**: 1974-1987.

Glud, R. N., J. K. Gundersen, N. B. Ramsing (2000). Electrochemical and Optical Oxygen Microsensors for In Situ Measurements, John Wiley & Sons Ltd.

Glud, R. N., J. N. Gundersen, N. P. Revsbech, B. B. Jorgensen. (1994). Effects on the benthic diffusive boundary layer imposed by microelectrodes. Limnology and Oceanography **39**(2): 462-467.

Glud, R. N., O. Holby, F. Hoffmann, D. E. Cainfield. (1998). Benthic mineralization and exchange in Artic sediments (Svalbard, Norway). Marine Ecology Progress Series **173**: 237-251.

Grenz, C., L. Denis, G. Boucher, L. Chauvaud, J. Clavier, R. Fichez, O. Pringault. (2003). Spatial variabilty in Sediment Oxygen Consumption under winter conditions in a lagoonal system in New Caledonia (South Pacific). Journal of Experimental Marine Biology and Ecology **285-286**: 33-47.

Gundersen, J. K., N. B. Ramsing, R. N. Glud. (1998). Predicting the signal of O_2 microsensors from physical dimensions, temperature, salinity and O_2 concentration. Limnology and Oceanography **43**(8): 1932-1937.

Guss, S. (1998). Oxygen Uptake at the sediment-water Interface Simultaneously Measured Using a Flux Chamber Method and Microelectrodes: Must a Diffusive Boundary Layer Exist? Estuarine, Coastal and Shelf Science **46**: 143-156.

Hall, P. O. J., L. G. Anderson, M. M. Rutgers van der Loeff, B. Sunby, AND S. F. G. Westerlund (1989). Oxygen uptake kinetics in the benthic boundary layer. Limnology and Oceanography **34**(4): 734-746.

IPCC. (2007). Summary for policy makers. In: *Climate change 2007*: *The Physical Science Basis. Contribution of Working Group I to the Fourth Assessment Report of the Intergovermental Panel on Climate Change,* Cambridge University Press.

Jorgensen, B. B., AND N. P. Revsbech (1985). Diffusive boundary layers and the oxygen uptake of sediments and detritus Limnology and Oceanography **30**(1): 111-122.

Jorgensen, B. B., R. N. Glud, O. Holby. (2005). Oxygen distribution and bioirrigation in Artic fjord sediments (Svalbard, Barents Sea). Marine Ecology Progress Series **292**: 85-95.

Kazumasa, O., K. Hiroshi, S. Takako, M. Kazuyo, R. N. Glud. (2004). Oxygen imaging using a planar optode system for biogeoenvironmental applications. Bioimages **12**(2): 106-119.

Kim, H. K., AND D. Kim. (2007). Seasonal and spatial variabilty of sediment oxygen fluxes in the Beobsan intertidal flat of Taean Bay, mid-western Korean Penisula. Geosciences Journal **11**(4): 323-329.

Kitazato, H., AND OTHERS (2003). Longterm monitoring of sedimentary processes in central Sagami Bay Japan. Rationale, Logistics and overview. In Glud, R. N., H. Stahl, P. Berg, F. Wenzhofer, O. Kazumas, AND H. Kitazato. (2009). In situ microscale variation in distribution and consumption of O_2: A case study from a deep ocean margin sediment (Sagami Bay, Japan) Limnology and Oceanography **54**(1): 000-000.

Klimant, I., M. Kuhl, R. N. Glud, G. Holst. (1997). Optical measurements of oxygen and other environmental parameters in microscale: strategies and biological applications. Sensors and Actuators **B 38/39**: 29-37.

Meysman, F. J. R., O. S. Galaktionov, R. N. Glud, AND J. J. Middelburg.(submitted) (2006). Oxygen penestration around burrows and roots in aquatic sediments. Limnology and Oceanography.

Middelboe, M., R. N. Glud, F. Wenzhofer, K. Oguri, H. Kitazato. (2006). Spatial distribution and activity of viruses in the deep-sea sediments of Sagami Bay, Japan. Deep-Sea Research I **53**: 1-13.

Middelburg, J. J., F. J. R. Meysman. (2007). Burial at sea. Science **316**(5829): 1294-1295.

Rasmussen, H., AND B. B. Jorgensen. (1992). Microelectrode studies of seasonal oxygen uptake in a coastal sediment: role of molecular diffusion. Marine Ecology Progress Series **81**: 289-303.

Reimers, C. E. (2007). Applications of Microelectrodes to Problems in Chemical Oceanography. Chemical Reviews **107**: 590-600.

Reimers, C. E., AND K. L. Smith. (1986). Reconciling measured and predicted fluxes of oxygen across the deep sea sediment-water interface. Limnology and Oceanography **31**(2): 305-318.

Revsbech, N. P. (1989). An oxygen sensor with a guard cathode. Limnology and Oceanography **34**(2): 474-478.

Revsbech, N. P., B. B. Jorgensen, T. H. Blackburn. (1980). Oxygen in the sea Bottom Measured with a Microelectrode. Science **207**(21): 1355-1356.

Revsbech, N. P., B. Madsen, B. B. Jorgensen. (1986). Oxygen production and consumption in sediments determined at high spatial resolution by computer simulation of oxygen microelectrode data. Limnology and Oceanography **31**(2): 293-304.

Revsbech, N. P., J. P. Lomholt. (1980). Distribution of oxygen in marine sediments measured with microelectrodes. Limnology and Oceanography **25**(3): 403-411.

Roy, H., M. Huettel AND B. B Jorgensen. (2002). The role of small-scale sediment topography for oxygen flux across the diffusive boundary layer. Limnology and Oceanography **47**: 837-847.

Sarmiento, J. L., N. Gruber. (2006). Ocean Biogeochemical Dynamics Princeton University Press.

Seiter, K., C. Hensen, M. Zabel. (2005). Benthic carbon mineralization on a global scale. *Global Biogeochem. Cycles* ***19***(GB1010): doi:10.1029/2004GB002225.

Soetaert, K., AND P. F. J. R. Meysman (2009). Reactive transport modellin in 1D or 2D.

Soetaert, K., AND P. M. J. Herman. (2009). A Practical Guide to Ecological Modelling: Using R as a Simulation Platform, Springer.

Soetaert, K. A. OTHERS. (2008). Datasets, constants, conversion factors, utilities for the marine and lacustrine environment. .

Stockdale, A., W. Davison, H. Zhang (2009). Micro-scale biogeochemical heterogeneity in sediments: A review of available technology and observed evidence. Earth-Science Reviews **92**: 81-97.

Thamdrup, B., AND D. E. Cainfield. (1996). Pathways of carbon oxidation in continental margin sediments off Chile. Limnology and Oceanography **41**(8): 1629-1650.

Unisense. (2008). http://www.unisense.com/Default.aspx?ID=568&Action=S.

Viollier, E., AND OTHERS. (2003). Benthic biogeochemistry: state of the art technologies and guidelines for the future of in situ survey. Journal of Experimental Marine Biology and Ecology **285-286**: 5-31.

Wenzhofer, F., AND R. N.Glud. (2002). Benthic carbon mineralization in the Atlantic: a synthesis based on in situ data from the last decade. Deep-Sea Research I **49**: 1255-1279.

Wenzhofer, F., AND R. N.Glud. (2004). Small-scale spatial and temporal variability in coastal benthic oxygen dynamics: Effects of faunal activity. Limnology and Oceanography **49**(5): 1471-1481.

Wenzhofer, F., O. Holby, O. Kohls. (2001). Deep penestrating benthic oxygen profiles measured in situ by oxygen optodes. Deep-Sea Research I **48**: 1741-1755.

http://www.hamburgerbildungsserver.de/welcome.phtml?unten=/klima/klimawandel/treibhausgase/carbondioxid/surfaceocean.html